Article

Multi-Disciplinary Computational Investigations on Asymmetrical Failure Factors of Disc Brakes for Various CFRP Materials: A Validated Approach

Vijayanandh Raja [1] , **Raj Kumar Gnanasekaran** [1] , **Abdul Razak Kaladgi** [2], **Parvathy Rajendran** [3,4,]*[], **Sher Afghan Khan** [5] and **Mohammad Asif** [6]

1 Department of Aeronautical Engineering, Kumaraguru College of Technology, Coimbatore 641049, Tamil Nadu, India
2 Department of Mechanical Engineering, P. A. College of Engineering (Affiliated to Visvesvaraya Technological University, Belagavi), Mangaluru 574153, Karnataka, India
3 School of Aerospace Engineering, Universiti Sains Malaysia, Engineering Campus, Nibong Tebal 14300, Pulau Pinang, Malaysia
4 Faculty of Engineering & Computing, First City University College, Bandar Utama 47800, Selangor, Malaysia
5 Department of Mechanical Engineering, Faculty of Engineering, International Islamic University, Kuala Lumpur 44000, Selangor, Malaysia
6 Department of Chemical Engineering, College of Engineering, King Saud University, P.O. Box 800, Riyadh 11421, Saudi Arabia
* Correspondence: aeparvathy@usm.my

Abstract: Finite element analyses (FEA) are flexible and advanced approaches, which are utilized to address difficult problems of aerospace materials that exhibit both structural symmetrical and structural asymmetrical characteristics. Frictional behavior effects are used as a crucial element in this multidisciplinary study, and other structural, thermal properties are computed using FEA. Primary lightweight materials such as glass fiber reinforced polymer (GFRP), carbon fiber reinforced polymer (CFRP), kevlar fiber reinforced polymer (KFRP), titanium alloy, tungsten carbide, steel alloys, and advanced lightweight materials, such as silicon carbide (SiC) mixer, based on aforesaid materials underwent comprehensive investigations on aircraft disc brake, two-wheeler disc brake, and ASTM general rotating test specimen (G-99). Standard boundary conditions, computational sensitivity tests, and theoretical validations were conducted because the working nature of FEA may impair output dependability. First, FEA calculations were performed on a standard rotating disc component with two separate material families at various rotational velocities such as 400 RPM, 500 RPM, 600 RPM, 800 RPM, and 10 N of external frictional force. Via tribological experiments, frictional force and deformation of FEA outcomes were validated; the experimental outcomes serve as important boundary conditions for real-time simulations. Second, verified FEA was extended to complicated real-time applications such as aircraft disc brakes and automobile disc brakes. This work confirms that composite materials possess superior properties to conventional alloys for aircraft and vehicle disc brakes.

Keywords: composite materials; ceramics; FEA; rotating disc; structural analysis; CAE; deformation analysis; frictional safety

1. Introduction

This research primarily targets complicated rotating parts such as brake shoes, disc brakes, gears, and etc., and also precisely focuses on the disc brake's structural, thermal, and frictional properties. Brakes turn kinetic energy into heat by putting pressure on the rudder pedals. Wheel hub, caliper, knuckle, piston, lining puck, gasket, brake pad, etc. are disc brake components. Pins, spring plates, etc. are used to secure a friction pad between the disc and piston. Disc brakes also have a bleeding valve and bleeding bolt.

Each cylinder features a rubber-sealing ring between the cylinder and piston. Because the wheel hub and rotors are joined, friction failure is common; hence strong materials are used between them. Composite materials and its allies have good integrated features, such as lightweight with high strength and high heat conductivity, and asymmetrical qualities along its directions. Carbon composites are good in these sensitive settings; thus, they are employed in the disc brakes of various advanced vehicles such as aircraft and heavyweight automotive vehicles. Disc brakes are used to land aircraft at a planned spot, and short runways benefit from disc brakes. Disc brakes operate between 250 and 3500 RPM; therefore, speed decrease in high-speed zones may affect both disc brake and brake pad. As a disc brake's lifetime is influenced by its materials and mechanical properties, this study focuses on the material selection procedure for various aforesaid advanced vehicle disc brakes. This study implements symmetrical alloys and asymmetrical composites. Three materials are chosen for aforesaid advanced vehicles' disc brakes, which have undergone experimental testing and CAE (Computer Aided Engineering) simulation to capture deformation and stress results. Two symmetrical alloys (Steel EN19, Steel EN 24) are already in use, and one asymmetrical composite material (carbon ceramic matrix composite (CCMC)) is planned to be used [1–4] in aircraft disc brakes. Automotive disc brake systems will test stainless steel, titanium alloy, tungsten carbide, GFRP, and CFRP. Apart from conventional composites and alloys, the CCMC is a primary disc brake material need. CCMC strengthens a ceramic matrix with continuous reinforcement and resins. Carbon fiber is employed as reinforcement in CCMC, and Epoxy HY951 and LY556 are used as adhesive. The matrix holds the reinforcing phase in place, transmits loads, and protects it from the environment. This technique uses carbon fiberto bolster a brittle matrix. Filler components like silicon carbide in particle form are added to CCMC matrix materials to improve electrical conductivity, thermal conductivity, thermal expansion, and hardness. Later machining creates intricate forms. Adding enough filler to the matrix improves primary composite qualities [5–10].

Failure factor analysis (FFA) is an effective approach to extend component life. FFA can uncover several mechanical component failure causes [6]. There are two types of failure factors: symmetrical (linear) and asymmetrical (non-linear). Symmetrical factors such as tensile failure and bending failure are directly connected to the applied external load and the produced internal resistive force [7]. In the case of non-linear (asymmetrical) failure, causes such as shear, impact loads are uncontrollable, generating an uncontrolled resistive force on the item's interior structure [8]. A change in atomic structure may cause catastrophic failure. For a long-lasting process, structural analysis must analyze asymmetrical (non-linear) failure variables [9]. Friction failure is the most unpredictable [9]. In friction, other from material reductions of both major and subordinate objects, temperature generation from material contact contributes greatly. Due to its unpredictability, the component's life under frictional loading is short. Frictional effects occur in various industries, including aerospace, automotive, electrical devices, marine, etc.

All available engineering techniques are emerging for predicting combined friction output [10]. Theoretical and experimental approaches are advancing rapidly, and complex engineering issues are usually solved using theoretical equations, modern computational tools, and well-equipped experimental settings [5]. Numerical simulation facilities are superior to the other two [11]. Improved simulation techniques are the best option for tackling all engineering challenges. Computer-based finite element simulations provide precise structural outputs, allow altering of circumstances at any point, and use a displacement-based solver approach, which boosts output reliability. Computational technologies struggle to model real-time things [12]. This projection issue may cause the fundamental object to collapse, impairing computational structural analysis. Improved modeling tools must bridge real-time objects and physical models. Due to these capabilities, nonlinear research uses modern computational methods. Flexibility at any moment and user-friendly procedures are the main elements that made computational simulation top in engineering methodology [13]. Advanced coupled structural simulations are utilized to achieve frictional (shear)

effect between moving and immovable objects. One-way coupling is majorly used to transform data between composite preparation and structural analyzing settings. This work is based on composite materials and nonlinear applications. Preparing composite materials with advanced matrix and reinforcements is quite complicated, and ordinary computational structural studies cannot produce satisfactory results. ANSYS ACP is used for composite construction and compression molding preparation. In the composite preparation tool, structural solving and post-processing are involved, thus the easiest numerical solver is unavoidable. To conduct this analysis successfully, a FEM-based solver is required, while an ANSYS structural tool is suggested. One-way coupling links these two powerful numerical instruments. Due to improved procedures, structural outputs are reliably achieved. Computational strategies are not always reliable. The experimental pin-on-disc test on the carbon fiber-based composite and steel alloys validates structural conclusions [14–20].

1.1. Problem Formulation and Method of Solution

This paper aims to select acceptable materials for disc brakes based on high thermal resistance and structural parameter assessment by computational simulation and experiments. Before the analysis begins, information about disc brake difficulties and reduction procedures are crucial [14–20].

1.1.1. Problems in Disc Brakes

Disc brake caliper and wheel failures are common. Pressure plate, smooth pins, and brake pads in the caliper also affect the lifetime of the advanced vehicle's braking system when subjected to external effects such as erosion, wear stress, corrosion, etc. Overheating the brakes can cause damage and failure of the braking equipment. When brake pad pressure is relaxed, brake heat dissipates [14–20]. High-intensity braking must be monitored for overheating and damage to guarantee safe operation. Disc brake failure can also be caused by sophisticated vehicle inoperability. During non-operational periods, frictional contact between brake components and thermal stress induction caused by sand dust, minor corrosion, etc. are major failure factors in sophisticated car disc brakes. In this work, material selection was used to improve the frictional performance and heat induction rate of advanced vehicle disc brakes at varied rotational average speeds [14–20].

1.1.2. Problem Solution Techniques

Brake discs should provide smooth, effective braking with minimum noise. Many compounds, such as asbestos, have caused health hazards during dissipation [20–25]. High-strength steel has been utilized for years. Rusting and loudness make it hard to maintain. Multiple segmented brakes enabled for higher braking intensities but increased vehicle weight, leading to carbon-fiber and similar disc brakes. Carbon-fiber-based composites are cost-effective and offer good load-resisting properties with low density. Lightweight and heat-resistant brakes are employed in high-performance vehicles. Carbon fiber can endure twice the heat of steel and is 50% lighter. Ceramic brake pads combine benefits, and ceramic compounds and copper fibers can replace steel [20–25]. This enables high-temperature braking and speedier recovery. It is quieter, dustier, and outlasts metallic brake pads. The selection of acceptable materials for non-linear applications is the most challenging job in material science; hence, our research imposed both physical tests and computer structural evaluations. Using a pin-on disc experiment, wear rate, frictional force, and kinematic friction coefficient are estimated for both primary and advanced composites. Using experimental test output, the computational structural and thermal analyses are performed to evaluate the advanced vehicle disc brake's total deformation, equivalent stress, frictional (shear) stress, and thermal stress [20–25]. FEA tool, i.e., ANSYS Workbench, analyzes the stresses and deformations. In this work, the frictional, structural, and thermal behaviors of CCMC and current steel materials were analyzed [20–25] for aerospace applications, and Ti-Alloy, tungsten carbide, CFRP, GFRP, and stainless steel were analyzed for automotive applications.

2. Methodology Used—Computational Engineering Analyses

2.1. Computational Model

In the modeling phase, a hollow circular plane with 55 mm outer and 6.5 mm inner diameters represents a disc's geometry. Another small circular plane, representing pin behavior, is given a 6 mm diameter. In general, 2D geometric modeling was sufficient for composite preparation. ANSYS ACP gives the disc composite characteristics. ASTM standard disc and pin thicknesses are 10 mm and 20 mm. As a result of this known thickness, the number of layers and its individual diameter are determined, with 0.1 mm fiber diameter and 100 layers employed for numerical production of composite materials. 'Rosette' is used to assign fiber direction, and 'Oriented Set-up' is used to assign laminate direction for composites. Solid model generation is used to precisely combine reinforcements and matrix. Figure 1 shows the consolidated pin-on-disc test specimen. The top coral-colored pin and blue-gray hollow disc are called pin and disc, respectively [26–30].
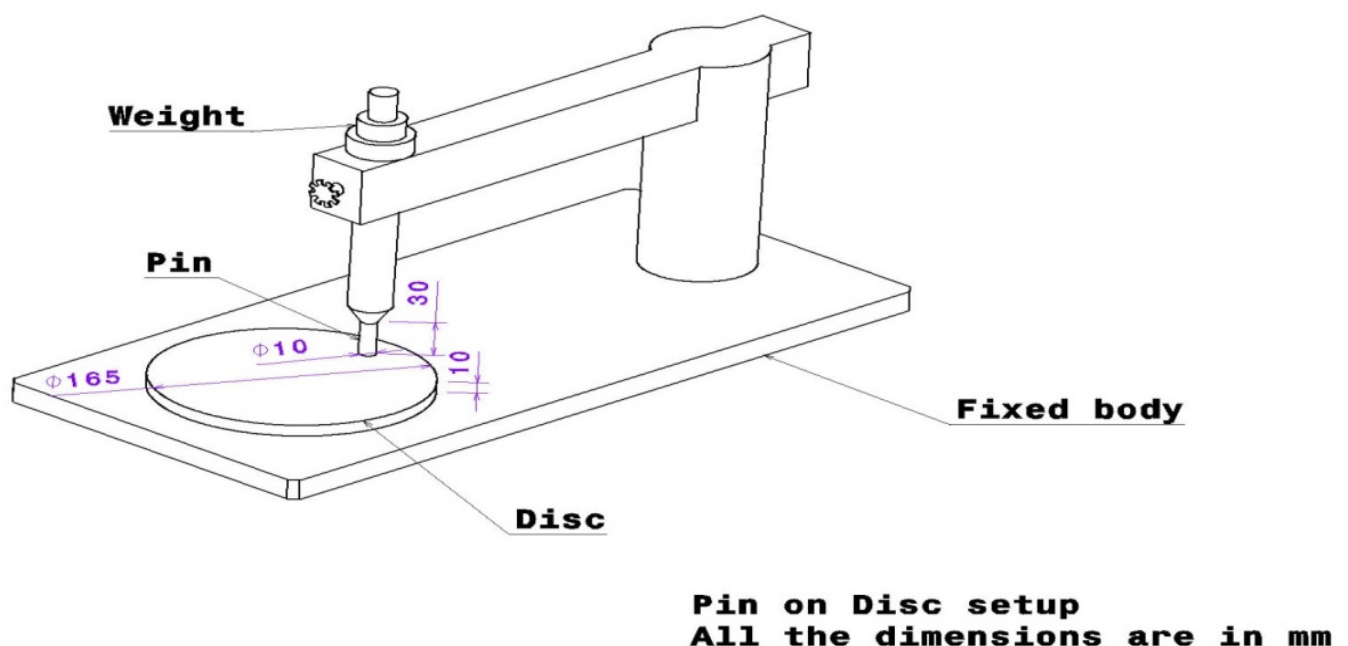

Figure 1. A typical isometric view of experimental set-up imposed for validation and base cases.

2.2. Discretization

In FEM-based simulations, the test set-up is partitioned into 3D finite elements. Nodes, line elements, and volume elements in 3D mesh calculate structural parameters. First, the structural outputs, i.e., deformations, are estimated at the nodal sites, and the various stresses are computed with the initial support of Young's Modulus, geometrical parameters, Poisson ratio, etc. In this study, 3D structural elements must be addressed using a stiffness-based dynamic technique using 15 governing equations. Fine setup is critical in the mesh process, which can capture the test object's physical model efficiently. Acceptable output requires complete capturization. This job is difficult; thus, in order to get accurate results, the ideal mesh must be designed and tested [31–35]. The complete test specimen is discretized with fine structural elements, and the mesh formation on the disc's top is altered by the pin. All the developed mesh cases are pictorially represented, wherein both structural and non-structural mesh cases are included. Among these five cases, one mesh case has been shortlisted as the best and most reliable platform for the provision of trustworthy outcomes.

2.3. Boundary Conditions

Rotational velocities and frictional force are major external loads in this scenario, which are given as 400 RPM, 500 RPM, 600 RPM, and 800 RPM and 10 N, respectively. In addition to these loads, modern composite mechanical properties play a key role in their boundary conditions. The imposed boundary conditions on the test specimen are revealed in Figure 2. Carbon fiber-based composites, glass-reinforced composites, and Kevlar fiber-based composites are also good at resisting mechanical loading; thus, they underwent numerical simulations. The numerical tool provides information on orthogonal characteristics, friction coefficient (0.15 for CFRP), density, thermal expansion coefficient, and melting temperature to represent the materials. To execute this sophisticated function well, the modeling and discretization phases must be linked and supported. After flawless composite material creation, discretized structures are sent to ANSYS using one-way coupling. This numerical model rotates clockwise. Between moving and immovable objects, friction is measured. This work compares frictional force on a fixed object (pin) [36–43].
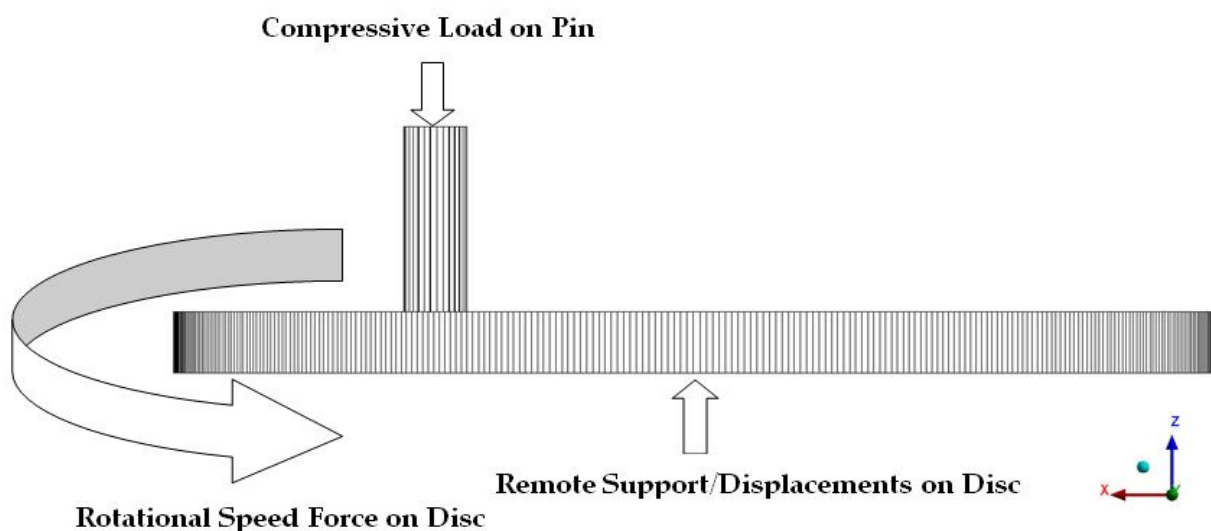

Figure 2. Details of imposed boundary conditions.

2.4. Details about the Analyses

The temperament of this study is rotodynamic, and the frictional effect of a disc brake, with an external load of 10 N, and the various rotating velocities are described. Therefore, cylindrical coordinate-based transient numerical investigations, in which the rotational velocities are provided with respect to different times, are used in a computational structural analysis of this nature. The dynamically based implicit equations are implemented in the solver phase as a result of this working behavior. The complete time-step, specifics of the time period for loading conditions, and fluctuations in rotational velocity acting on the disc brake with regard to time are significant parameters in this research. Since the applied force is known in this work, the stiffness-based methodology is used. Additionally, the calculation takes into account the mass of the entire system, as well as its velocities. Last but not least, the geometrical characteristics of the item, density and mass pertinent information, time dependent parameter data, and applied stress are crucial for properly carrying out the dynamic simulation [36–43].

2.5. Grid Convergence Study-1

The mesh must be optimized for its correctness, which depends on its quality, when it comes to the grid convergence research. Finding the least amount of output variation across all mesh configurations and selecting the fewest numbers of pieces based on these minute variations are key components of this optimization investigation. In this grid optimization, the mesh was separated into five categories based on its capturing quality:

coarse, medium, fine, fine with individual set-ups, and fine with inflation. The face mesh setup, curvature cum proximity setup, and inflation setup are three additional complex mesh settings used in this investigation. The aforementioned boundary criteria also apply without any modifications when the Kevlar composite is used consistently throughout all five circumstances. The coarse mesh configuration, which was the initial situation, is shown in Figure 3. Figure 4 shows a situation where the fundamental components are of average quality. Figuratively, Figures 5–7 might represent the top three meshes. Since they are essential for stress induction, face mesh facilities were included in Case 3 on the top and bottom sides of the disc. Because they more effectively capture warp and area variation zones, Case 4 meshes leveraged the curvature and proximity facilities. Finally, in Case 5, where the growth rate is set at 1.2, inflation had a large impact on how things turn out. Normally, only the top surface of the disc, or the primary portion, is inflated. Table 1 displays node and element information for all mesh scenarios. Except for the mesh modifications, all five mesh-based Kevlar composite test setups for which computational structural assessments are computed were therefore studied using the same input conditions.
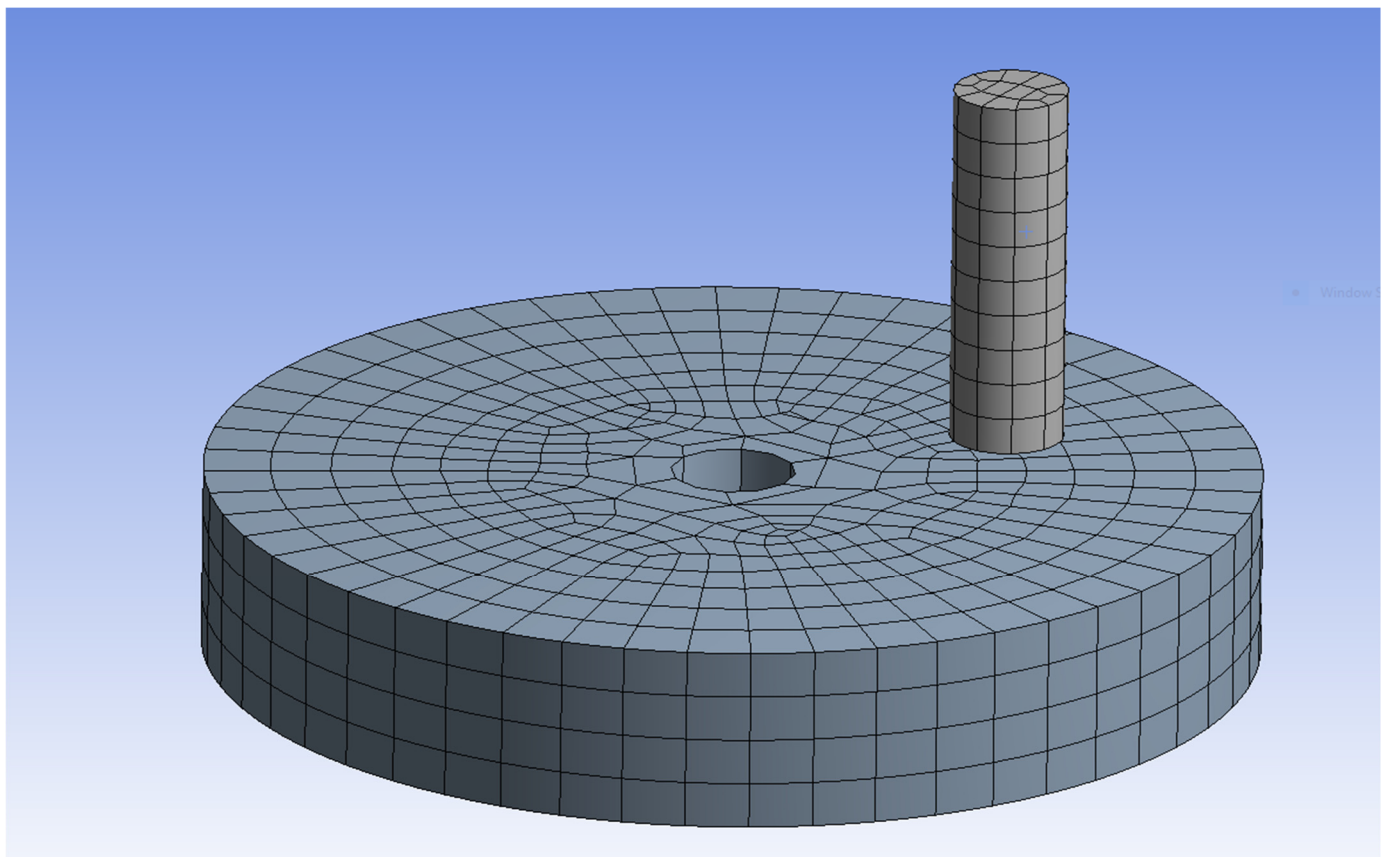

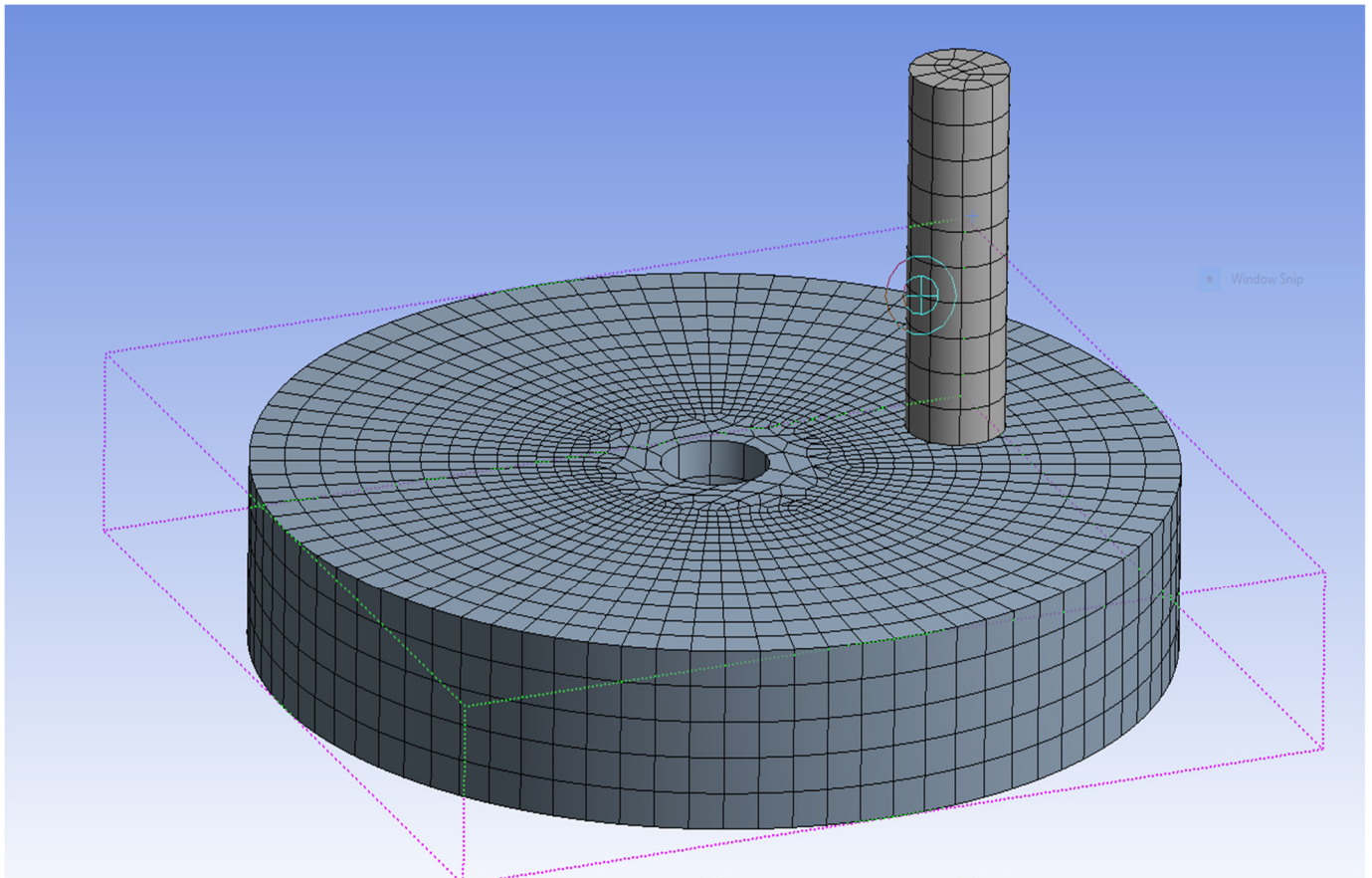**Figure 3.** A typical isometric view of coarse mesh [mesh, Case 1].

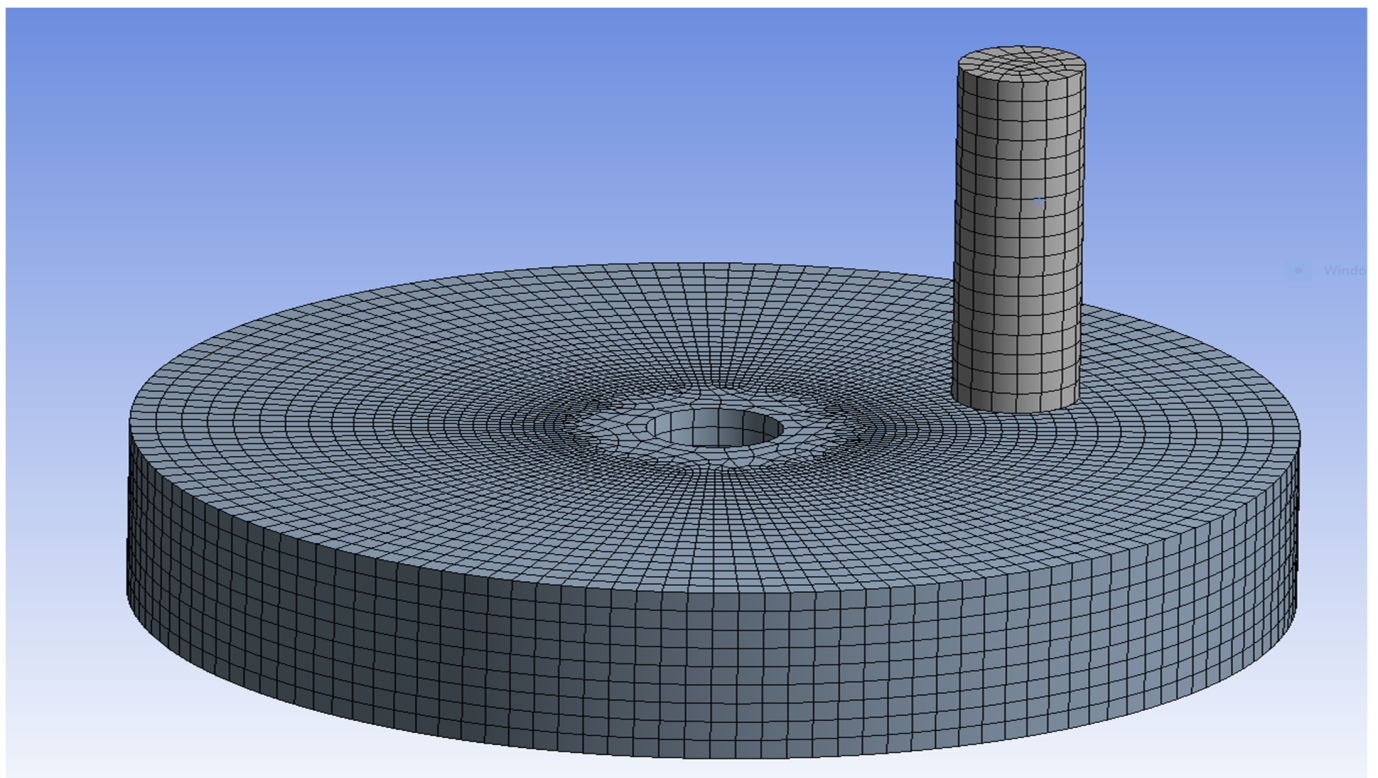**Figure 4.** A typical isometric view of medium mesh [mesh, Case 2].

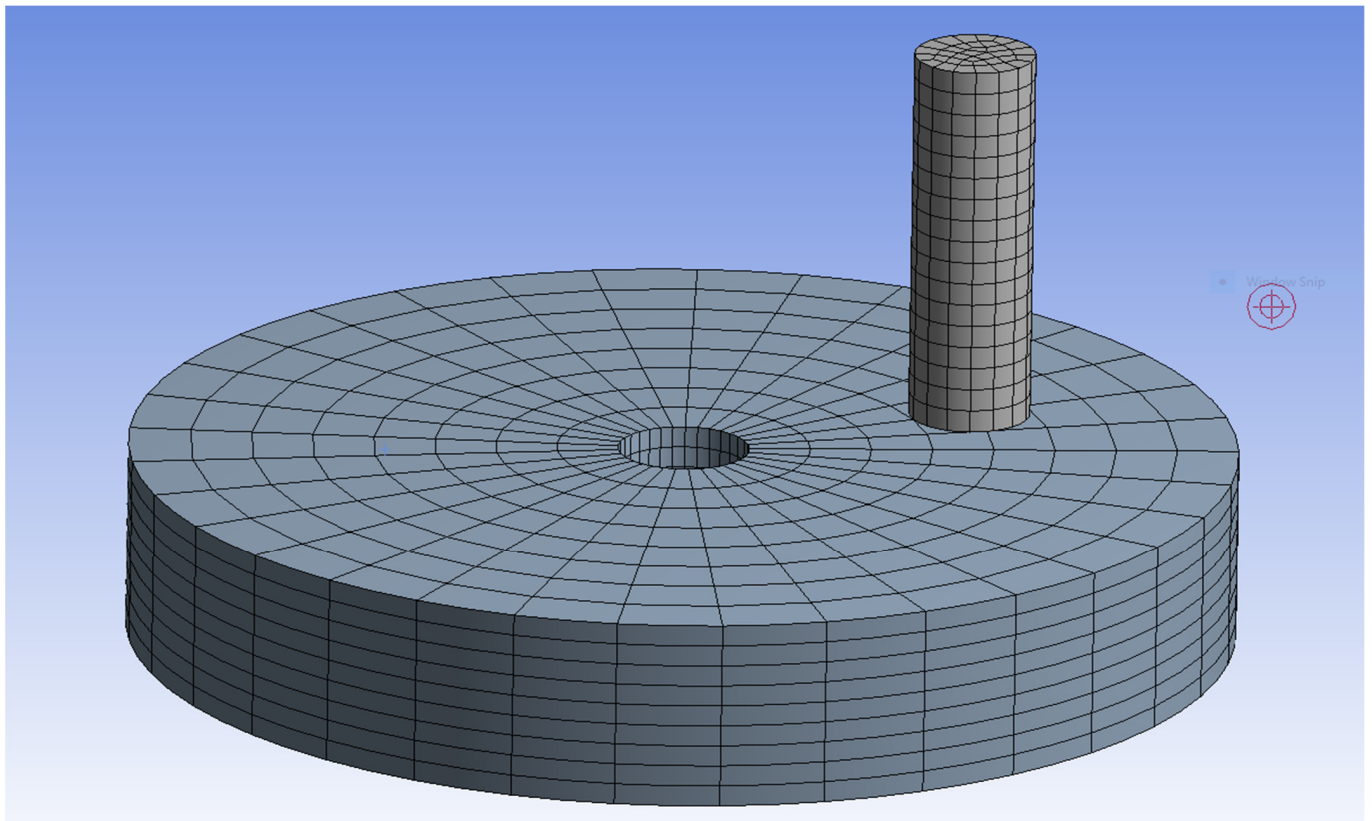**Figure 5.** A typical isometric view of fine with face mesh [mesh, Case 3].

Figure 6. A typical isometric view of fine with mesh set-up [mesh Case 4].
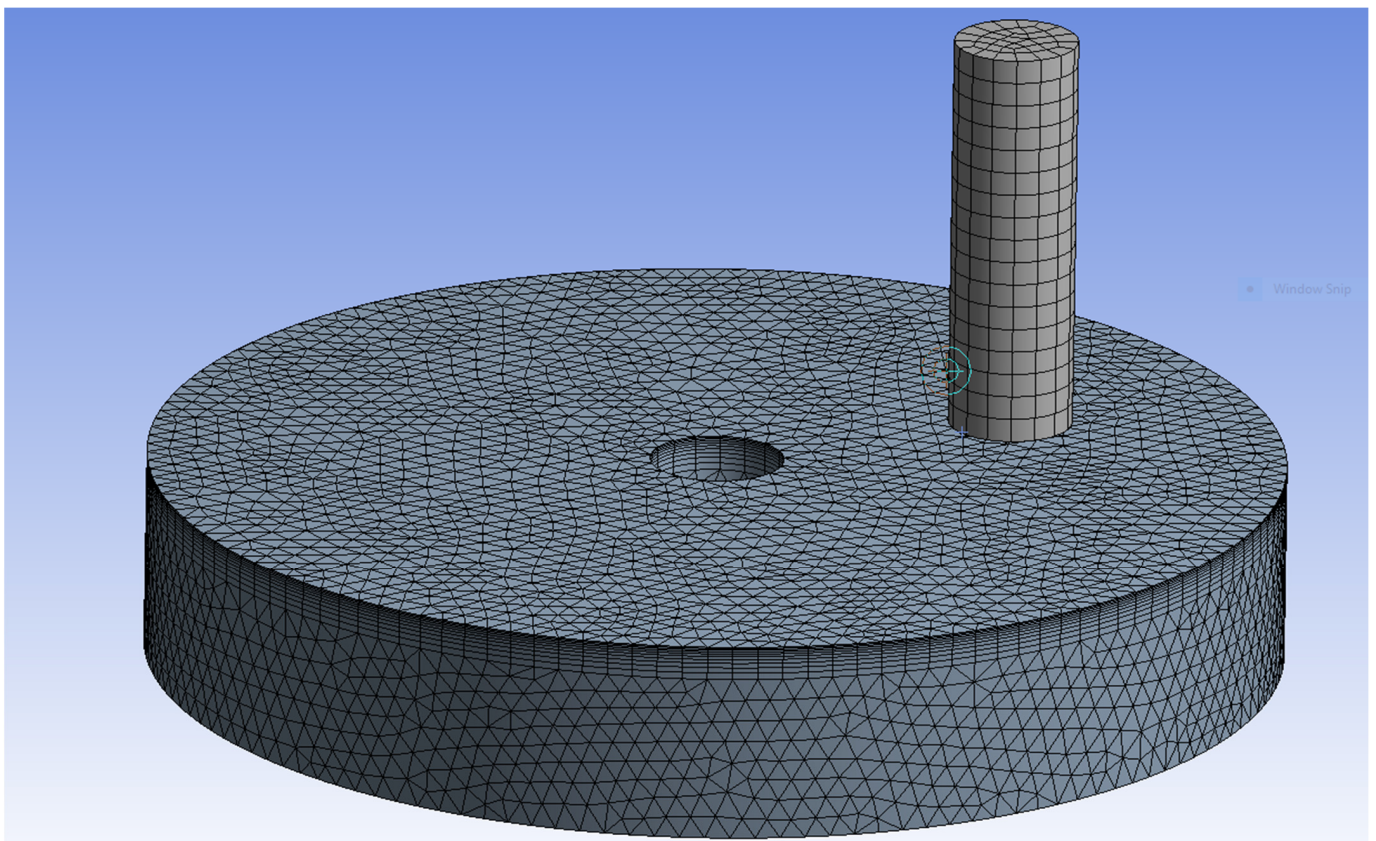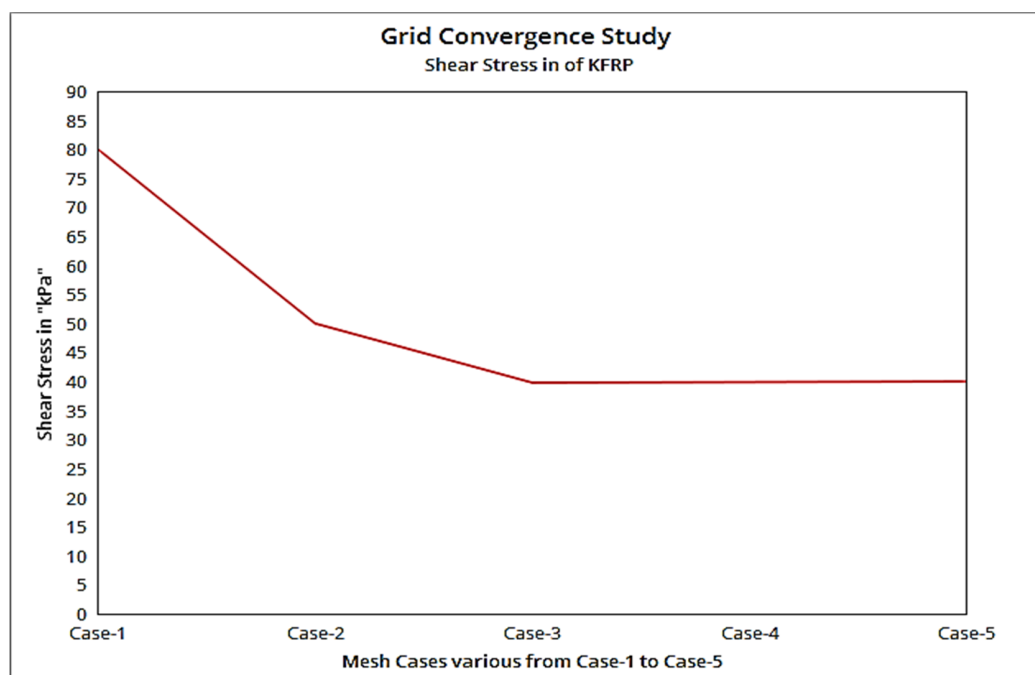

Figure 7. A typical isometric view of fine mesh with inflation set-up [mesh, Case 5].

Table 1. Comparative data of imposed mesh details for grid sensitivity test.

Sl. No	Type	Mesh Details	Number of Nodes	Number of Elements
1	Mesh1	Coarse	8505	1692
2	Mesh2	Medium	30,973	6580
3	Mesh3	Fine with face mesh set-up	14,126	2954
4	Mesh4	Fine	150,004	34,103
5	Mesh5	Fine with inflation	161,138	81,381

Figure 8 shows mesh cases versus shear stresses for a Kevlar-based composite. All mesh circumstances have the same major boundary conditions, such as the spinning disc's rotational velocity, external force on the pin, inner hub displacement, and pin surface support. Enhanced cumulus mesh capabilities build mesh instances with more compositional parts. Figure 8 prefers mesh Case 3 above the others. Case 4 mesh setups are always employed. Because mesh Cases 3 and 5 differ slightly, a decision is made. This is why mesh Case 3 is the best further extensor [36–43].

Figure 8. Grid convergence test on KFRP test specimen.

2.6. Results and Discussions of Base Cases

The aforementioned boundary requirements were put into practice, and structural simulations were run for all of the advanced composite materials with indents. Figure 9 depicts the structural outcome of a composite made of Kevlar, which is a material that is often utilized in engineering applications. The stress fluctuations of different glass fibers (S-Glass and E-Glass) are then displayed in Figures 10 and 11. Because S-Glass fiber outperforms all other glass fibers in terms of strength and ability to handle complex applications, it has become the standard to choose S-glass fibers. However, in the case of E-glass, the integrated check is entirely responsible for fiber selection. The results of all other materials are shown in Figures 12–14, where Figure 12 shows the total deformation variations for all materials, Figure 13 shows the equivalent stress, and Figure 14 shows the shear stress variations for composite materials.
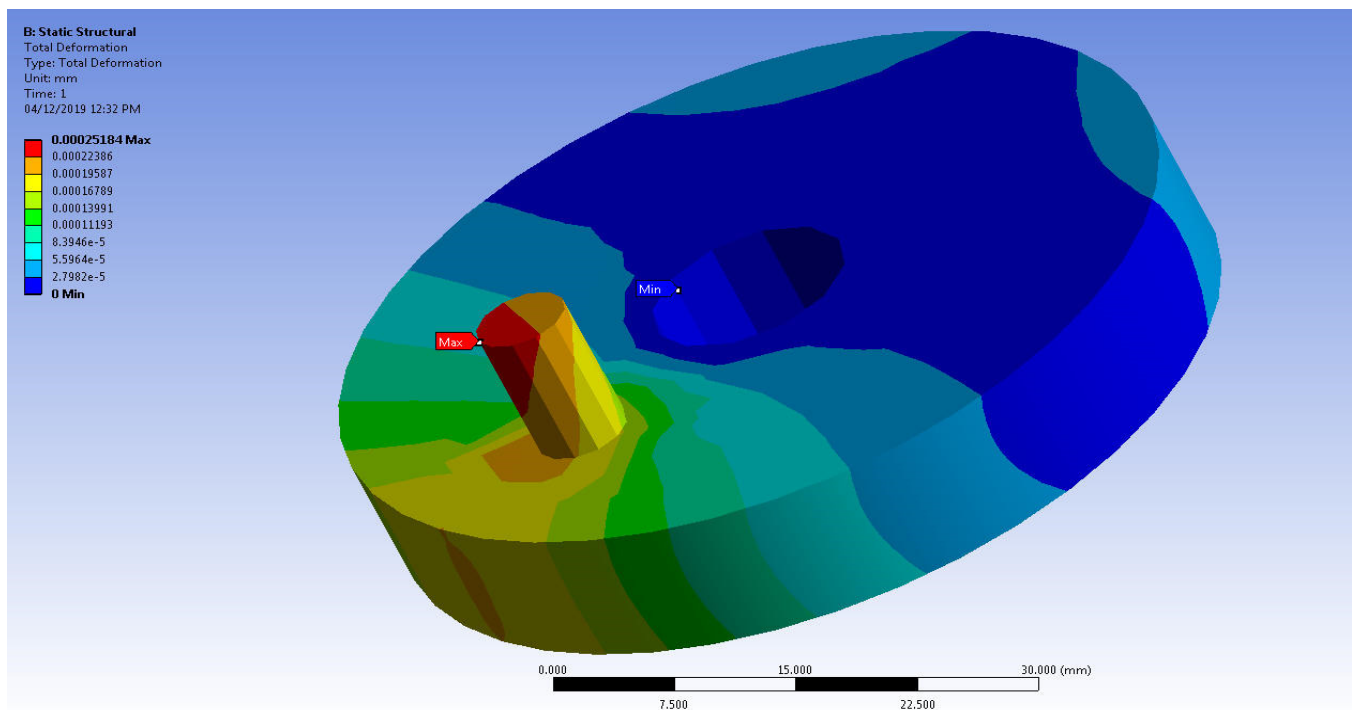
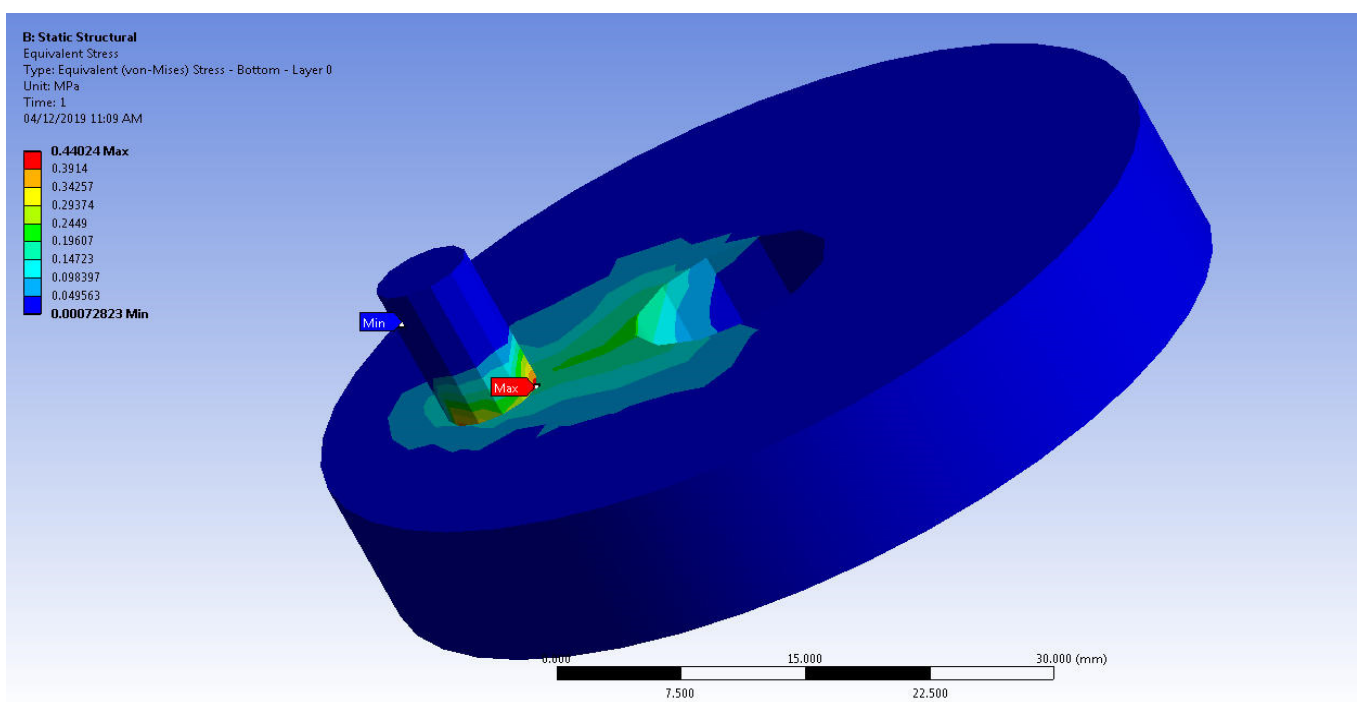**Figure 9.** Deformed structure of CFRP-UD wet-based test specimen.

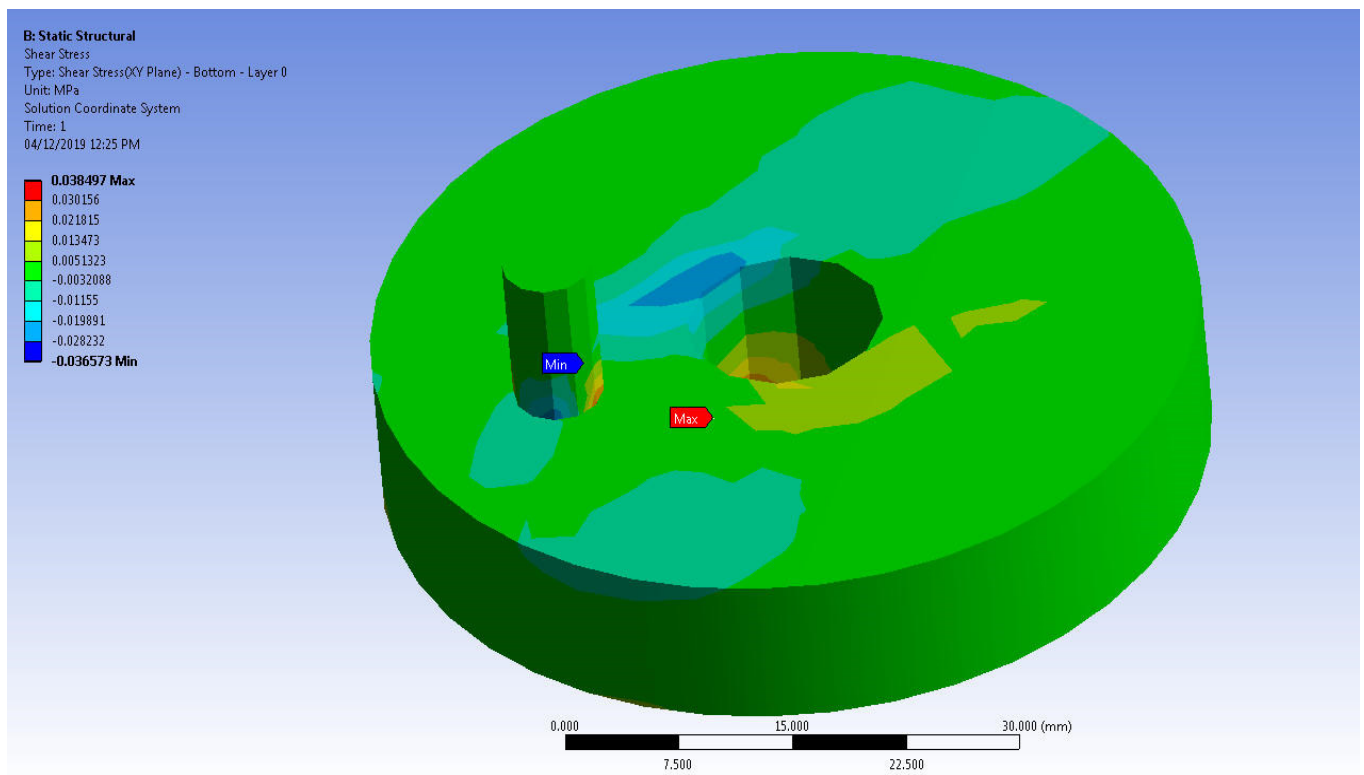**Figure 10.** Equivalent stress variations on the E-UD-GFRP-based test specimen.

Figure 11. Shear stress variations on the CFRP-UD-prepreg-based test specimen.
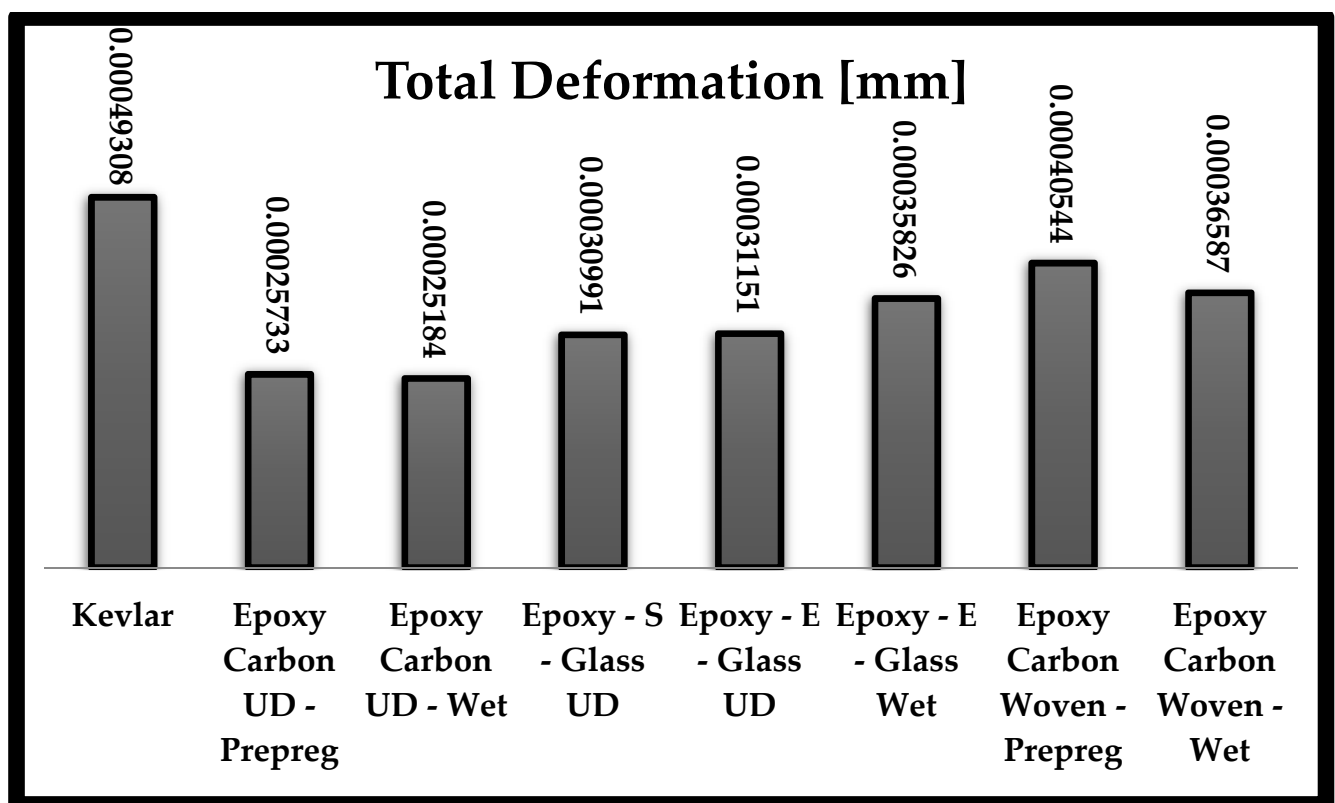

Figure 12. Comparative results of total deformations of all the composite materials.
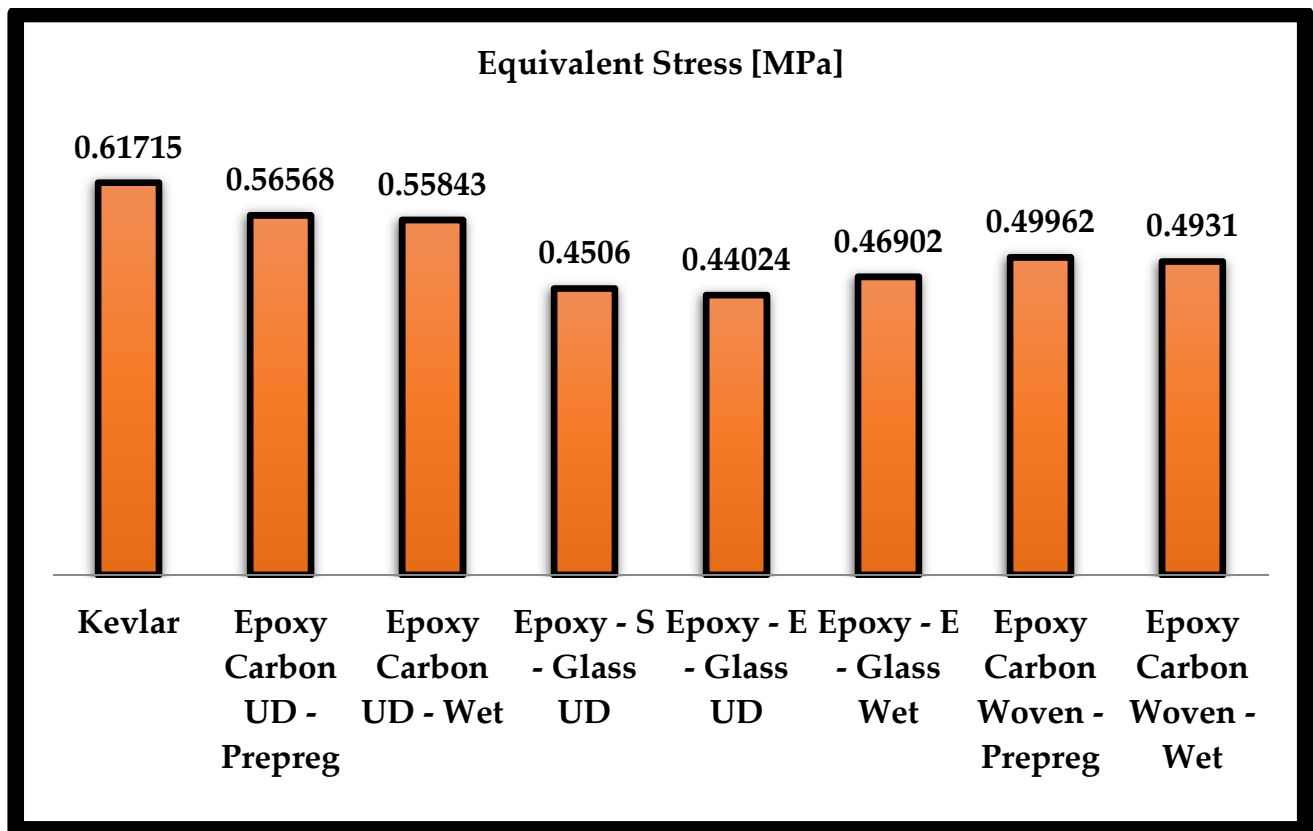
Equivalent Stress [MPa]

Material	Value
Kevlar	0.61715
Epoxy Carbon UD - Prepreg	0.56568
Epoxy Carbon UD - Wet	0.55843
Epoxy - S - Glass UD	0.4506
Epoxy - E - Glass UD	0.44024
Epoxy - E - Glass Wet	0.46902
Epoxy Carbon Woven - Prepreg	0.49962
Epoxy Carbon Woven - Wet	0.4931

Figure 13. Comparative results of equivalent stresses of all the composite materials.

Shear Stress [MPa]

Material	Value
Kevlar	0.039979
Epoxy Carbon UD - Prepreg	0.038497
Epoxy Carbon UD - Wet	0.039249
Epoxy - S - Glass UD	0.053203
Epoxy - E - Glass UD	0.053503
Epoxy - E - Glass Wet	0.057588
Epoxy Carbon Woven - Prepreg	0.13316
Epoxy Carbon Woven - Wet	0.12736

Figure 14. Comparative results of shear stresses of all the composite materials.

2.6.1. Results and Discussions of Base Cases

It is evident from Figures 12–14 that composites made of carbon fiber and Kevlar are better able to tolerate frictional loading. However, because carbon fibers outperform Kevlar composites in terms of the overall effect, carbon fibers are added to the best combinations to further reduce stresses.

2.6.2. Extension of Other Advanced Materials

Composite materials have good mechanical characteristics and resist mechanical loading well. In the case of frictional study and its side effect parameter, thermal stress induction, composites can react at a low level in difficult real-time applications, but not as much. Thus, application-oriented mixtures are important in non-linear research. Valid amounts of mixtures can boost the qualities of composite materials in relevant domains. In this paper, silicon carbide was chosen as a good frictional combination. In order to improve the composite's properties, the mixing level must be considered during preparation. In this numerical simulation, 5% (0.5 mm in disc thickness) silicon carbide was employed for the carbon-fiber-based composite with a composite preparation tool. Good structural findings on deformation, shear stress, and equivalent stress of carbon-woven-230-GPa-wet–SiC are shown in Figures 15–17. The comparative analyses of advanced frictional-based composite materials were evaluated, and the comprehensive results are shown in Figures 18–20. Figure 18 shows deformation outputs, Figure 19 shows equivalent stresses, and Figure 20 shows shear stresses.
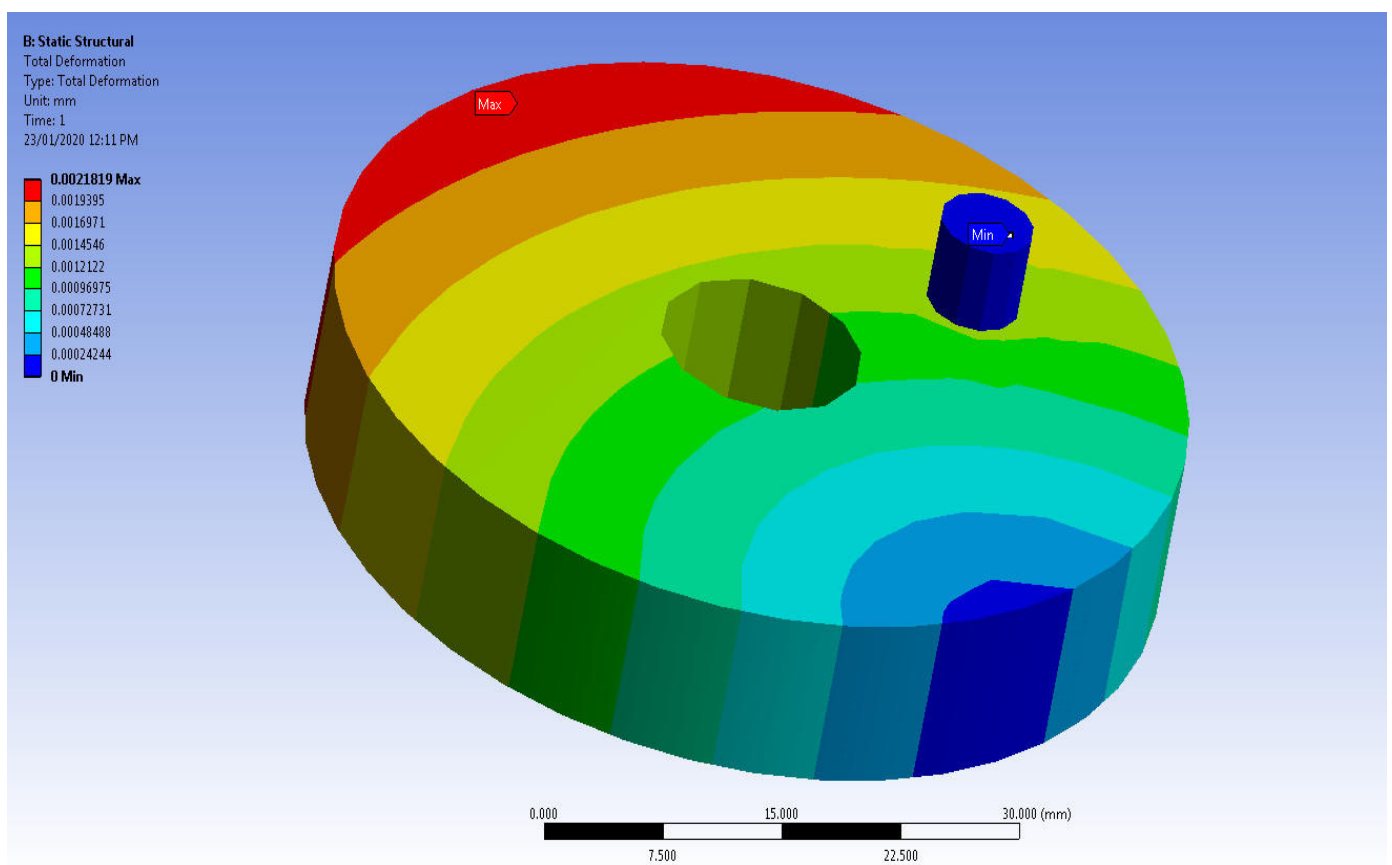

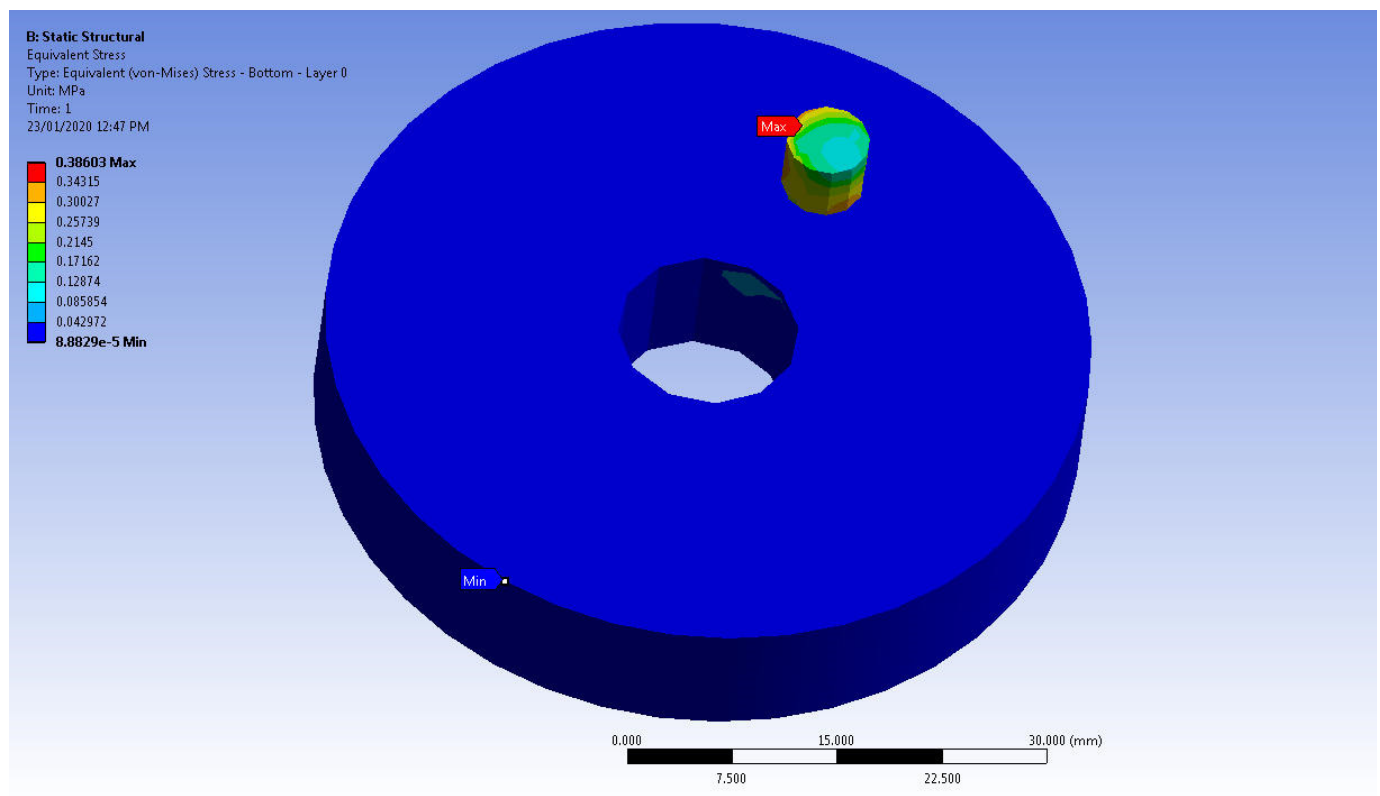**Figure 15.** Variations of deformation of UD-prepreg carbon-fiber-based composite with SiC.

Figure 16. Equivalent stress variations on the woven-prepreg-based CFRP composite with SiC.
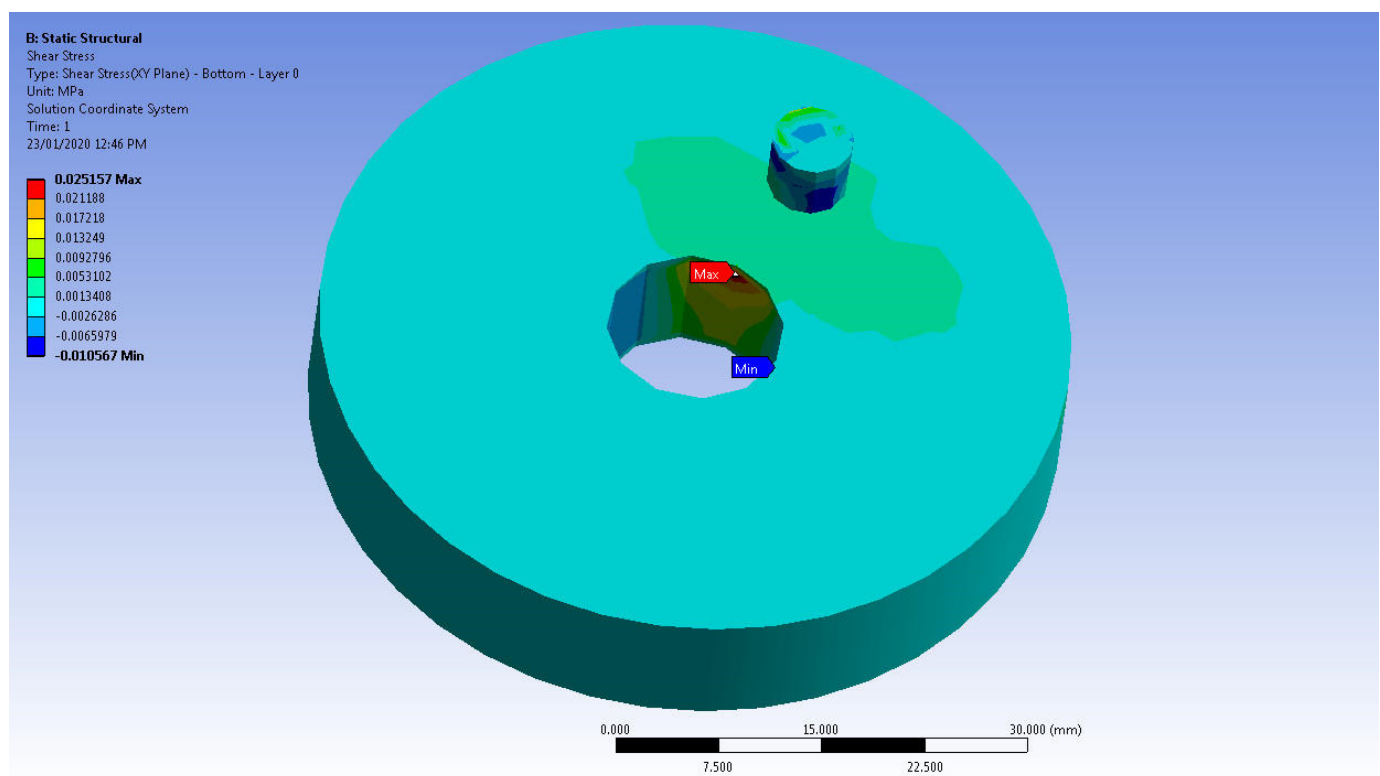

Figure 17. Shear stress variations on the woven-prepreg-based CFRP composite with SiC.
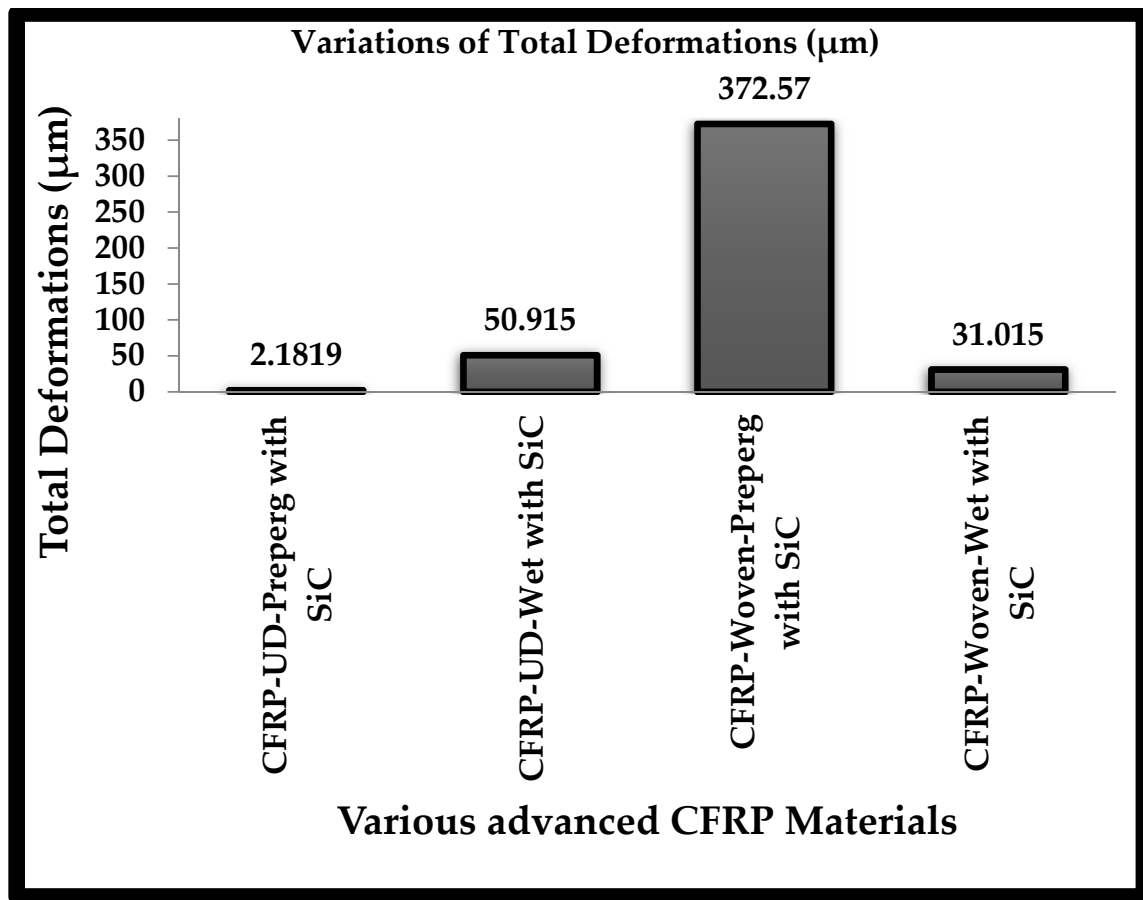
Figure 18. Comparative analysis of deformation values of best composite materials.
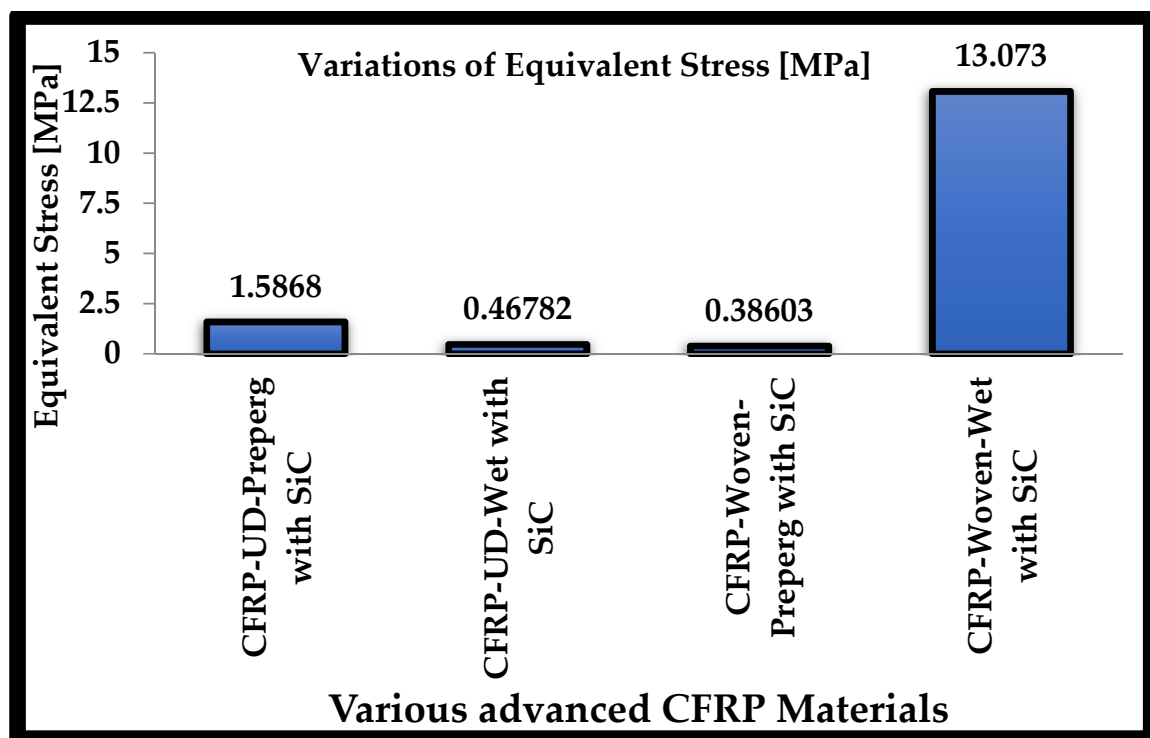

Figure 19. Comparative analysis of equivalent stress values of best composite materials.
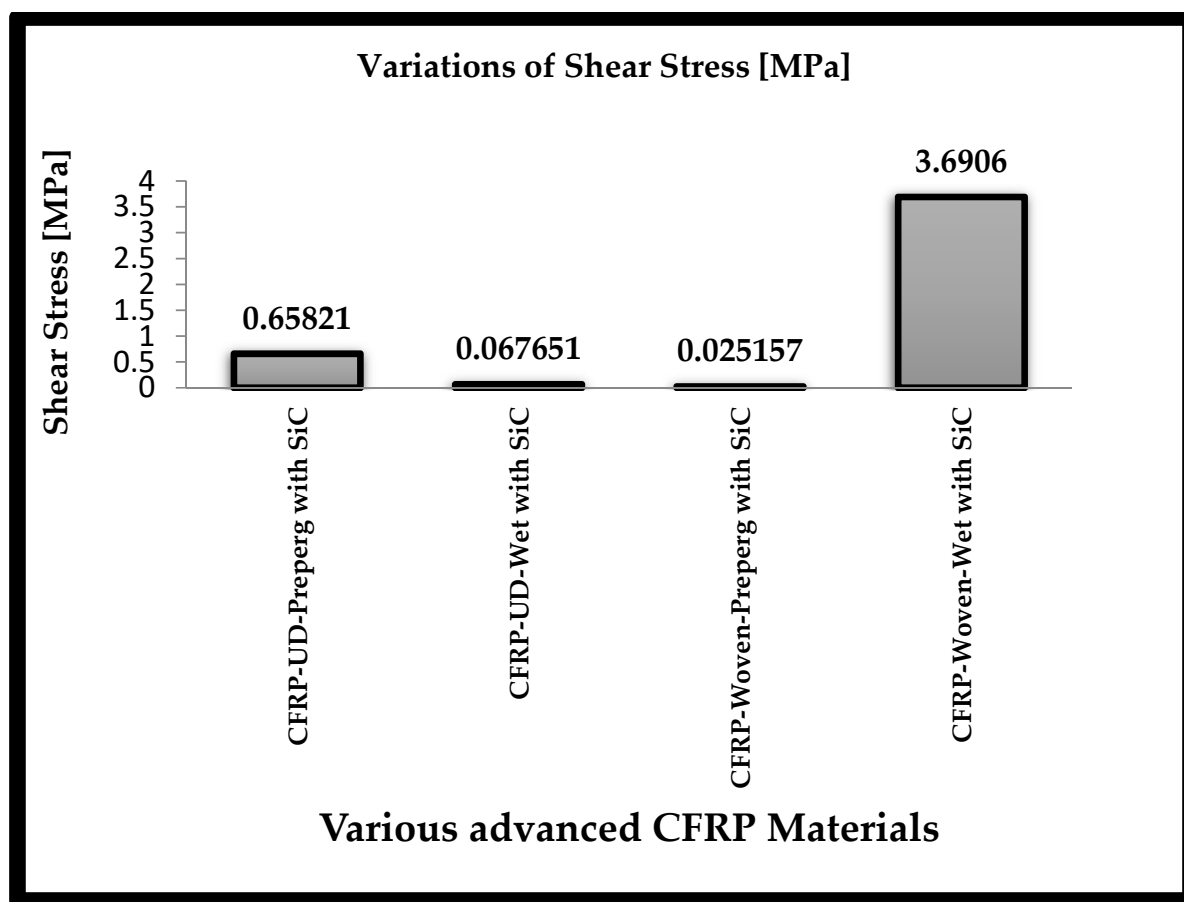
Variations of Shear Stress [MPa]

Figure 20. Comparative analysis of shear stress values of best composite materials.

Figures 18–20 show that frictional stresses were much lower than in conventional composites. Epoxy-carbon-UD-230 GPa-prepreg is the best material to endure frictional loading based on the initial comparative investigation. Second, compared to other composites, frictional stresses were drastically decreased. The carbon-woven-230-GPa-prepreg mixed with SiC is better for frictional loading under complex situations.

2.7. Validation Investigation of Base Cases

This comparative study relied on computer-based computational structural analysis. Validation was required to confirm the estimated output, as real-time applications prefer these results. Experimental pin disc equipment validated the carbon fiber composites results.

Computational Structural Analysis

Pre-processing, solution, and post-processing are the primary families in numerical simulation for trustworthy output with uniform direction. In pre-processing of this shear test, dimensions of the test specimen were modeled, testing environments were chosen to involve theoretical formulae, materials were represented using mechanical properties, and support and external loads were provided. Theoretical formulas were used for numerical simulation. The implementation of essential standard equations could be simplified for the solving step. Post-processing provided modifications of evaluation parameters such as total deformation, strain energy, etc. Structural simulation was conducted on carbon fiber composite [14–16]. Figures 21 and 22 are exhibit epoxy-carbon-UD-230-GPa-prepreg stress and deformation.
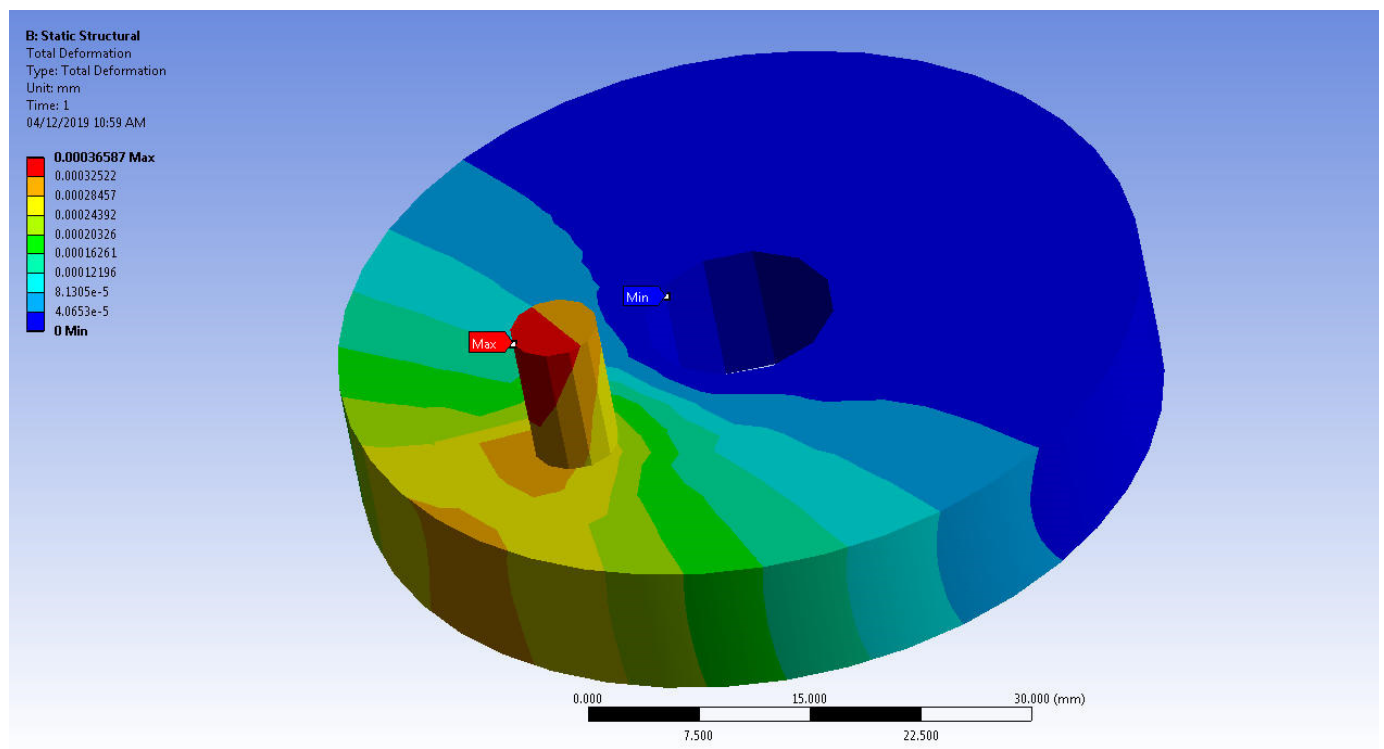
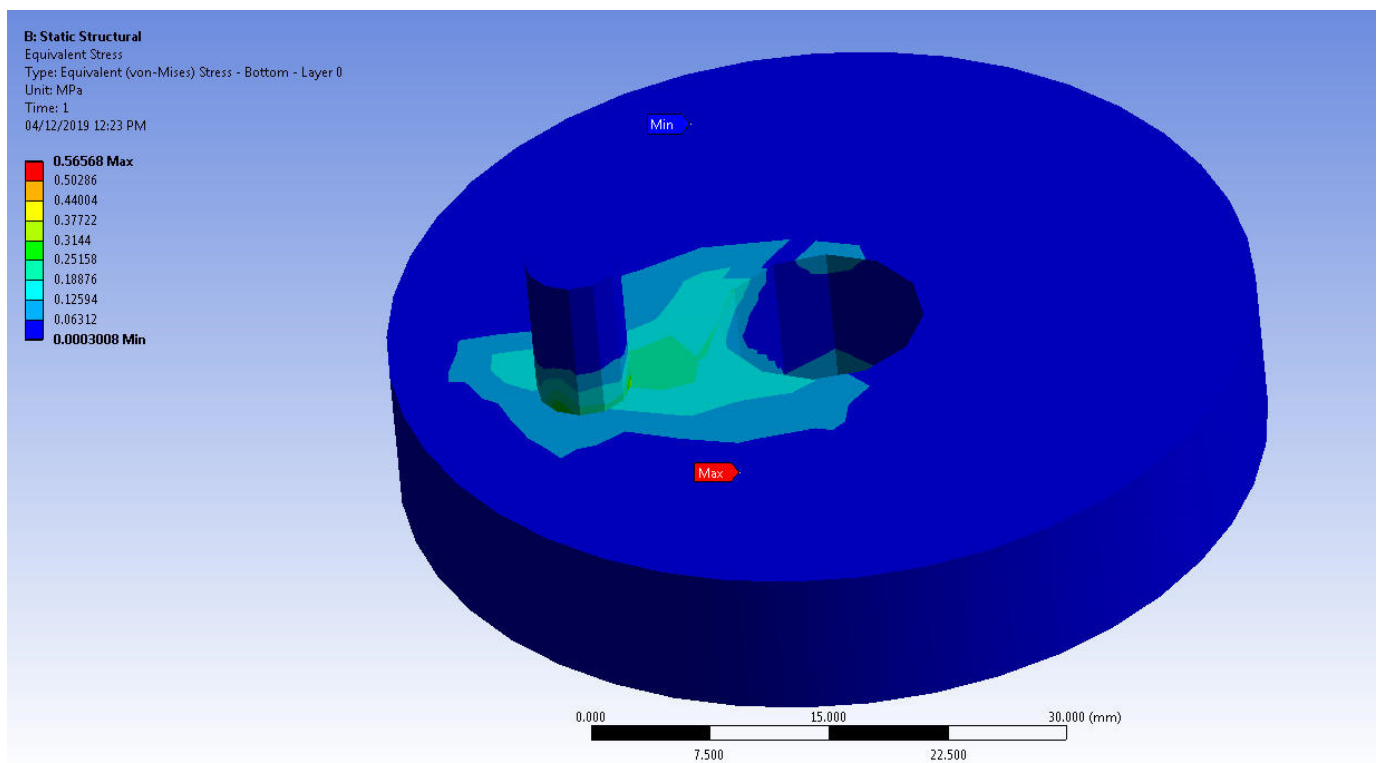**Figure 21.** Deformed structure of CFRP-woven-wet-based test specimen.

Figure 22. Stress variations on the carbon specimen through FEA outcomes.

The validation section of this work compares simulation findings with carbon fiber composite test results. In the experimental test, woven and UD carbon fibers with a Young's modulus of 230 GPa were employed, while in the numerical simulations, unidirectional

and bidirectional fibers were used and compared. Figure 23 shows the test specimen and setup. The coefficient of friction results of this imposed CFRP test specimen for various rotational velocities such as 400 RPM, 500 RPM, and 600 RPM are shown in Figures 24–26 respectively. Figure 27 compares the structural results of experimental and numerical engineering approaches, showing that the implemented boundary conditions in the structural simulation can provide acceptable solutions. This methodology is suggested to execute other leading CFRP-composite materials [20–29].

$$\text{Error \%}_{\text{UD}} = \frac{[\text{Computational Structural Result} - \text{Experimental Result}]}{[\text{Computational Structural Result}]} \Rightarrow \frac{(0.258184 - 0.254471)}{(0.258184)} \Rightarrow \text{Error \%}_{\text{UD}} = 1.44$$

$$\text{Error \%}_{\text{Woven}} = \frac{[\text{Computational Structural Result} - \text{Experimental Result}]}{[\text{Computational Structural Result}]} \Rightarrow \frac{(0.40544 - 0.38754)}{(0.40544)}$$
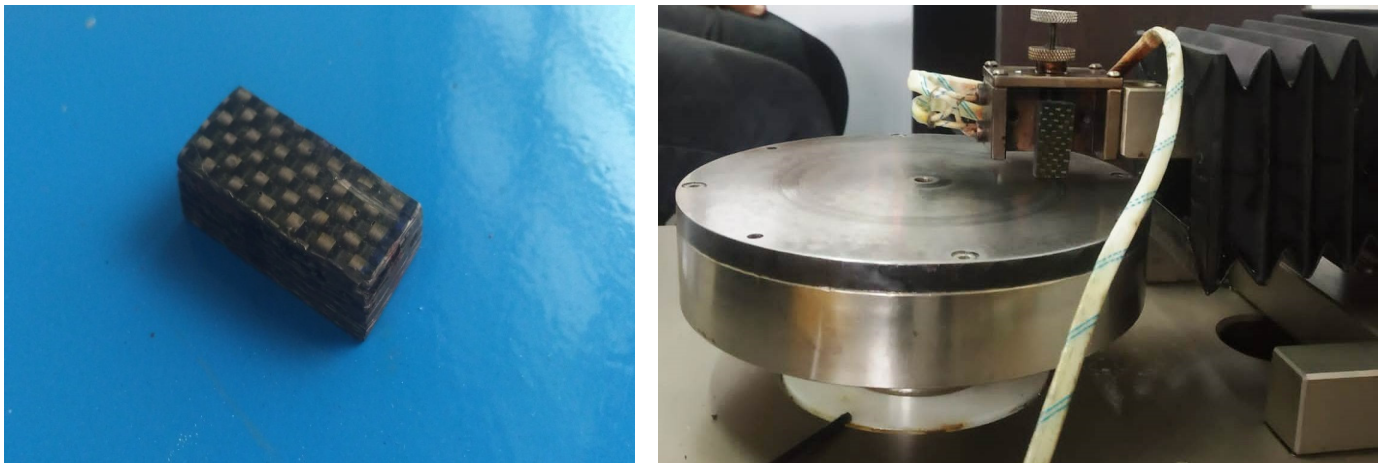$$\Rightarrow \text{Error \%}_{\text{Woven}} = 4.415$$

Figure 23. The combined views of a developed CFRP test specimen and its loading condition on the experiment.

Less than 5% error was obtained from this validation investigation, which is in the acceptable range. Thus, the followed procedures were confirmed with the help of experimental tests, and thereby, the results confirmed the applicability of the proposed materials in real-world contexts.

2.8. Validation Investigation of Advanced Cases

2.8.1. Test Specimen Preparation—Experimental Prototype—Steel

Machining removes metal via turning, milling, and drilling. It is a factory finishing procedure that results in great precision. In this study, a lathe was utilized to convert the test material to the necessary dimensions. Turning reduces the rod's diameter by rotating it around a tool. Machines should finish unfinished work. A finished product will be smooth and the size of the plan draught used to machine it. A lathe removes the rod's extra diameter to give it a smooth outer diameter. The Material removing rate (MRR) is crucial for evaluating thermal characteristics. Figure 28 shows the development process involved in the steel-alloy-based test specimens for experimental testing.
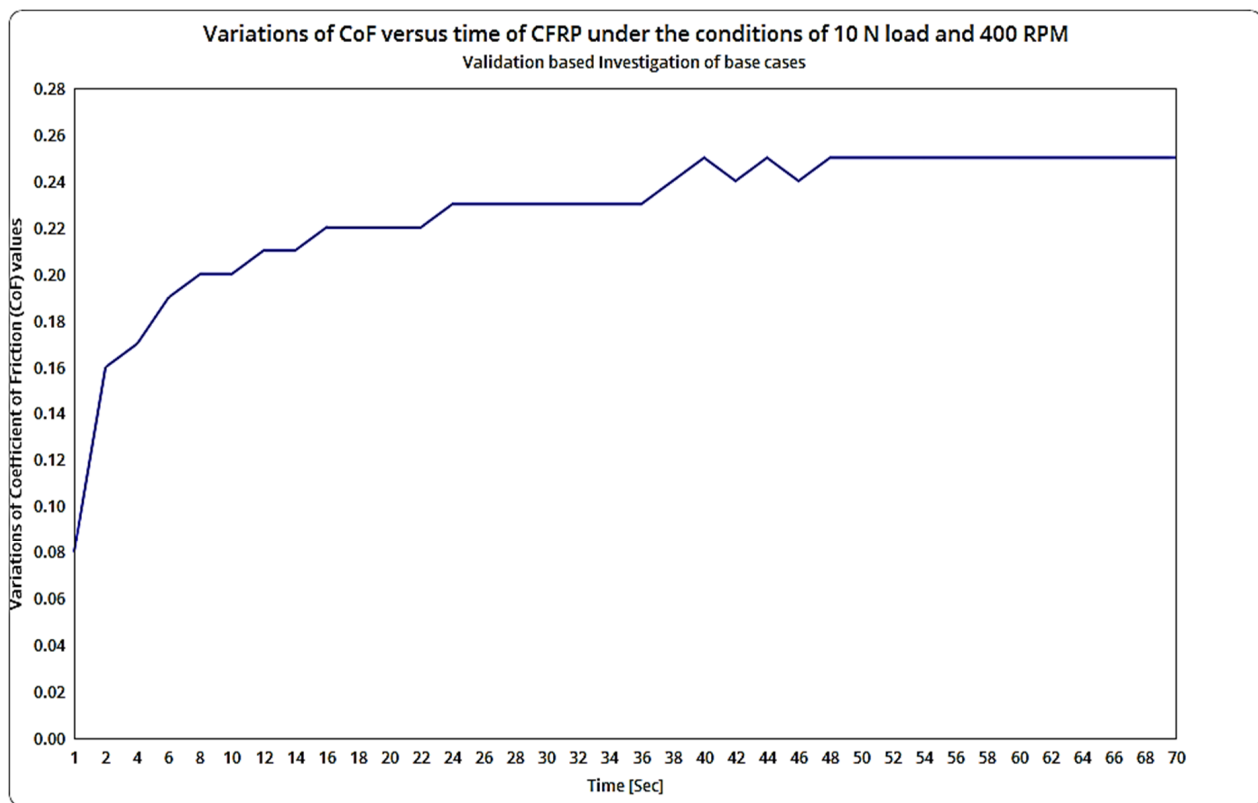
Figure 24. Variations of CoF versus time of CFRP under the conditions of 10 N load and 400 RPM.
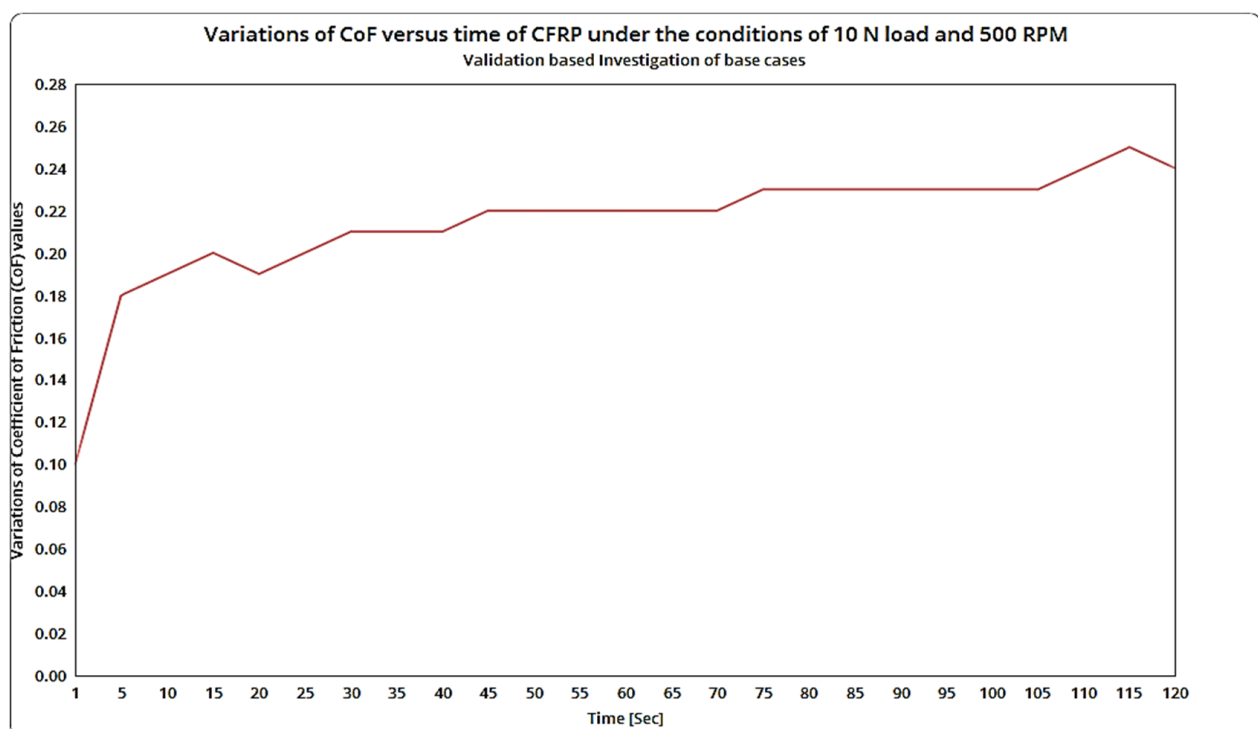

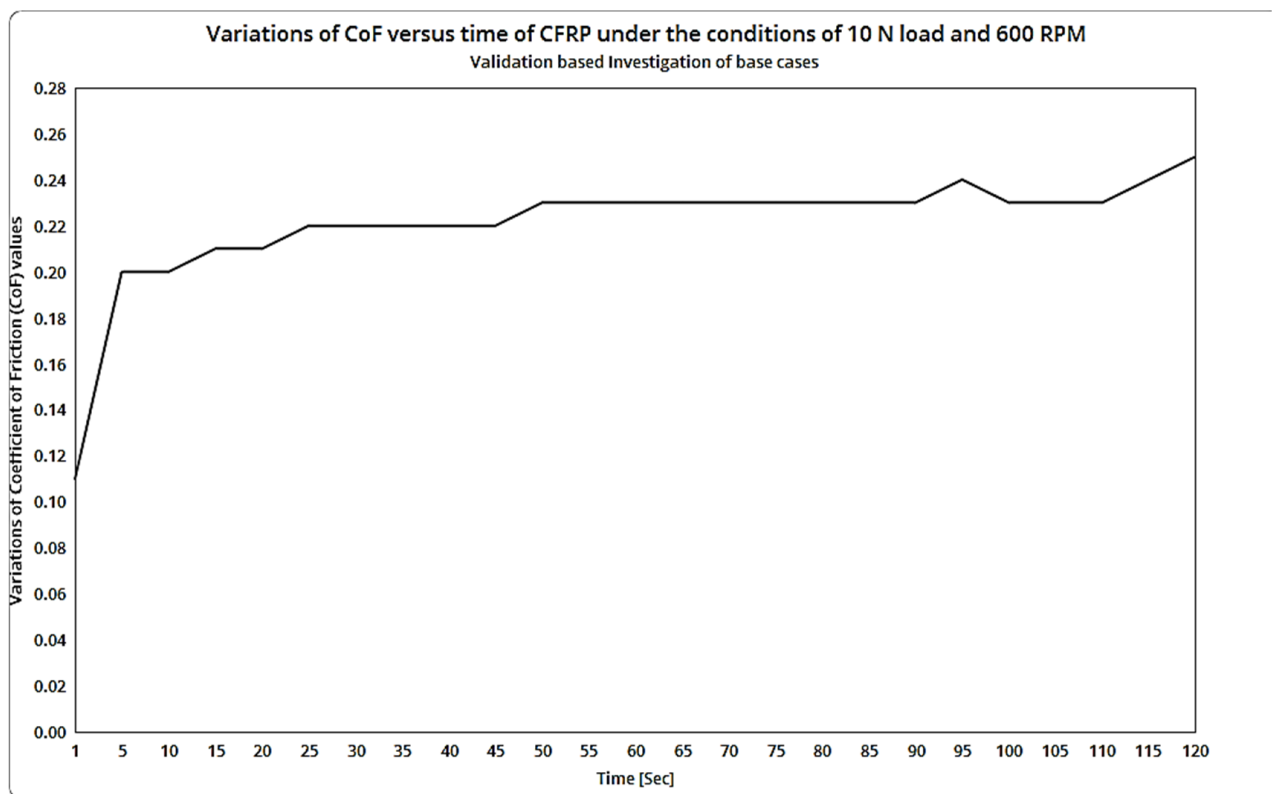**Figure 25.** Variations of CoF versus time of CFRP under the conditions of 10 N load and 500 RPM.

Figure 26. Variations of CoF versus time of CFRP under the conditions of 10 N load and 600 RPM.
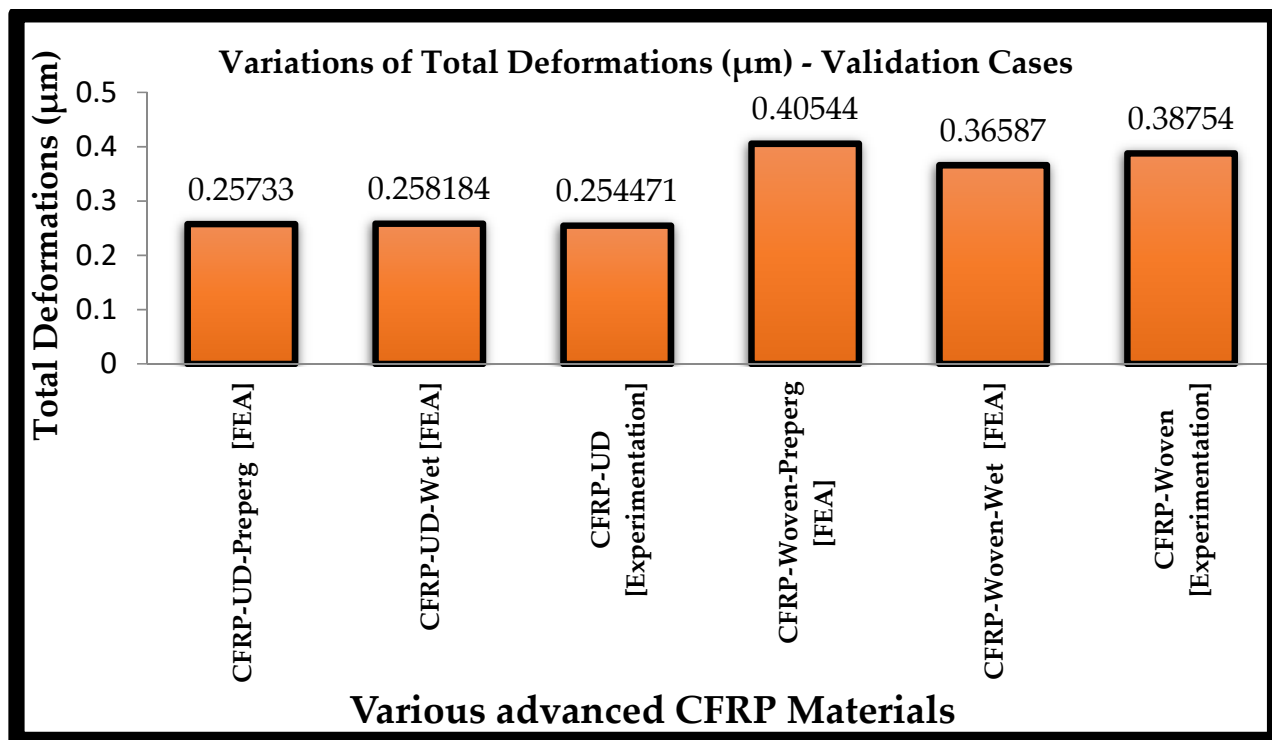

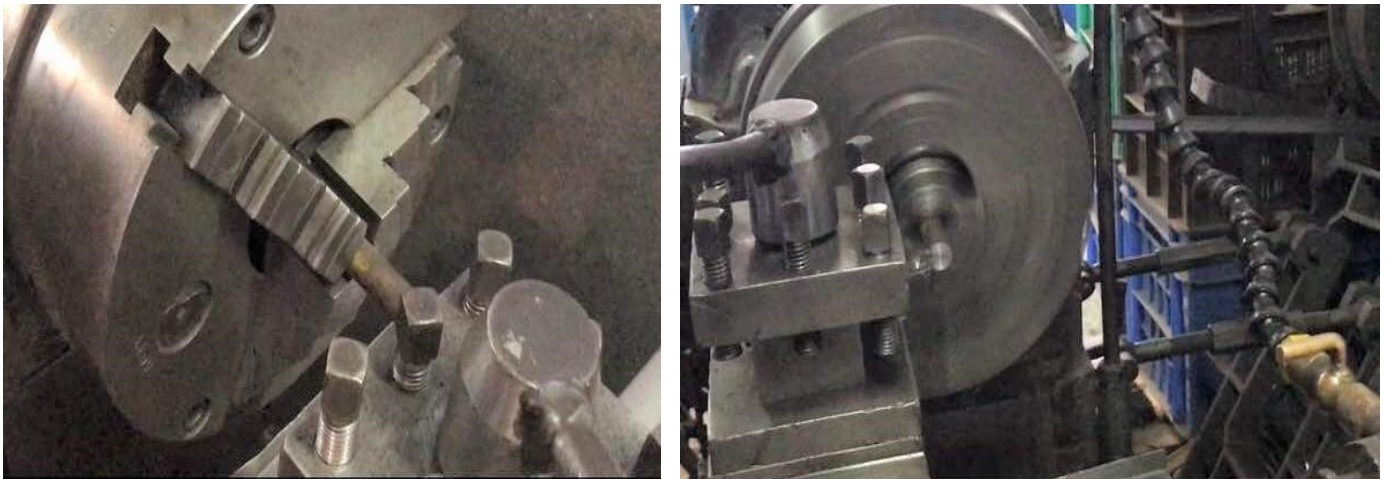**Figure 27.** Comparative structural results of both approaches.

Figure 28. A distinctive view of test specimen preparation of steel alloys.

A complete test specimen is shown in Figure 29, wherein the length and diameter were measured as 33 mm and 8 mm, respectively, for Steel EN-19. Also, the length and diameter were measured as 35 mm and 8 mm, respectively, for Steel EN-24.

Figure 29. A typical top view of steel specimen end-products.

2.8.2. Development of CCMC

Compression molding uses a preheated, open mold chamber. All parts of the mold are then sealed with a pressure-applied top plate. Heat and pressure are maintained until the material cures. Fibers are encased in thermosetting polymers. Carbon fiber reinforcements can be high-volume, high-pressure molded. In compression molding, heated components generate semi-finished parts. It converts powdered material under high pressure and temperature. Non-melting powdered particles form a dense, solid framework [11]. These sectors produce high-quality parts efficiently and precisely, reducing manufacturing time. Table 2 details the manufacturing process and the details of the CCMC-based test specimen.

Table 2. The basic details of CCMC.

Detail about Test Material				
Fiber Material	**Length (cm)**	**Width (cm)**	**Thickness (micron)**	**No of Layers**
Carbon fiber	12	7	0.6	15
Matrix material	Epoxy		**Hardener**	Silicon Carbide
Quantity	300 mL		30 mL	15 g
Apparatus Setup	**Temperature (°C)**			**Load (kg)**
Compression molding	150			40

Figure 30 shows the manufacturing processes involved in the preparation of composite test specimen.

Figure 30. Composite Compression Molding.

Figure 31 shows the carbon fiber end-product, which will be further modified and fine tuned as per the ASTM standard, in which the used fiber is Carbon Woven—230 GPa—Wet.

2.8.3. Experimental Test and Results—Pin on Disc Frictional Testing

The material's coat faded away due to interaction with another. Easy-to-setup pin-on-disc wear tests were utilized in labs. Pin-on-disc tribometer measured the specimen's wear. A disc tribometer loaded a "pin" in contact with a spinning disc. Spherical tip pins are the most common. The coefficient of friction relates frictional force to pin loading force. The wear rate can be calculated from the specimen's weight before and after testing. The pin-on-disc tribometer material wear depends on applied force, sliding speed, and sliding distance. The specimen has a pin-sized wear track. The pin should be harder than the sample. Figure 32 depicts the typical components and test set-up for experimental testing of three shortlisted test specimens. The experiments were carried out, and thereby, outcomes were observed. For the 600 RPM case, the run time was kept as 5 min, whereas for the 800 RPM case, the run time was kept as 3 min. Traditional measures of material wear are weight loss and wear rate. The wear coefficient is more accurate since it considers the wear rate, applied force, and pin hardness.

Figure 31. A typical top view of CCMC test specimen before final development.

Figure 32. A typical view of another pin on disc experiment with test specimen.

The graphical representation of wear rate versus time for 600 and 800 RPM, respectively, is shown in Figures 33 and 34. In this diagram, the variation in carbon ceramic composite is shown by the brown color, the variation in steel EN 19 is shown by the blue color, and the variation in steel EN 24 is shown by the dark green color. The frictional force

versus time graph for 600 and 800 RPM is shown in Figures 35 and 36, respectively. The graphical variation of the friction coefficient versus time for 600 and 800 RPM, respectively, is shown in Figures 37 and 38.
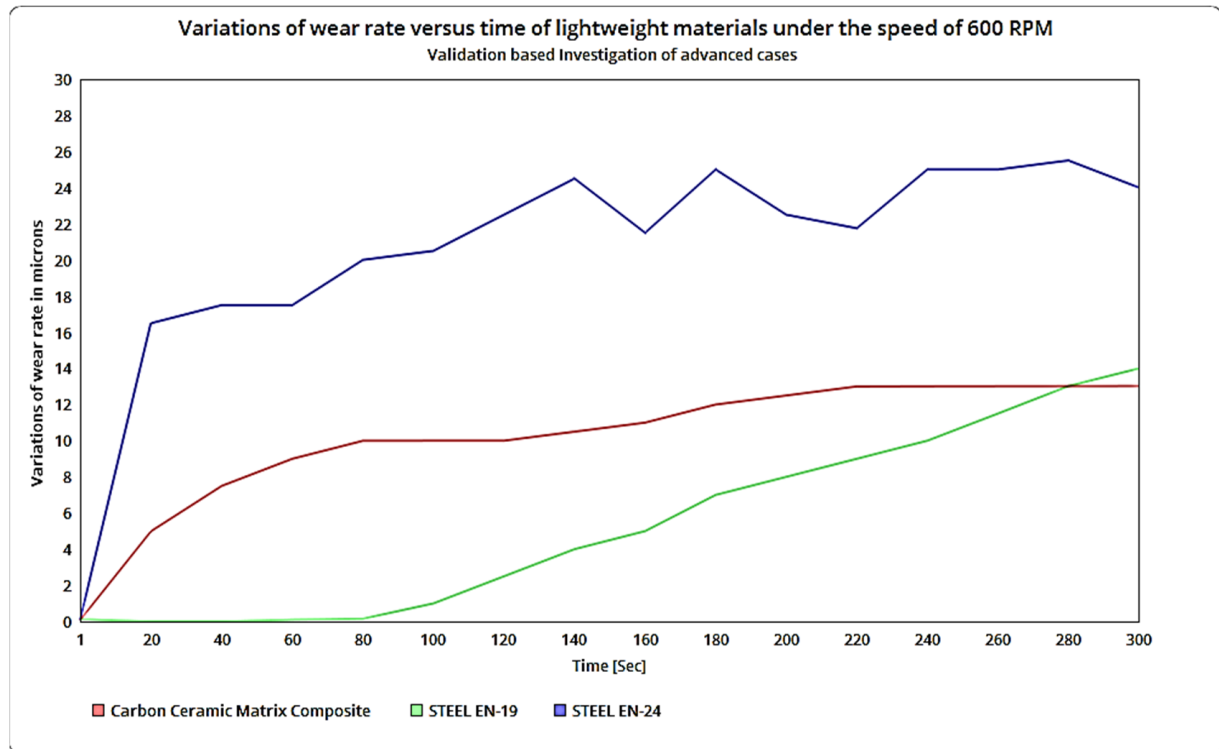

Figure 33. Variations of wear rate versus time of lightweight materials under the speed of 600 RPM.
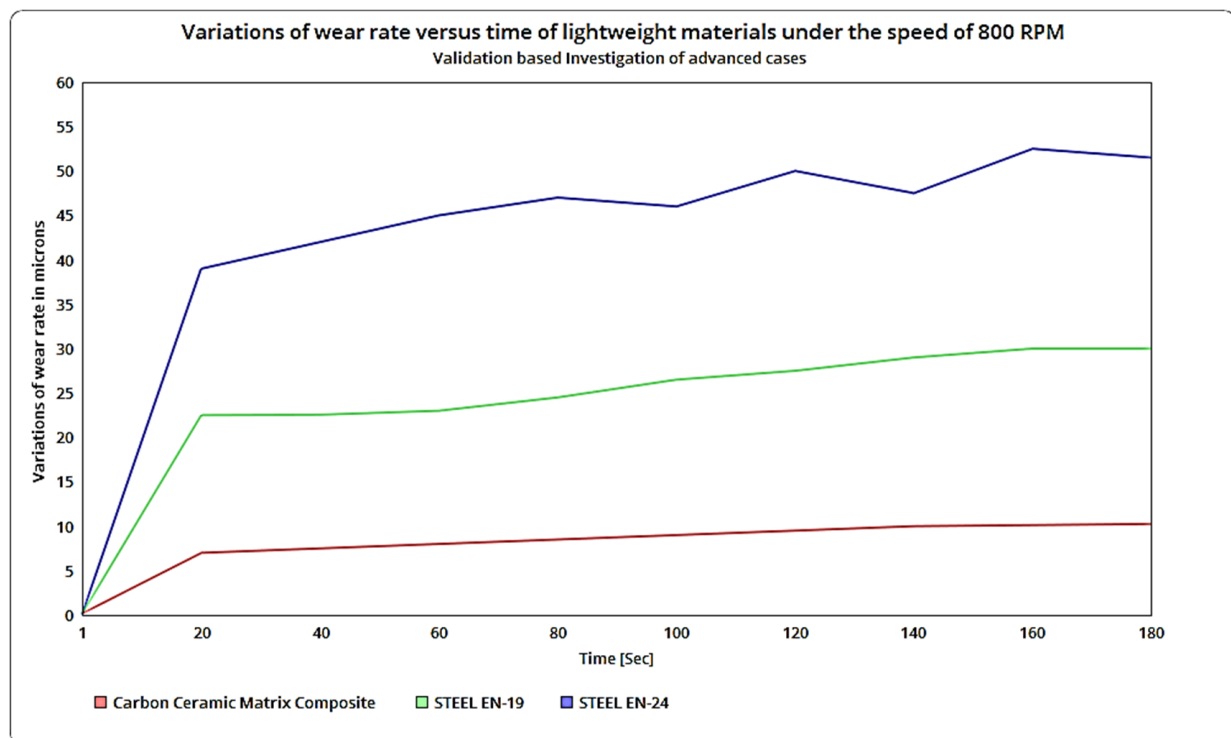

Figure 34. Variations of wear rate versus time of lightweight materials under the speed of 800 RPM.
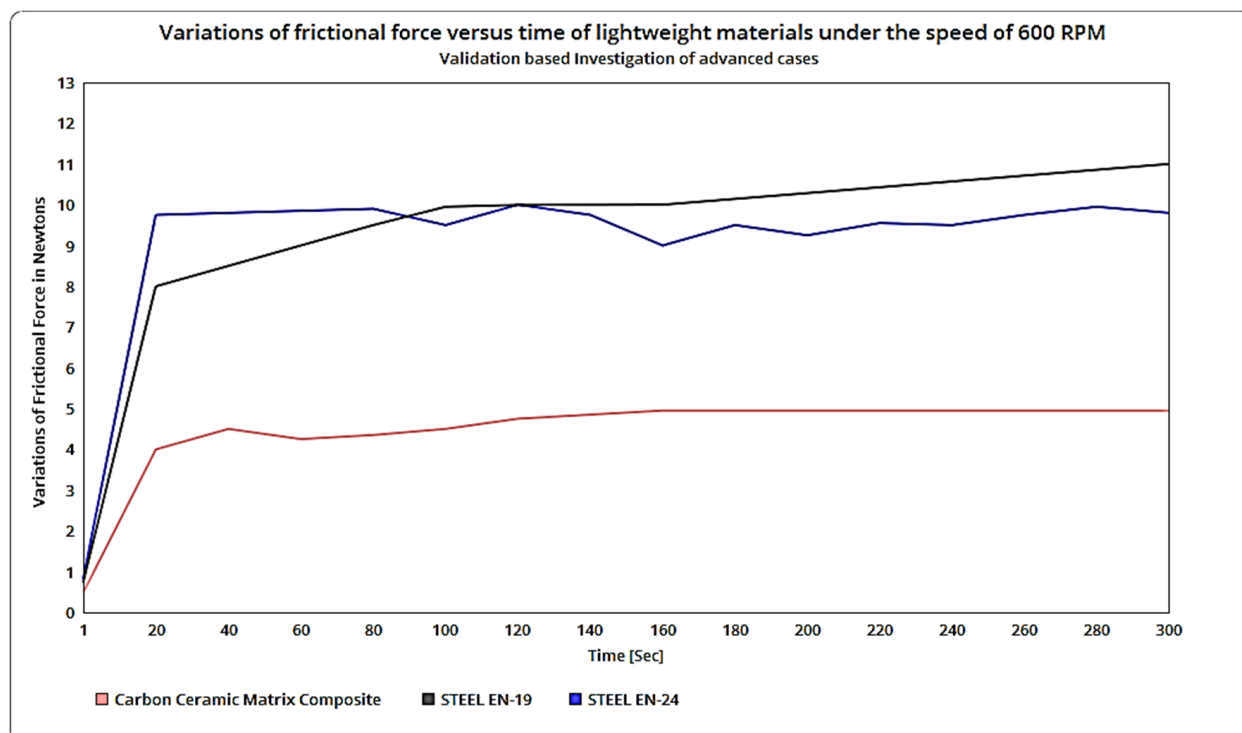
Figure 35. Variations of reaction force versus time of lightweight materials under the speed of 600 RPM.
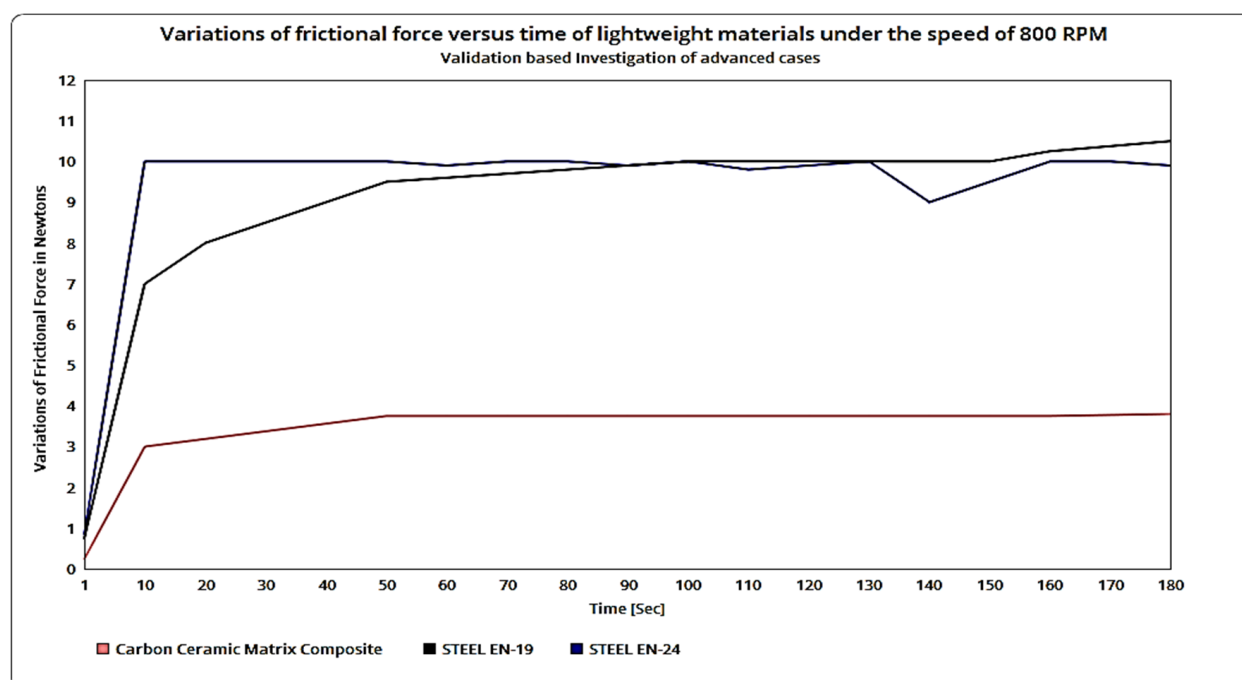

Figure 36. Variations of reaction force versus time of lightweight materials under the speed of 800 RPM.
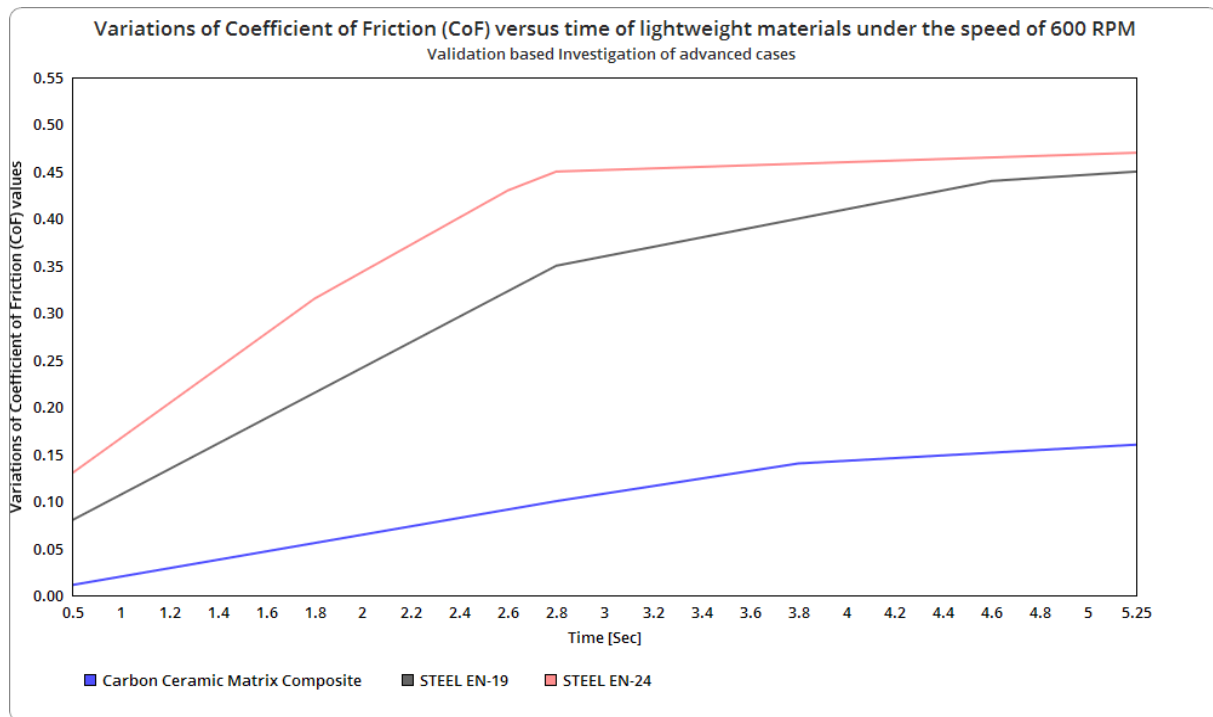
Figure 37. Variations of CoF versus time of lightweight materials under the speed of 600 RPM.
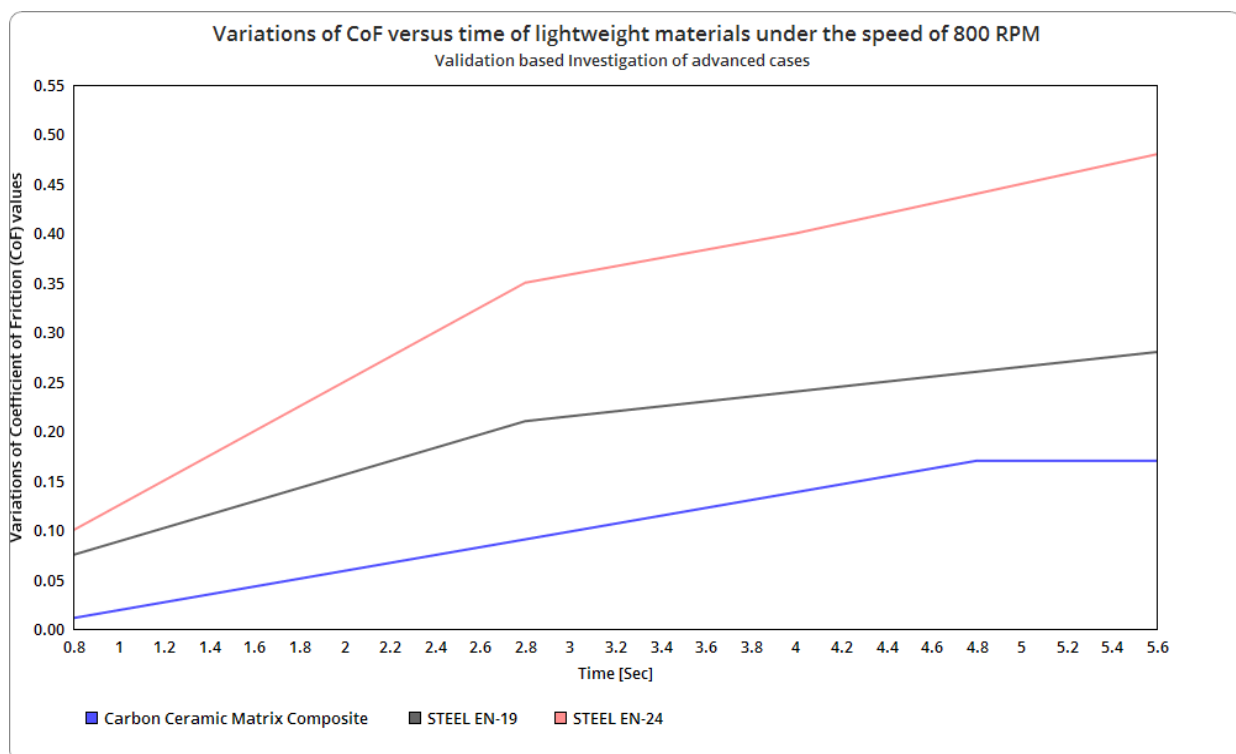

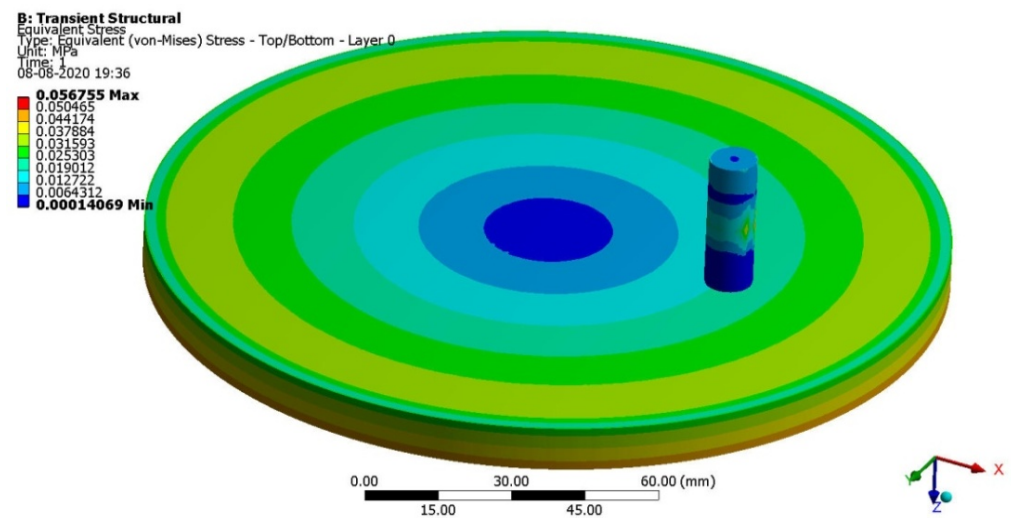**Figure 38.** Variations of CoF versus time of lightweight materials under the speed of 800 RPM.
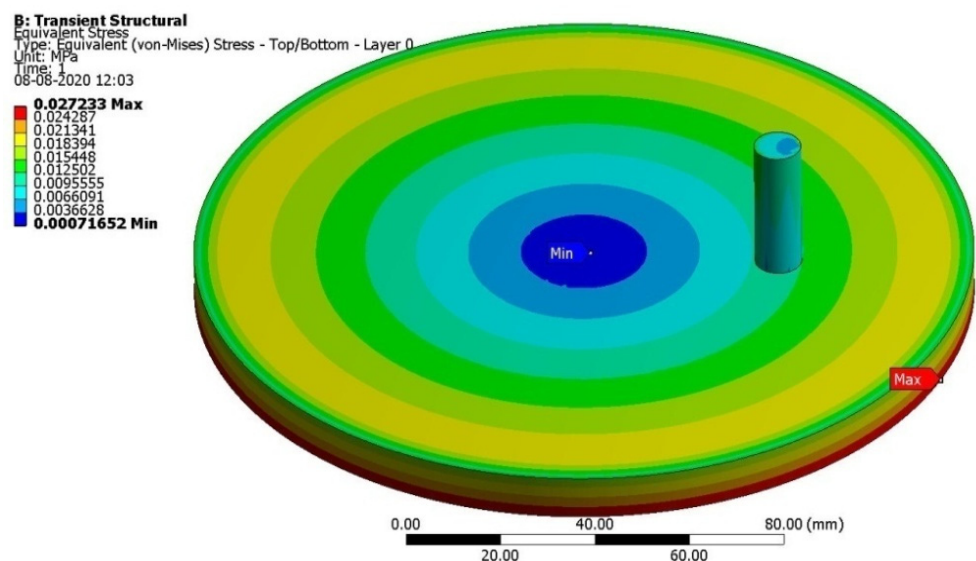
The complicated tests are executed with the help of pin on disc experiment and the entire results are listed in Table 3. From Table 3, the CCMC is picked as best performer based on its positive outcomes. Also, all of the experimental outcomes listed in Table 3 are imposed as initial conditions for computational simulations.

Sl. No.	RPM	Experimental Tastings Results	Steel EN19	Steel EN24	CCMC
1		Wear rate (Microns)	13	25	12
2	600	Frictional force (N)	10.5	9.5	3.5
3		Co-efficient of Friction	0.43	0.45	0.15
4		Wear rate (Microns)	29	54	9
5	800	Frictional Force	11	10	3
6		Co-efficient of Friction	0.28	0.48	0.17

2.8.4. Computational Structural Analyses for Validation

For the given co-efficient of friction, wear rate, the frictional force acting on the test specimen is obtained, which are isometrically reveals in Figures 39–41 and the data are compared with the pin on disc experimental results in Table 4.

Figure 39. Stress variations on the pin on disc CCMC's test specimen under 800 RPM.

Figure 40. Stress variations on the pin on disc Steel EN-19′s test specimen under 600 RPM.
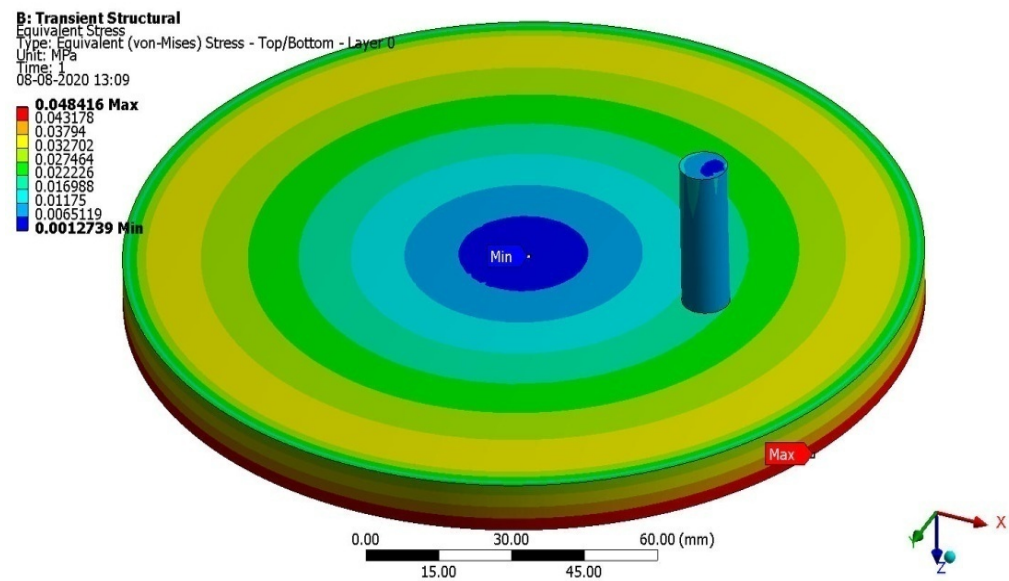
Figure 41. Stress variations on the pin on disc Steel EN-24's test specimen under 800 RPM.

Table 4. Comparative results of experimental and transient structural results.

Sl. No	RPM	Materials Name	Experimental Results (N)	FEA Results (N)	Error %
1		Steel EN19	10.5	9.7906	6.76
2	600	Steel EN24	9.5	9.7949	3.01
3		CCMC	3.5	3.2542	7.02
1		Steel EN19	11	10.034	8.78
2	800	Steel EN24	10.5	10.04	4.38
3		CCMC	2.75	2.5265	8.13

Similar to the base case, the advanced case also obtained acceptable error percentages between experimental outcomes and computational outcomes. Thus, through base and advanced validation cases, the computational procedures were validated and thereafter extended for real-time applications.

3. Real Time Applications and Its Results

After validation, the same computational approach was used for an aircraft disc brake and an automotive disc brake. These two disc brakes have different functioning conditions and designs. First, the aircraft disc brake was employed at 600 RPM, the average working speed of various aircraft. In pre-processing, the frictional coefficient [0.15] was estimated. This application uses the same computational technique and captures the results. The reference model was modified based on existing designs. This paper's brake disc was built using CATIA's easy modeling approach. The design is first sketched. Outer and inner diameters were measured. The sketch was then extruded into a 3-D object. The solid is then slotted. This is then patterned around the solid and extruded to generate heat-dissipating grooves. Next, four disc brake hubs were designed. The hubs were extruded to the desired thickness and patterned around the disc. The fit-to-spline procedure was used to add grooves to the inner disc brake. This was patterned and extruded to make the disc brake rotor.

3.1. Aircraft Disc Brake

3.1.1. Computational Model

In the modeling phase of the aircraft disc brake, complicated components like calipers, smooth pins, and brake pads were provided so that CATIA could complete the conceptual design. Figure 42 shows a CATIA-modeled 3-D aircraft disc brake. Table 5 lists all design parameters.
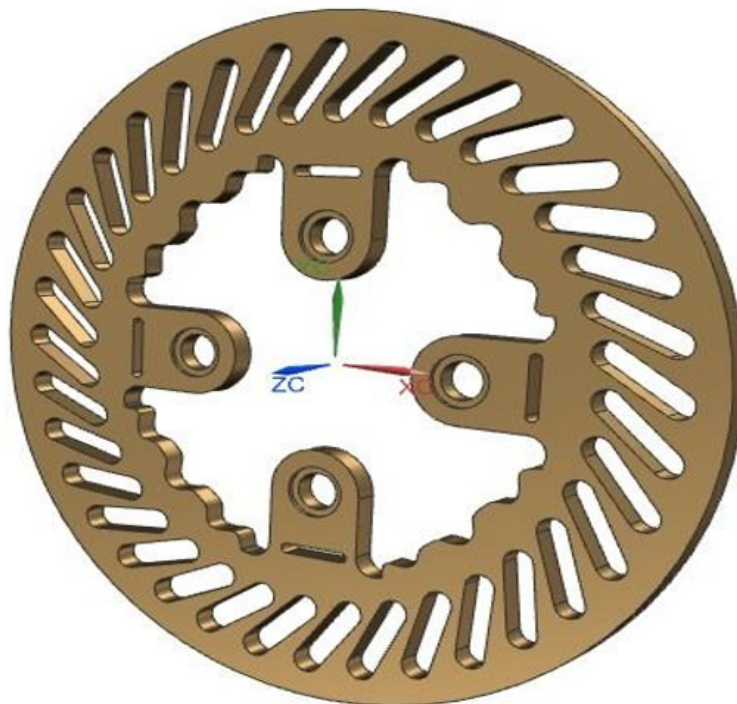

Figure 42. A systematic view of the 3-D model of the aircraft disc brake.

Table 5. Design parameters of aircraft disc brake.

Size (mm)	Design Parameters	Size (mm)	Design Parameters
160	Total disc diameter	5	Disc brake thickness
160	Outer diameter	21	Slot length
100	Inner diameter	5	Wheel hub mount diameter

3.1.2. Materials Applied

Carbon-woven–wet, Steel EN19, and Steel EN24 were utilized for this aircraft disc brake. For a long service life, disc brake materials must have acceptable mechanical and electrical properties. Low wear rate, frictional force, high melting point, and anti-corrosive characteristics are criteria. Cost and mechanical qualities are also essential. Table 6 is comprises of all the needful properties of the imposed materials.

3.1.3. Finite Element Model

A computational structural analysis can predict a model's deformations, stresses, and strains given particular constraints. This work simulated pad materials such as CCMC, Steel EN19, and Steel EN24 using FEM software ANSYS Workbench for structural and thermal analysis. Finite element structural and non-structural problems commonly require boundary value difficulties for PDEs. The technique approximates unknown values at a few discrete locations in the domain. FEA's key component is discretization. The problem is broken into smaller, more manageable pieces, allowing for more precision and better

solutions. Figure 43 shows the results of a finite element study of an aviation disc brake with 0.7 mm elements and a 3-D tetrahedral configuration.

Table 6. Material properties comparison.

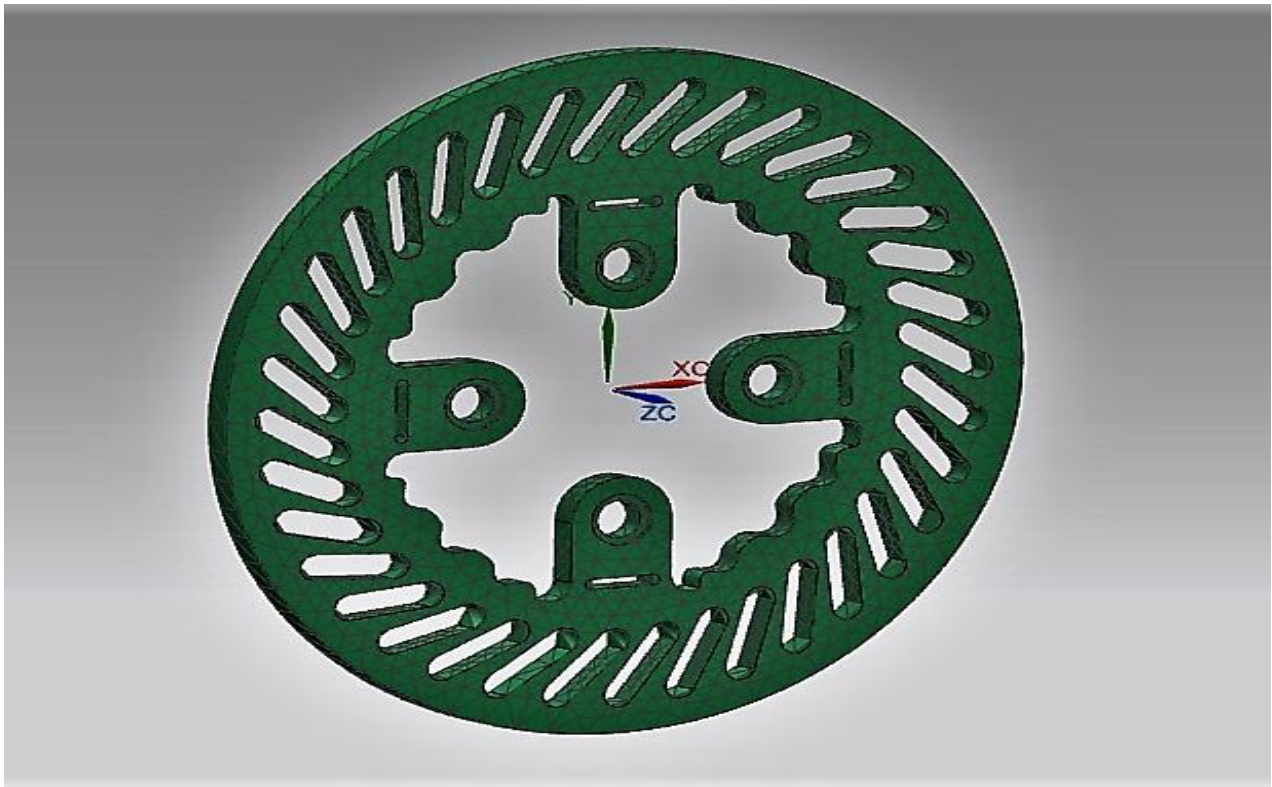| Material Properties	Steel EN 24	Steel EN 19	CCMC
Mass Density (kg/mm^3)	7.85×10^{-6}	7.81×10^{-6}	1.451×10^{-6}
Young's Modulus (kPa)	193,000	204,000	70,000
Yield Strength (kPa)	1,178,000	861,000	250,000
Ultimate Tensile Strength (kPa)	1,240,000	931,800	513,000
Poisson's Ratio	0.284	0.272	0.16
Thermal Expansion Co-efficient (/°C)	1.23×10^{-5}	1.17×10^{-5}	2.2×10^{-6}
Thermal Conductivity (K)	44,500	22,658	52,000
Specific Heat (micro J/kg·K)	4.75×10^8	4.2×10^8	5.1×10^8
Hardness (HB)	248–302	248–302	390–453

Figure 43. A typical view of the finite element model of the aircraft disc brake.

3.1.4. Boundary Conditions

Equation (1) was used to calculate the disc brake's rotating speed. The calculations require aircraft speed and wheel diameter. This work selected minimum, average, and maximum speeds [13]. Maximum speed was 288 mph (463.491 km/h). Minimum speed was 20 mph (32.1869 km/h). The reference diameter was 27 × 7.75R15, the size of Boeing 737 tires. From Equation (1), the rotational speed ranges were expected to be 25 to 3500 RPM, so the typical speeds are 600 to 800 RPM. Table 7 lists remaining boundary requirements.

$$k = 0.001885 \times d \times r \tag{1}$$

where "*k*" is kilometer per hour (km/h), "*d*" is wheel diameter (cm), and "*r*" is revolution per minute (RPM).

Sample Calculation—I:
$32.1869 = 0.001885 \times 68.58 \times RPM \Rightarrow RPM = 249$
Sample Calculation—II:
$273.5885 = 0.001885 \times 68.58 \times RPM \Rightarrow RPM = 2116.36$
Sample Calculation—III:
$463.491 = 0.001885 \times 68.58 \times RPM \Rightarrow RPM = 3585.36$

Table 7. Details of imposed boundary conditions.

Material	Steel EN19	Steel EN24	CCMC
Speeds	100 knots	100 knots	100 knots
	135 knots	135 knots	135 knots
RPMs	600	600	600
	800	800	800
Heat Flux (w/m^2)	1,666,667.485	1,666,667.485	1,666,667.485
	7,025,254.6	7,025,254.6	7,025,254.6
Angular Velocity (rad/s)	64.25	64.25	64.25
	86.7	86.7	86.7
Angular Acceleration (rad/s^2)	11	11	11
	20.06	20.06	20.06
Pressure (psi)	500	500	500
	500	500	500
Constraint	Fixed	Fixed	Fixed

3.1.5. CAE Results of Aircraft Disc Brake and Discussion—Structural Analysis

The development of deformation under the speed of 600 RPM for three different materials, namely steel EN 19, steel EN 24, and carbon fiber, were computed with the help of aforesaid boundary conditions. After the simulations, the results were noted carefully in order to capture the physics involved in the structural behavior on the aircraft disc brake, in which the maximum deflection of steel EN 19 was 0.70642 mm; in Steel EN 24, the maximum deflection was 0.79673 mm, and in the case of carbon fiber, the maximum deflection was 0.1151 mm. In all cases, the maximum deflection occurred at the outer boundary of the aircraft disc brake for the given 600 RPM. The deformation plots of 800 RPM for three different materials, namely steel EN 19, steel EN 24, and carbon fiber, were plotted for the given fixed boundary condition at the inner part. Figures 44 and 45 represent the deformation variation of the aircraft disc brake for Steel EN 24 and CCMC with speeds of 600 RPM and 800 RPM, respectively.

From the deformation results, we came to know that the carbon fiber material has a high stiffness–weight ratio compared to other materials. The stiffness–weight ratio plays a vital role in aerospace industry; hence, carbon fiber is a very suitable material for disc brakes for the aerospace industry. After the successful completion of the deformation study, stress variations on the disc brake were also executed for the different boundary conditions. After deformation, the equivalent stresses of all the foresaid materials were computed for the developed aircraft disc brake; the results are revealed in Figures 46 and 47. Figure 46 comprises of equivalent stress variations of Steel EN 19 with a rotating speed of 600 RPM, and Figure 47 comprises of equivalent stress variations of CCMC with a rotating speed of 800 RPM.
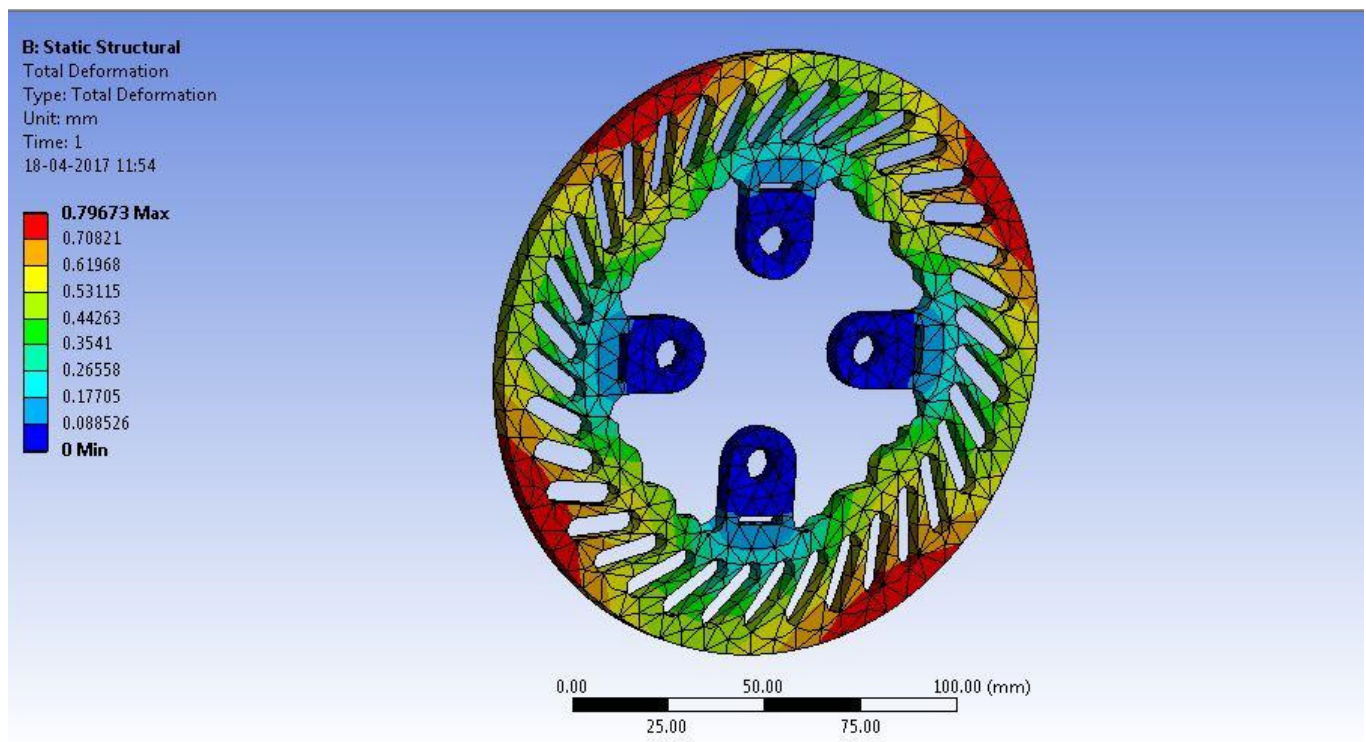
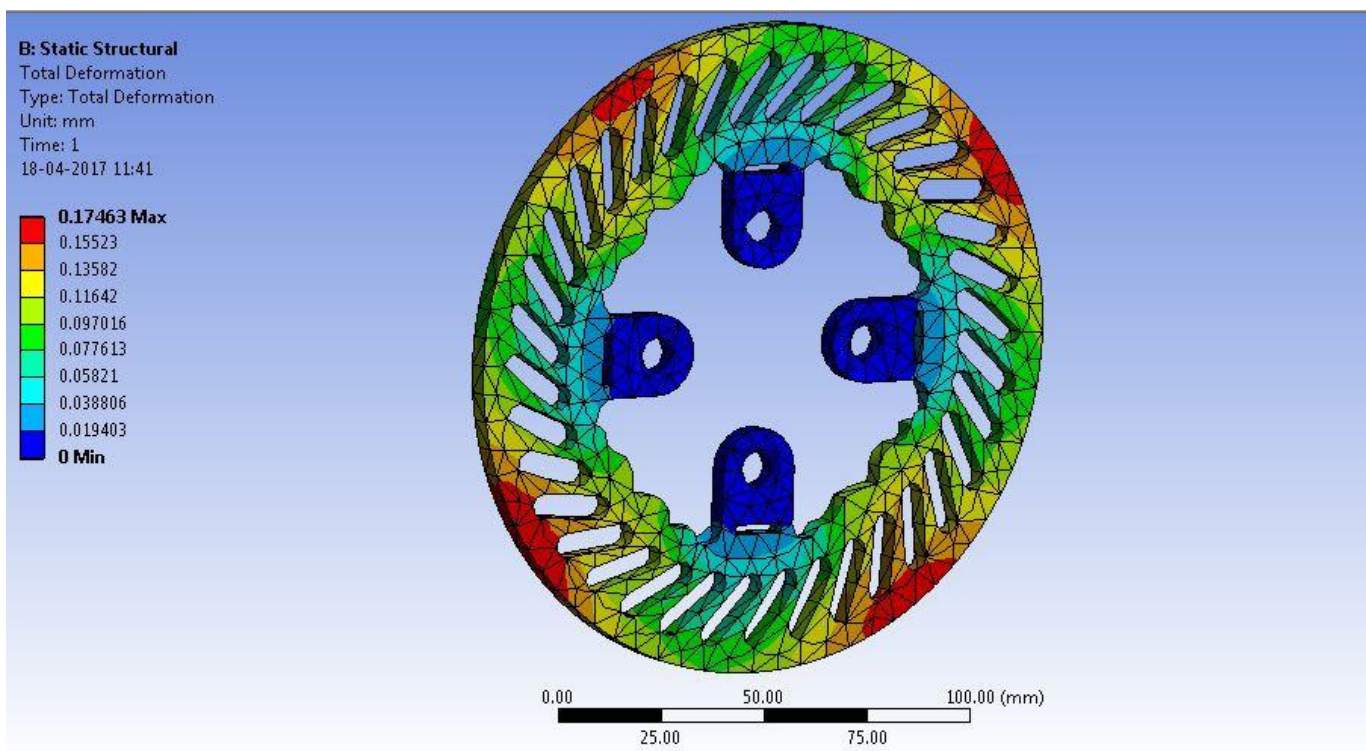**Figure 44.** A typical representation of deformed structure of Steel EN 24 under 600 RPM.

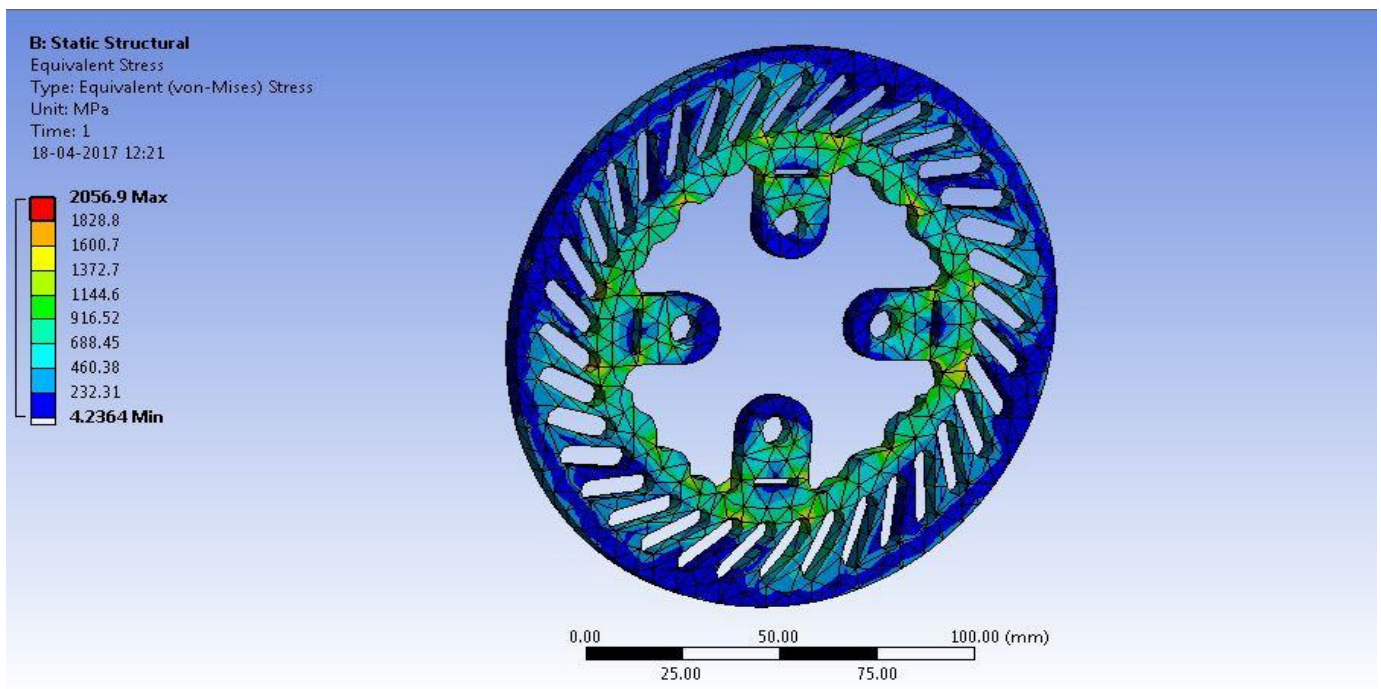**Figure 45.** A typical representation of deformed structure of CCMC under 800 RPM.

Figure 46. A systematic projection of equivalent stress variations of Steel EN 19 under 600 RPM.
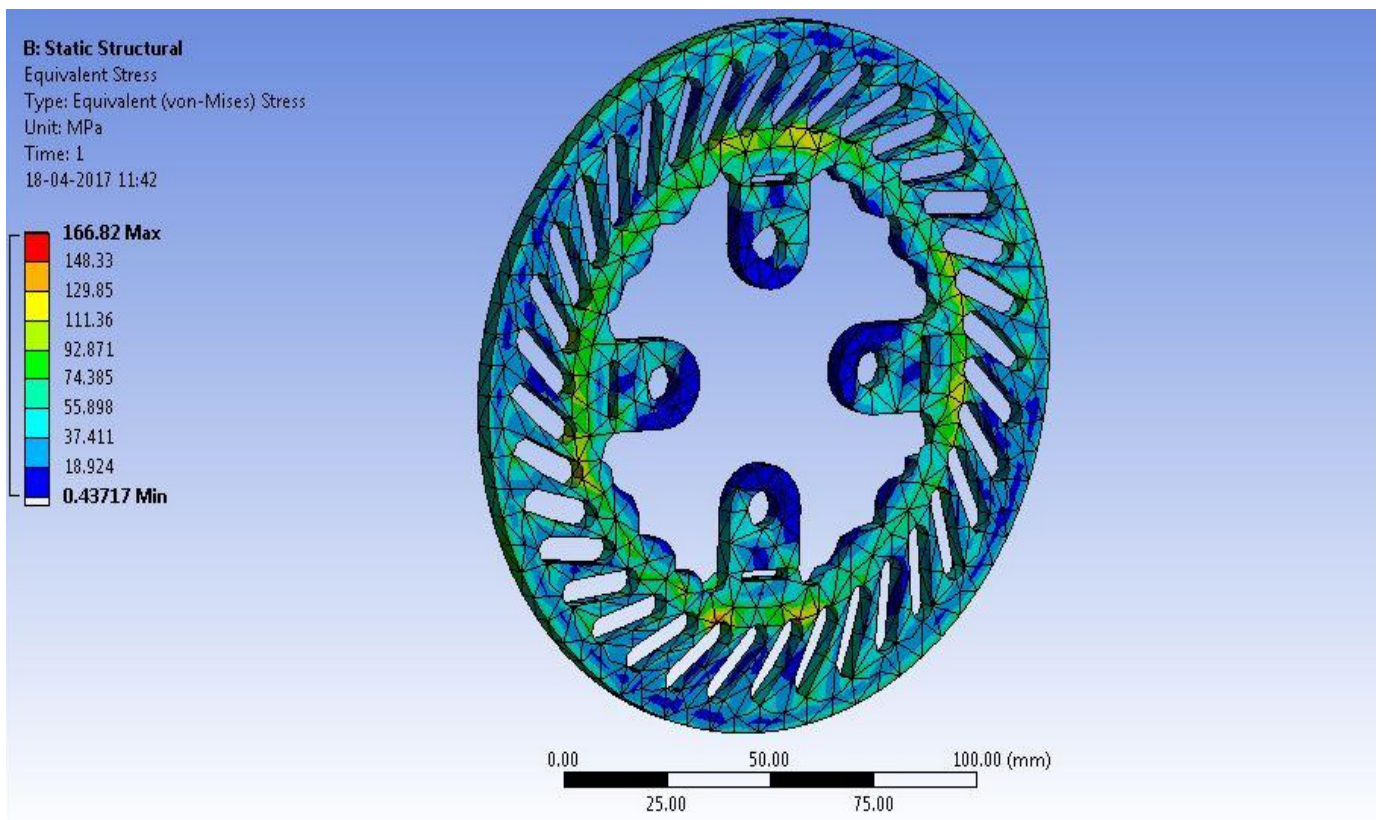

Figure 47. A systematic projection of equivalent stress variations of CCMC under 800 RPM.

The induced resisting force with respect to stress, the location of maximum and minimum stress on the disc brake, strain energy variation along the object, and stress reduction techniques are important takeaways from this structural simulation. From the mechanical stress plots, it was understood that the maximum stress occurred at the inner

region of the disc brake due to reaction force, in which the maximum stress value of 2056.9 MPa had been induced in the Steel EN19, and the low value of resisting force had been induced in the CCMC (100.06 MPa) for the given same boundary conditions. From the mechanical stress results, we learned that carbon fiber material has high load-withstanding capability compared to the other materials. The stress induced in the steel EN 19 and EN 24 was approximately 20 times greater than the stress induced in the carbon fiber for the applied boundary conditions of RPM and structural displacement. In the aerospace industry, the major issue is impact load due to gust, which has been solved with the help of safety consideration factors. Similarly, in this case, the safety factor was also included in the selection phase for an aircraft disc brake's material. The safety factor value of carbon fiber is 20 times that of other steel alloys, hence it is capable to withstand any impact load while subject to critical environments.

3.1.6. CAE Results of Aircraft Disc Brake and Discussion—Thermal Analysis

In this paper, heat transfer plays a predominant role in determining the lifetime of aircraft disc brakes. The same three different materials are analyzed for the given boundary conditions, such as rpm, structural displacement, and temperature. In general, thermal analysis is used to calculate the heat flux, temperature gradient, and temperature variation on the respective object. Figures 48 and 49 are showing the important results of thermal analysis under the various velocities of 600 RPM and 800 RPM, respectively. Also, Figure 48 corresponds to CCMC, and Figure 49 corresponds to Steel EN 24. From the temperature nodal distribution plot, it has been observed that carbon fiber has linear temperature variation along its body; also, its thermal withstanding capability is quite high compared to other materials.
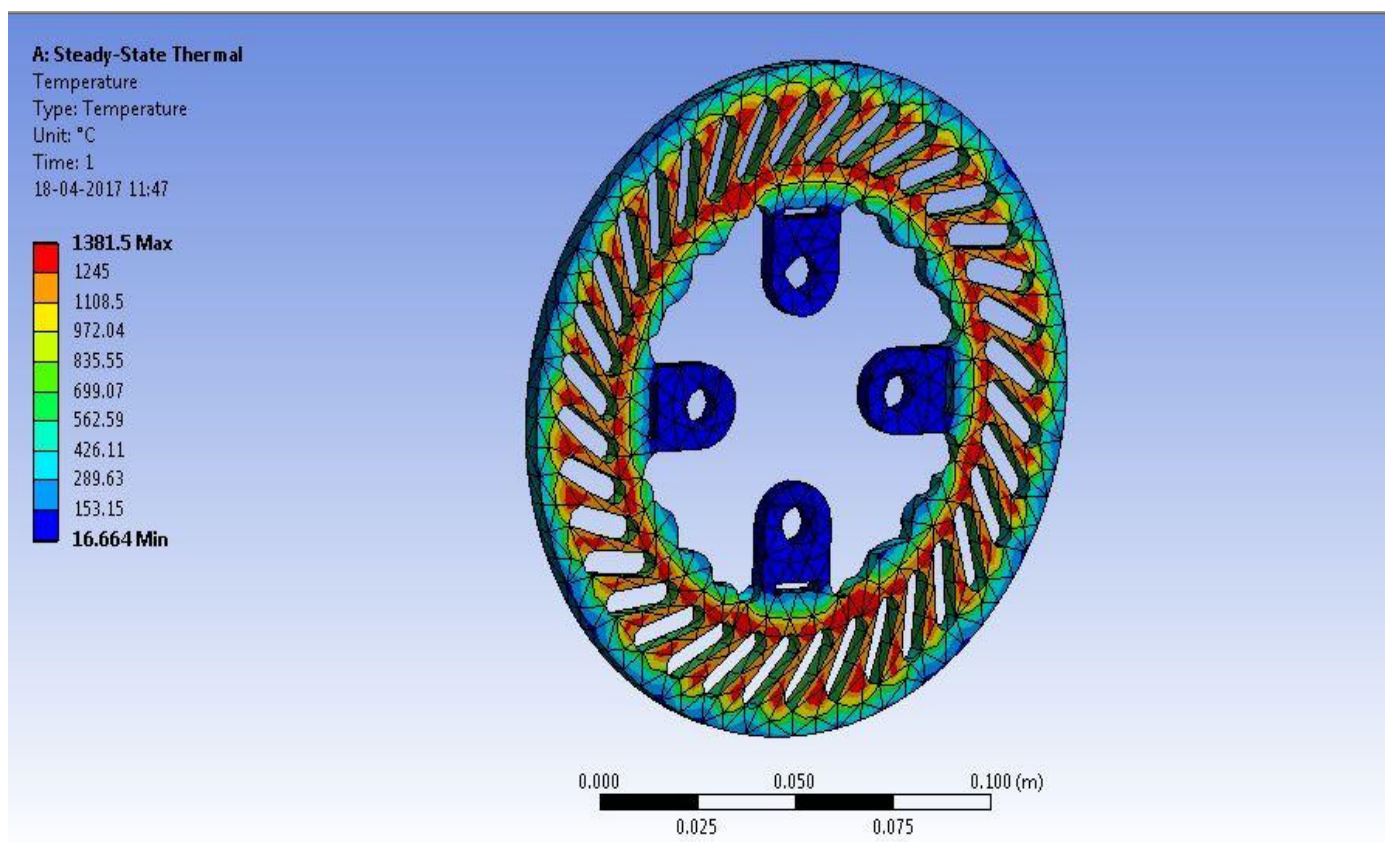

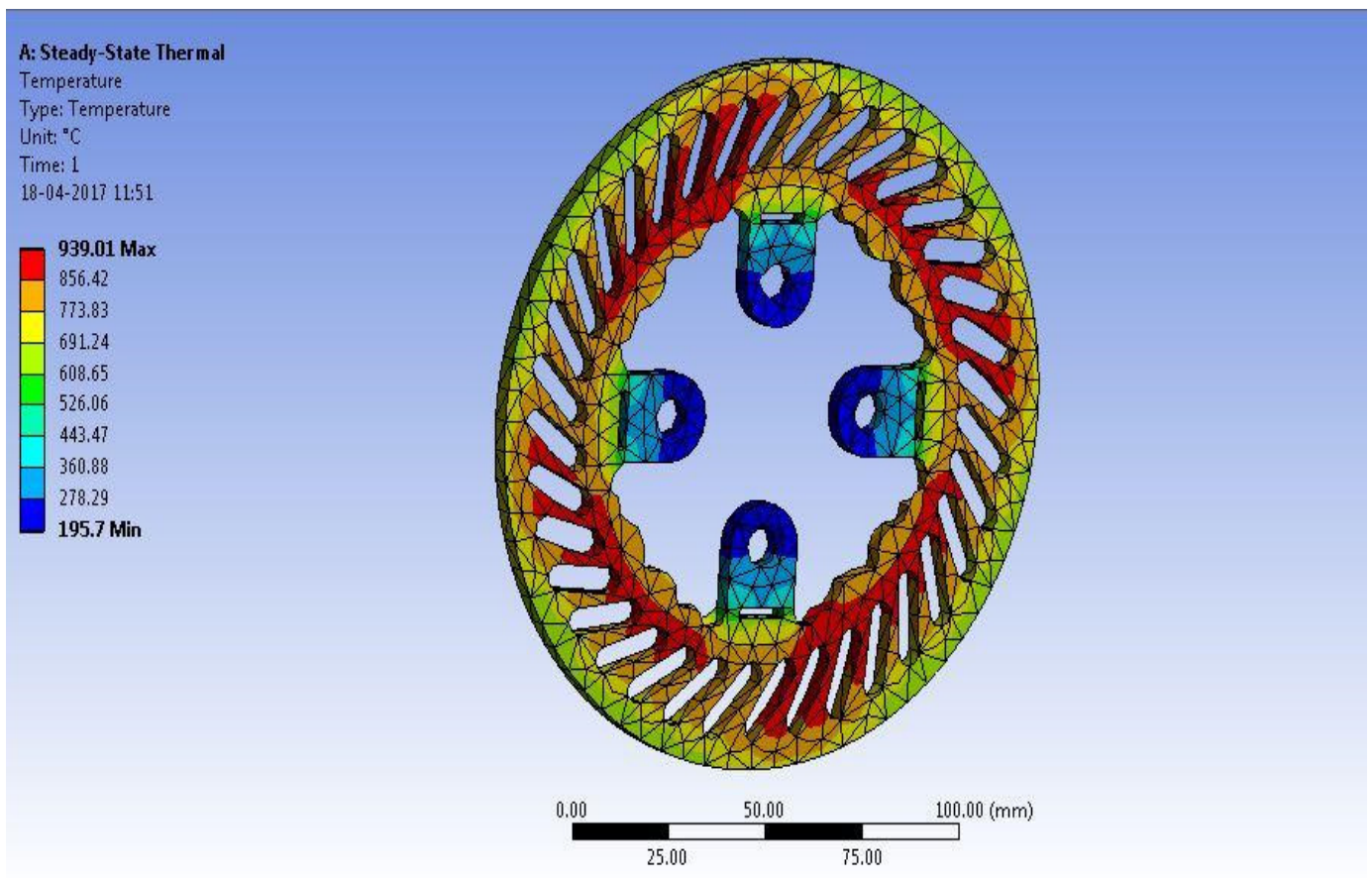**Figure 48.** A characteristic depiction of temperature distributions of CCMC under 600 RPM.

Figure 49. A characteristic depiction of temperature distributions of Steel EN 24 under 800 RPM.

3.1.7. Comparative Analysis of All CAE Structural Cases

Comparative studies of typical structural parameters for 600 and 800 RPMs were carried out; the values are shown through comprehensive representation in Figures 50–55.
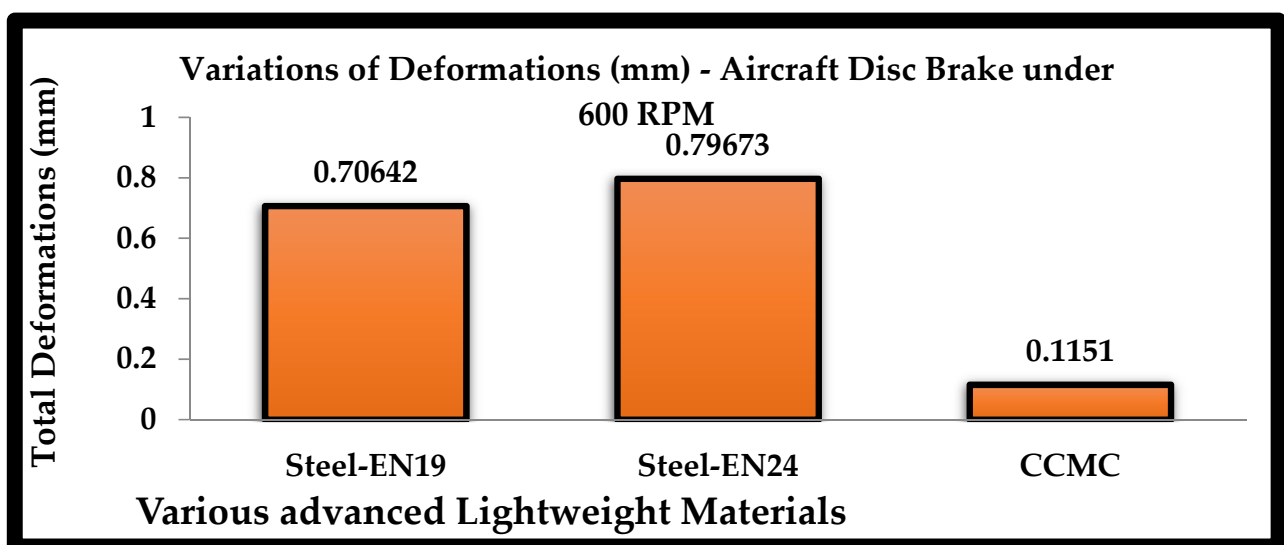

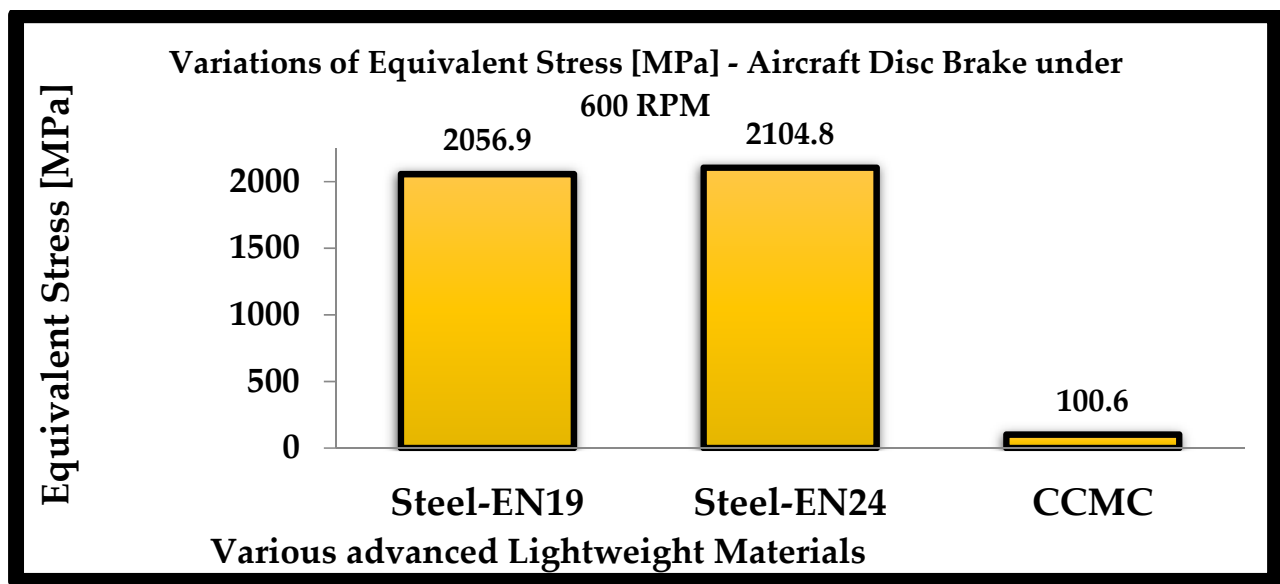**Figure 50.** Comparative results of total deformations—600 RPM.

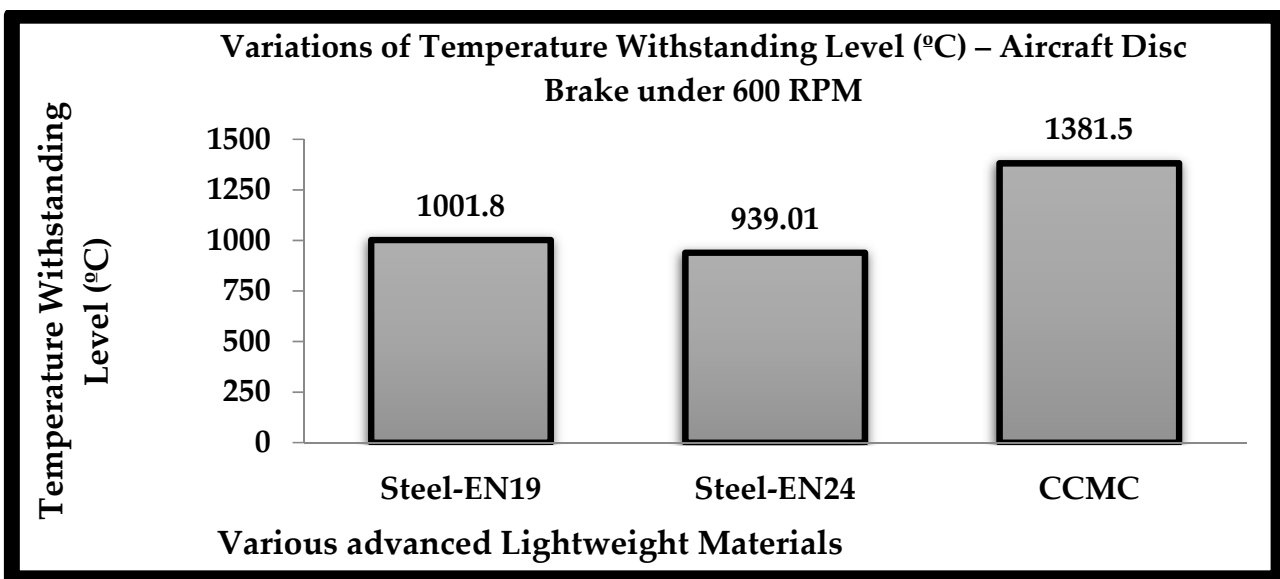**Figure 51.** Comprehensive equivalent stress results—600 RPM.

Figure 52. Comparative outcomes of thermal withstanding rate—600 RPM.

Based on the comprehensive investigations and Figures 50–55, it can be observed that the carbon ceramic matrix demonstrated better wear resistance and temperature capability than the other materials [14].

3.2. Automotive Disc Brake

The primary mechanism that can be used to slow or stop a moving vehicle is the braking system. As automobile technology developed, the drum brake was made available. Drum brakes are a straightforward system. The effective function, which is the brake shoe pressure or force supplied to the drum, stops the rotational moment of the drum. The next improvement in the braking mechanism was the use of disc brakes. The brake caliper is where the stationary brake pad components and disc brake rotors make contact. This work examined shear stress analysis over a disc brake. To overcome the technological challenges, all possible economic technologies should be applied, and experimental research

should be closely supervised. The aerospace and automotive sectors concurrently place many components under mechanical and thermal pressures. High stresses can result in deformation and possibly system collapse. This study's main objective was to collect information on the shear force that discs constructed of pertinent materials encounter. The brake system was designed using CATIA software (Figure 56), and it was simulated using ANSYS structural tool. The meshed model is revealed in Figure 57. Comparative studies have been done on stainless steel, titanium alloy, tungsten carbide, GFRP, and CFRP. In Figures 58–60, the example computational outcomes are displayed [44–50].
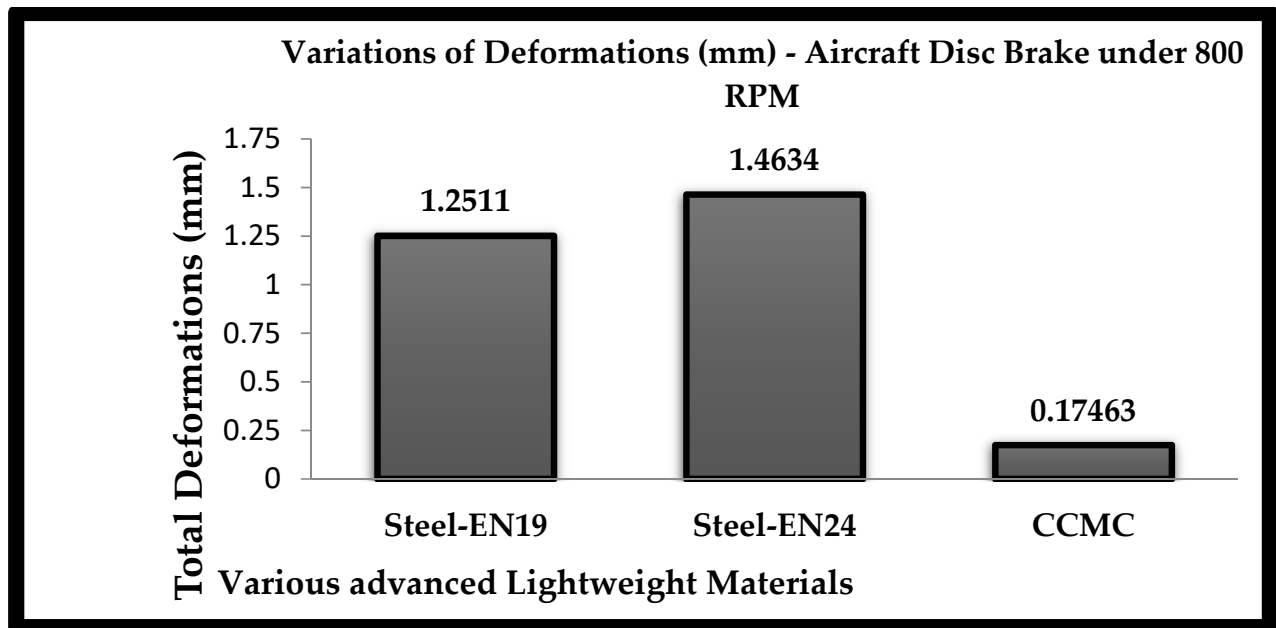

Figure 53. Comprehensive deformed outcomes of aircraft disc brakes under the speed of 800 RPM.
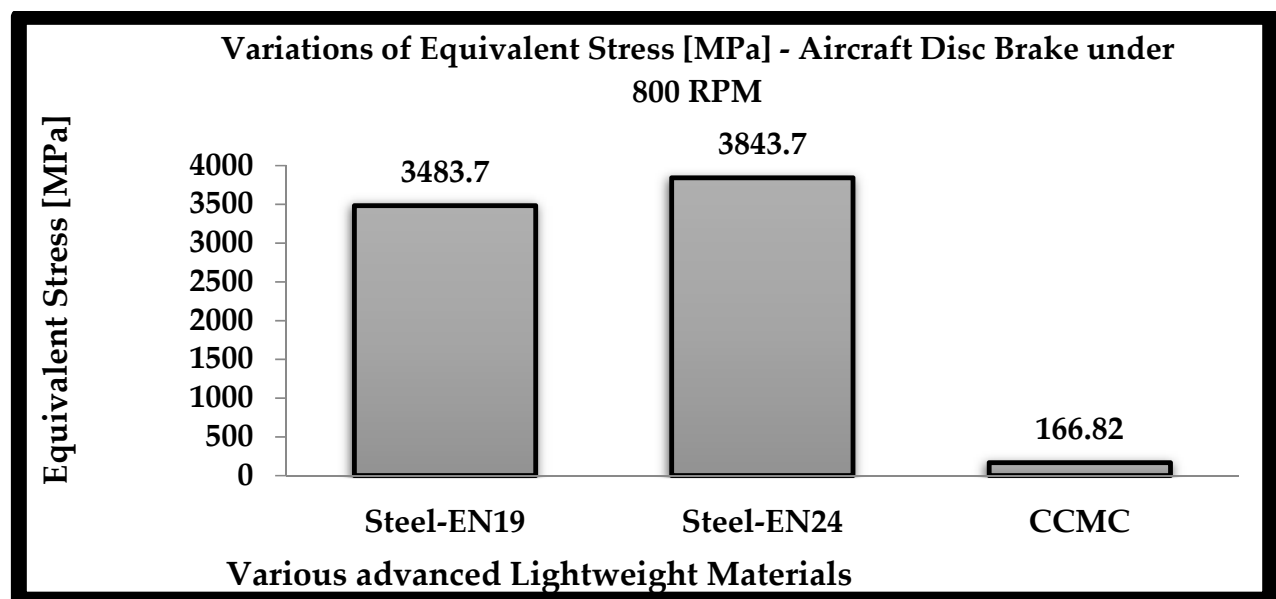

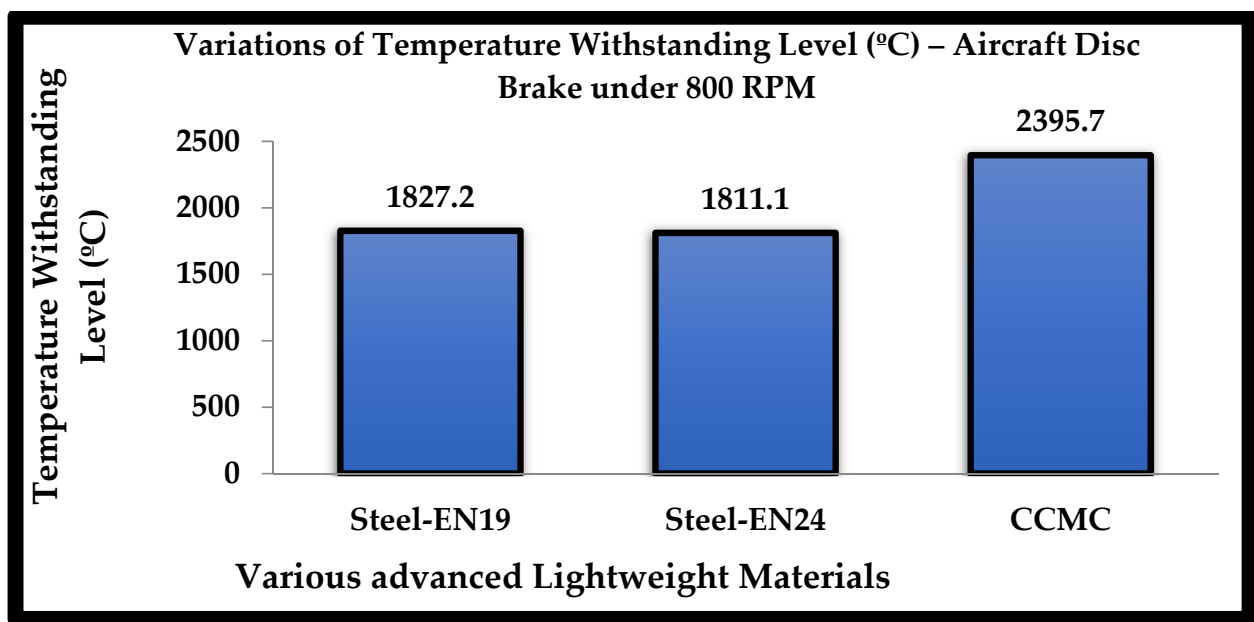**Figure 54.** Comprehensive outcome of equivalent stress of aircraft disc brakes under 800 RPM.

Figure 55. Comprehensive thermal resisting rate of various lightweight materials under 800 RPM.
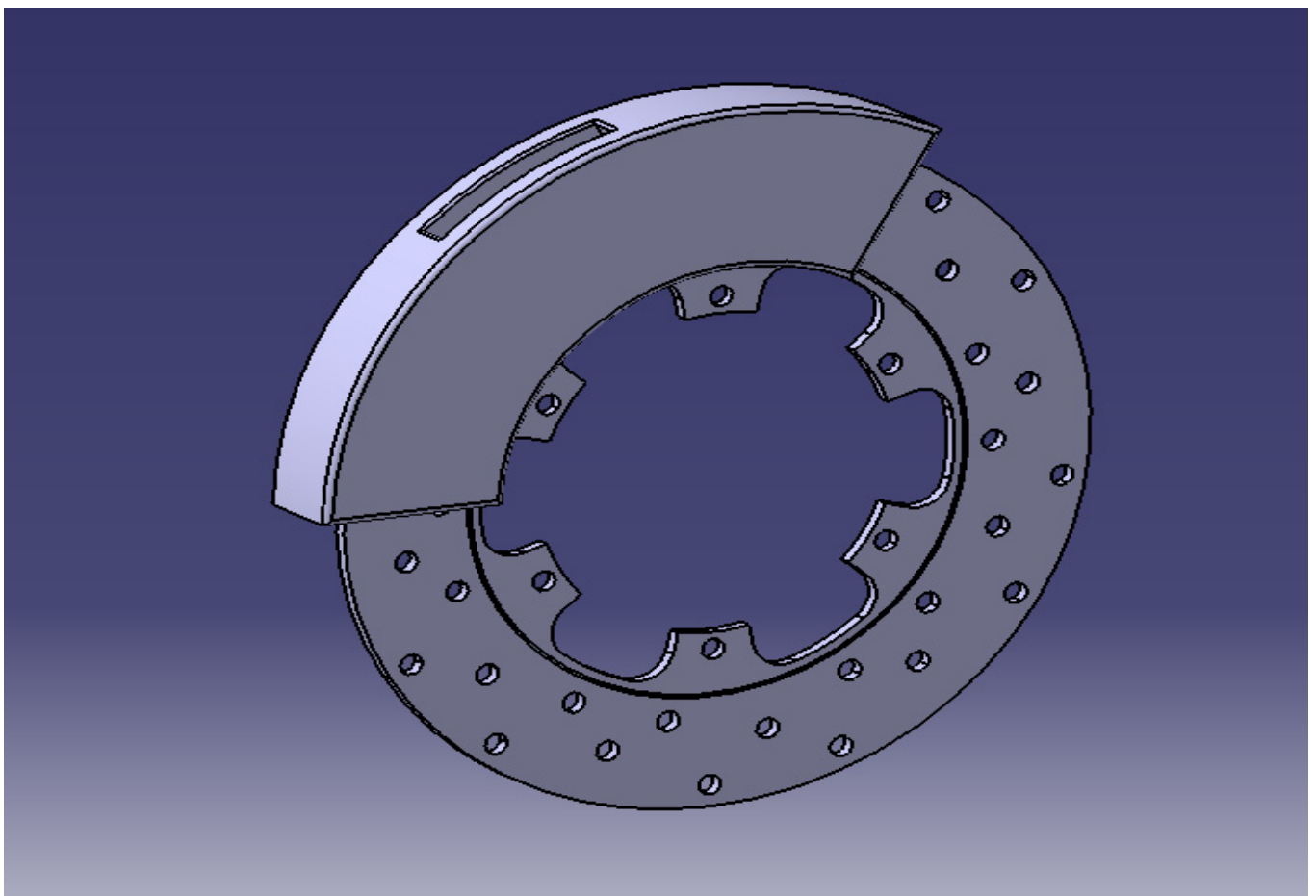

Figure 56. A typical isometric view of a developed automotive disc brake.
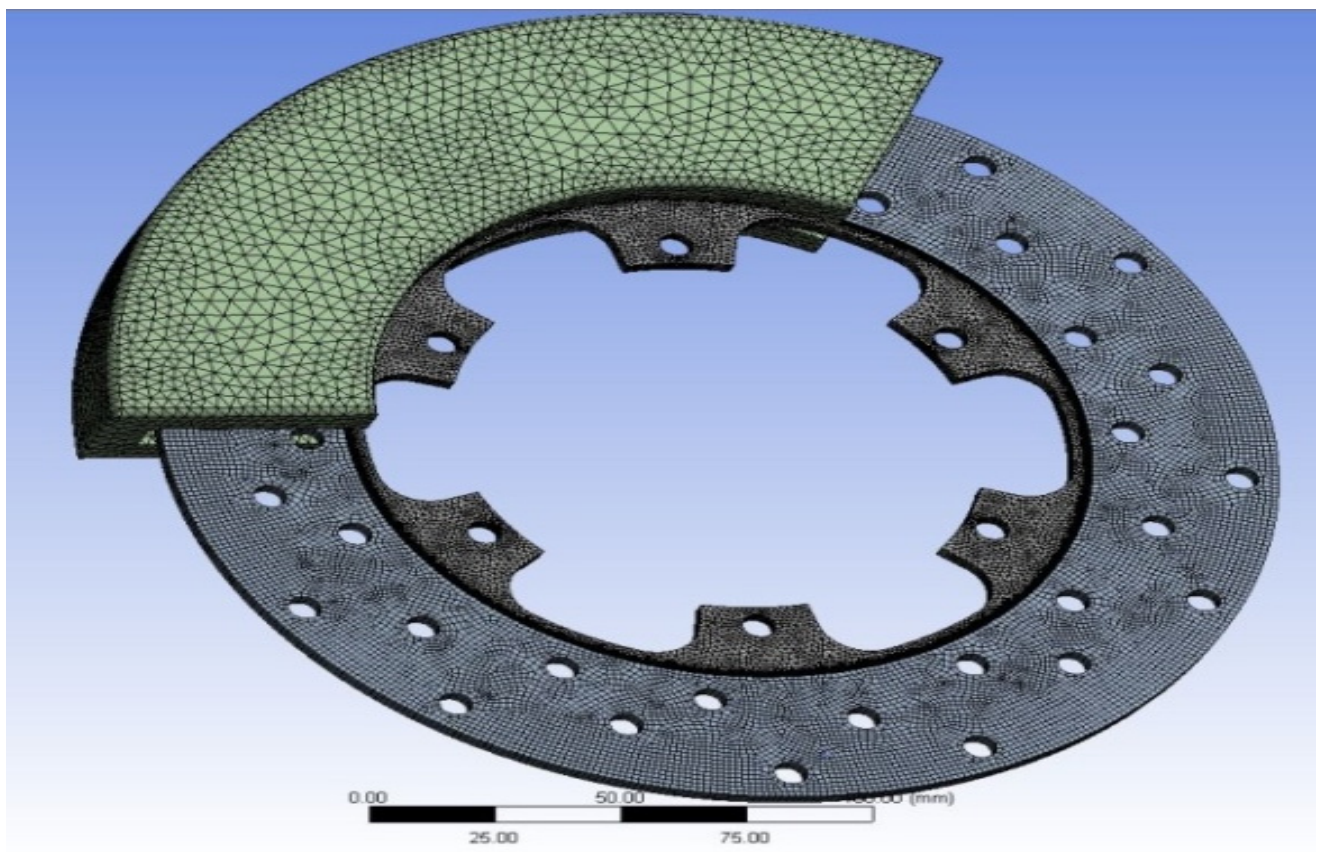
Figure 57. Discretized structure of two-wheeler disc brake.
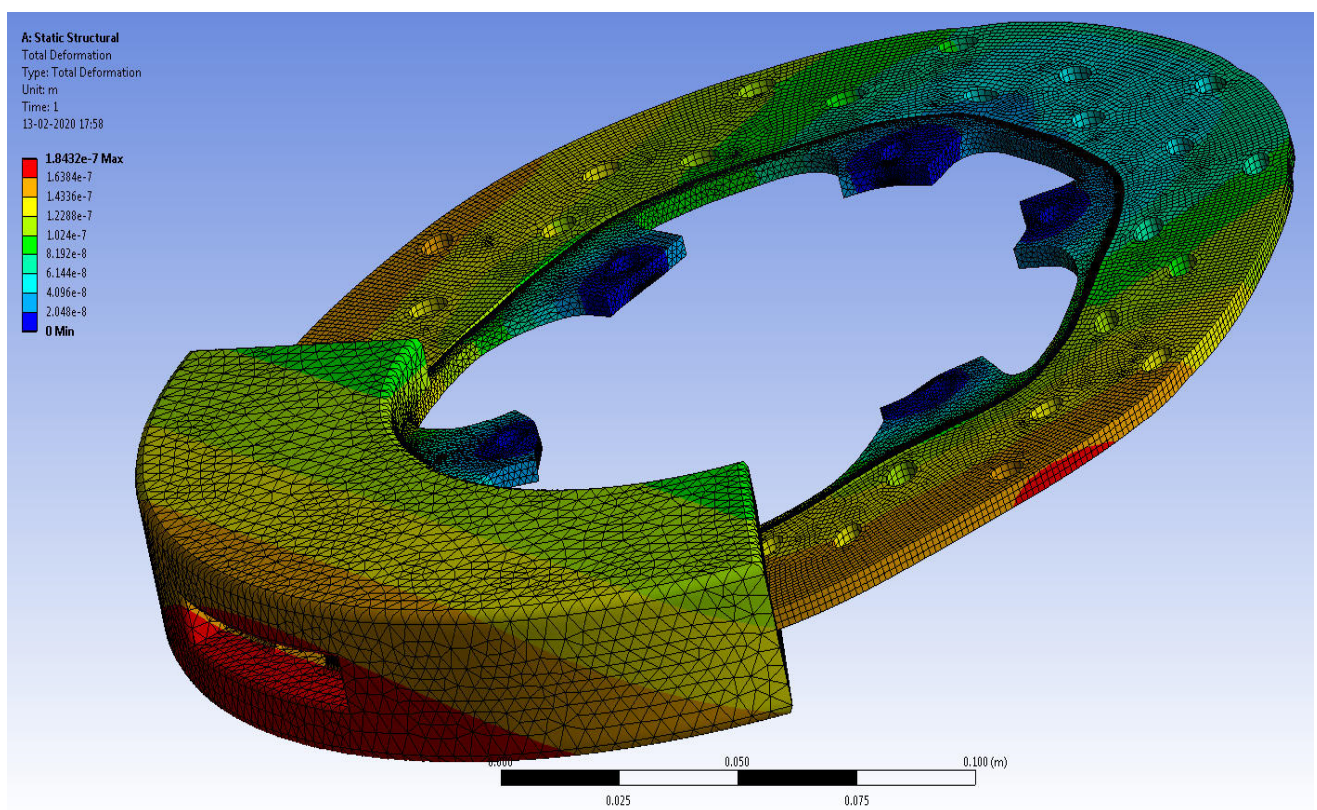

Figure 58. Deformation variations of disc brake based on CFRP-woven-wet based composite.
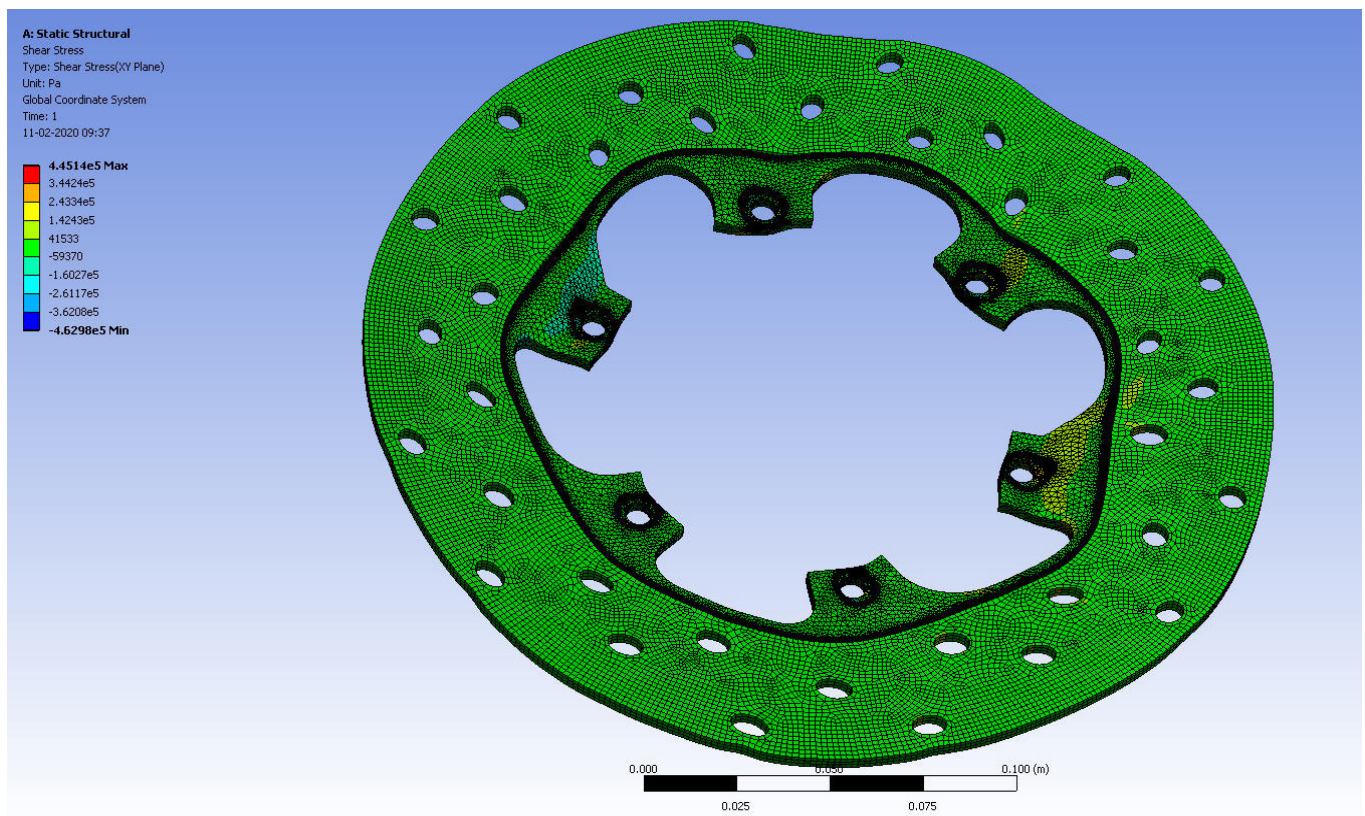
Figure 59. Frictional stress variations of disc brake based on CFRP-UD-prepreg composite.

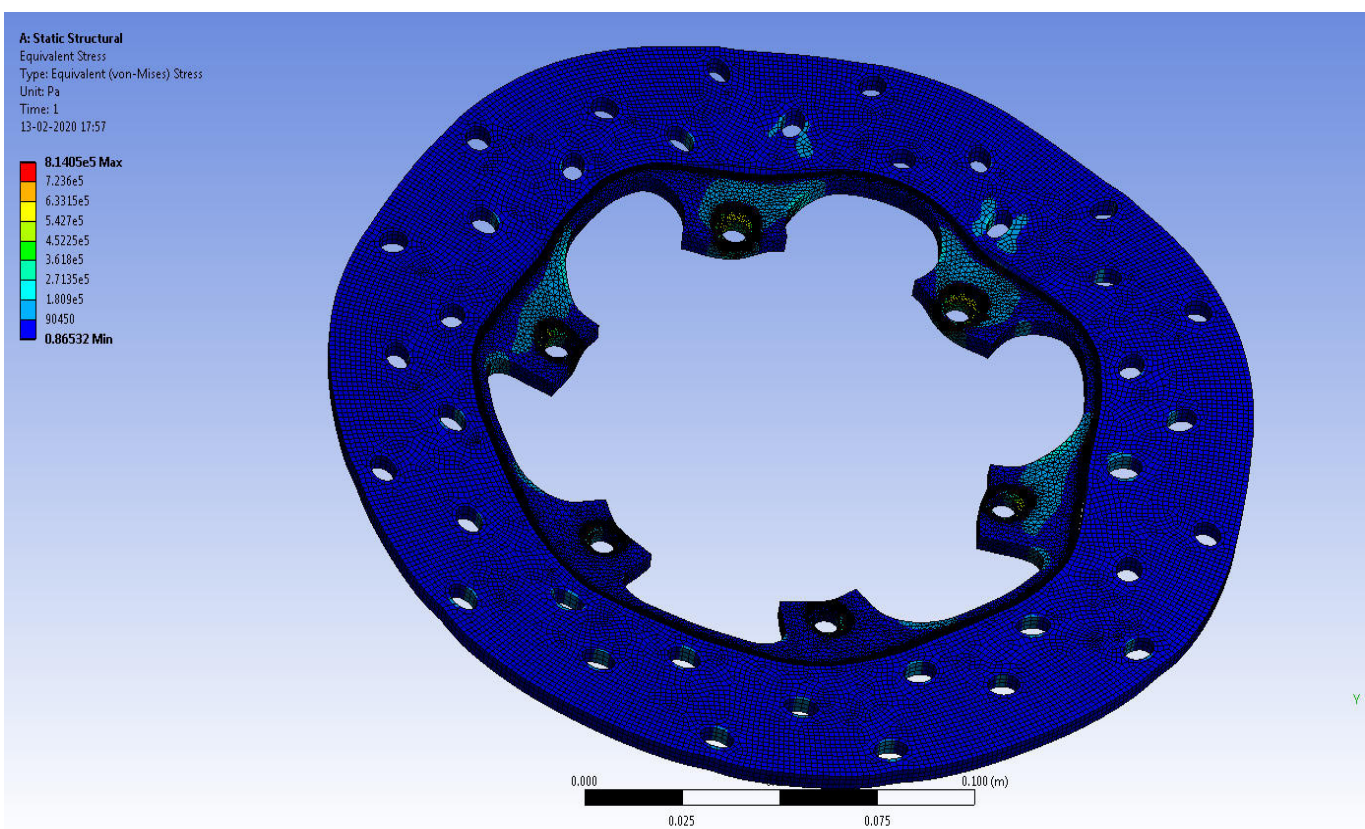**Figure 60.** Equivalent stress variations of disc brake using stainless steel.

All of the short-listed materials' structural outputs were created using a FEA software tool, and the data are given in detail in Figures 61–63.
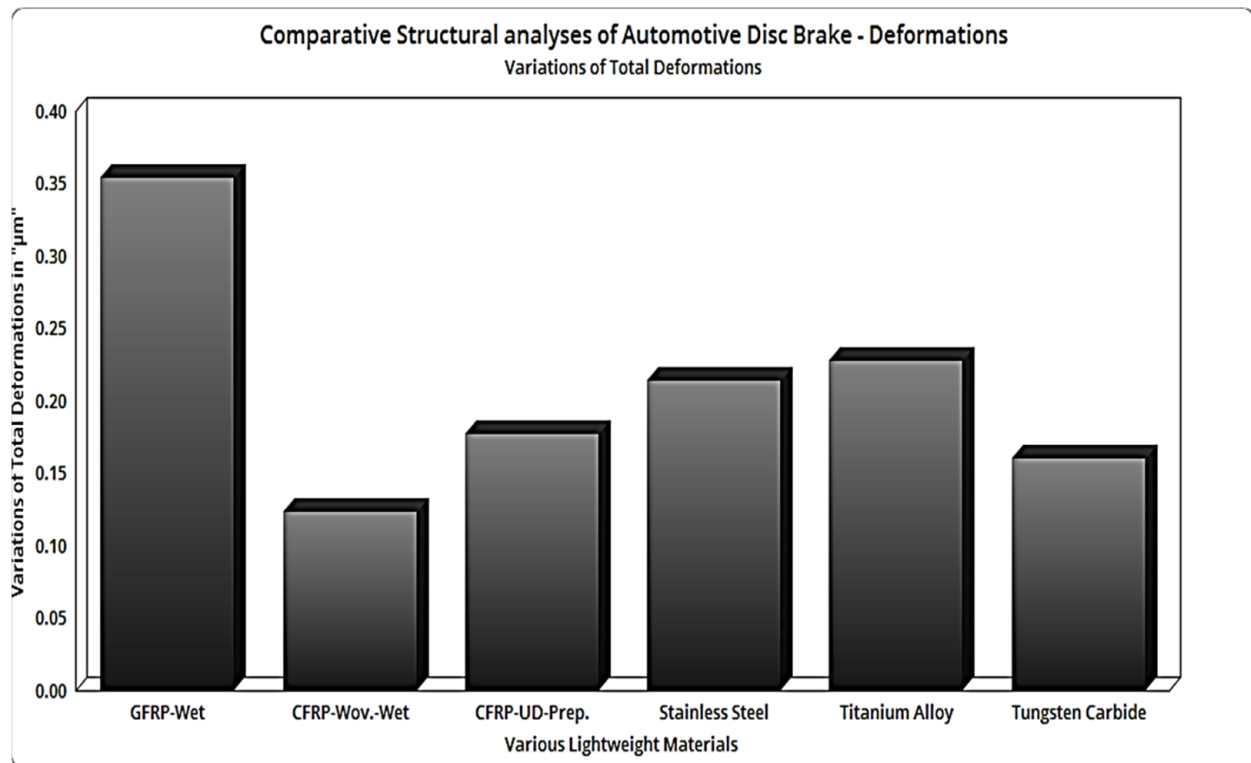

Figure 61. Comparative structural analyses of automotive disc deformations.
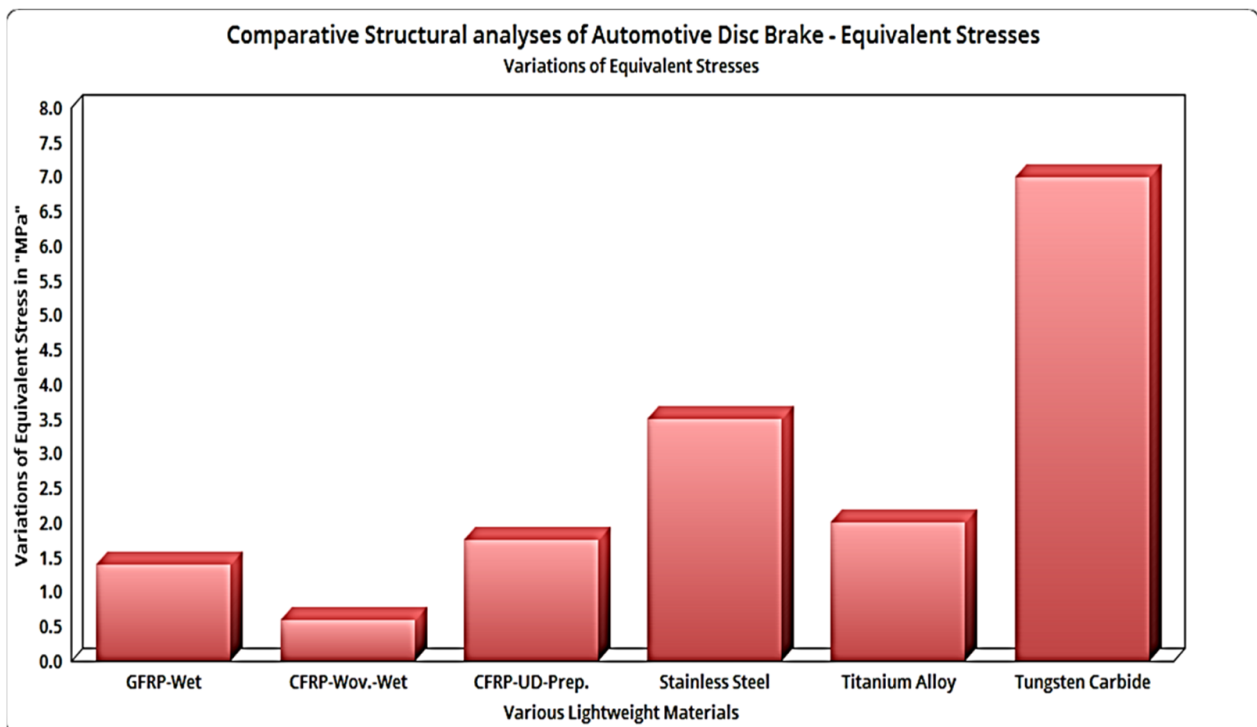

Figure 62. Comparative structural analyses of automotive disc equivalent stresses.
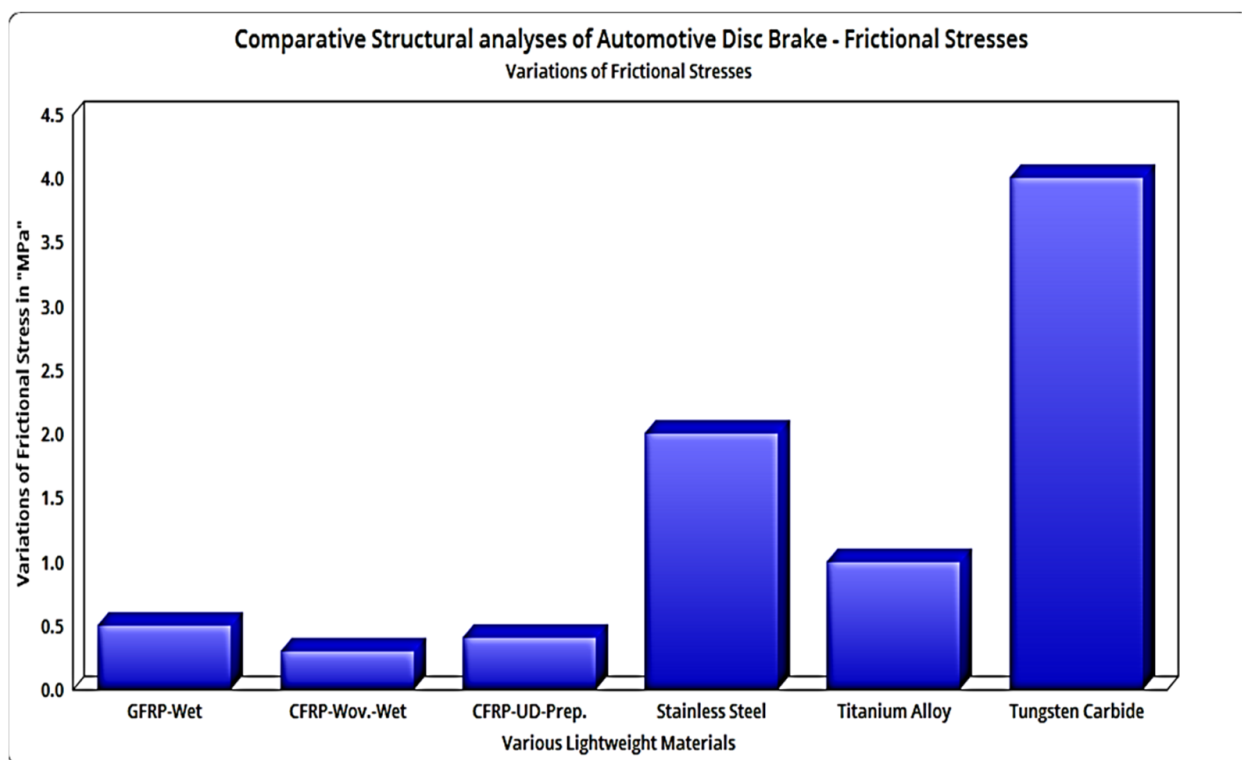
Figure 63. Comparative structural analyses of automotive disc frictional stresses.

Given its low deformation and equivalent stress, carbon-woven-wet reacts to static rotating loading, while carbon-UD-prepreg reacts to low shear stress under static rotating loading, as seen in Figures 61–63. Carbon-woven-wet was selected as the ideal material for disc brakes because of its ability to endure the natural loading conditions that occur. Carbon fiber-based polymer matrix composites performed well in the comparative research; therefore, they should be used in real-world applications.

4. Conclusions

ANSYS Workbench performed advanced coupled structural studies on composite materials. Experimental validation was performed to strengthen the trustworthiness of computational structural assessments. In a validation study, carbon fiber results were matched with Pin on disc test results, and the error rate was 3.1%. Comparative computational structural investigations showed that epoxy-carbon-UD-230-GPa–prepreg fiber composite (asymmetrical material) induces reduced frictional shear stress. This study used ANSYS ACP for composite generation and ANSYS Static Structural Tool as a solver. ANSYS ACP and Static Structural Tool shared data via ANSYS Workbench's one-way coupling feature. A comparison was essential to appreciate the property enhancement and high load absorption level of advanced composite materials. Finally, structural models were extended for several CFRP–SiC combinations, which had minimal frictional stresses. The epoxy-carbon-woven-230-GPa-prepreg mixture with SiC (asymmetrical material) is better for protecting against frictional loads in complex situations. ANSYS Workbench was used to analyze seven primary composite specimens, including carbon-UD-prepreg–SiC, carbon-UD-wet–SiC, carbon-woven-prepreg–SiC, carbon-woven-wet–SiC, E-glass-UD–SiC, E-glass-wet–SiC, S-glass-UD–SiC, and steel alloys. It was clear after confirmation that the stresses predicted by both engineering procedures were identical. Finally, this work constructed and analyzed large solid disc brake rotors made of the aforementioned materials. Advanced aircraft brakes ensure smooth braking and passenger safety. Braking materials must be high-quality and reliable. Through experimental testing and CAE simulations,

the properties of the selected materials (EN19, EN24, both steel and carbon fiber ceramic composite) were evaluated, resulting in carbon fiber ceramic matrix demonstrating superior properties. This paper's reference aircraft model was modeled in CATIA and simulated in ANSYS Workbench. Standard tribological experimental setups were used to estimate material wear. According to engineering techniques, carbon fiber can sustain higher temperatures with less deformation than steel alloys and 20 times less stress. Carbon fiber has a low frictional coefficient and frictional force; hence, it wears the least. Carbon fiber can survive hard braking conditions and has a longer life cycle than standard materials. Carbon-woven-wet reacts to static rotating loading with minimal deformation and equivalent stress, while carbon-UD-prepreg reacts to low shear stress. Carbon-woven-wet is the optimum material for automotive disc brakes due to its durability. Carbon-fiber-based polymer matrix composites performed well in comparative studies; they should be employed in real-world for both aerospace and automotive applications.

References

1. Kumar, G.R.; Vijayanandh, R.; Kamaludeen, M.B.; Balasubramanian, S.; Jagadeeshwaran, P.; Ramesh, M. Comparative Structural Characterization of Fiber Reinforced Composite Rotating Disc: A Validated Investigation. *Tribol. Ind.* **2020**, *42*, 608–620. [CrossRef]
2. Udhaya Prakash, R.; Raj Kumar, G.; Vijayanandh, R.; Senthil Kumar, M.; Ram Ganesh, T. Structural analysis of aircraft fuselage splice joint. *IOP Conf. Ser. Mater. Sci. Eng. J.* **2006**, *149*, 012127. [CrossRef]
3. Shahzamanian, M.M.; Sahari, B.B.; Bayat, M.; Ismarrubie, Z.N.; Mustapha, F. Transient and thermal contact analysis for the elastic behavior of functionally graded brake disks due to mechanical and thermal loads. *Mater. Des.* **2010**, *31*, 4655–4665. [CrossRef]
4. Sahari, B.B.; Shahzamanian, M.M.; Bayat, M.; Ismarrubie, Z.N.; Mustapha, F. Comparison OfThermoelastic Results in Two Types of Functionally Graded Brake Discs. *Int. J. Automot. Mech. Eng.* **2012**, *5*, 660–669. [CrossRef]
5. Shahzamanian, M.M.; Sahari, B.B.; Bayat, M.; Mustapha, F.; Ismarrubie, Z.N. Elastic Contact Analysis of Functionally Graded Brake Disks Subjected to Thermal and Mechanical Loads. *Int. J. Comput. Methods Eng. Sci. Mech.* **2013**, *14*, 10–23. [CrossRef]
6. Shahzamanian, M.M.; Sahari, B.B.; Bayat, M.; Mustapha, F.; Ismarrubie, Z.N. Finite element analysis of thermoelastic contact problem in functionally graded axisymmetric brake disks. *Compos. Struct.* **2010**, *92*, 1591–1602. [CrossRef]
7. Daoud, A.; El-Khair, M.T.A. Wear and friction behavior of sand cast brake rotor made of A359-20 vol% SiC particle composites sliding against automobile friction material. *Tribol. Int.* **2010**, *43*, 544–553. [CrossRef]
8. Naveen Kumar, K.; Vijayanandh, R.; Bruce Ralphin Rose, J.; Swathi, V.; Narmatha, R.; Venkatesan, K. Research on Structural behavior of Composite Materials on different Cantilever Structures using FSI. *Int. J. Eng. Adv. Technol.* **2019**, *8*, 1075–1086. [CrossRef]
9. Alpas, A.T.; Zhan, J. Effect of SiC particulate reinforcement on the dry sliding wear of aluminium-silicon alloys (A356). *Wear* **1992**, *155*, 83–104. [CrossRef]
10. Raj Kumar, G.; Senthil Kumar, M.; Vijayanandh, R.; Sekar, K.R.; Mohamed Bak, K.; Varun, S. The Mechanical Characterization of Carbon Fiber Reinforced Epoxy with Carbon Nanotubes. *Int. J. Mech. Prod. Eng. Res. Dev.* **2019**, *9*, 243–255.
11. Cuevaa, G.; Sinatora, A.; Guesser, W.L.; Tschiptschin, A.P. Wear resistance of cast irons used in brake disc rotors. *Wear* **2003**, *155*, 1256–1260. [CrossRef]
12. Kumar, G.R.; Vijayanandh, R.; Kumar, M.S.; Kumar, S.S. Experimental Testing and Numerical Simulation on Natural Composite for Aerospace Applications. ICC 2017. *AIP Conf. Proc.* **2017**, *1953*, 090045.

13. Howell, G.J.; Ball, A. Dry sliding wear of particulate-reinforced aluminium alloys against automobile friction materials. *Wear* **1995**, *181–183*, 379–390. [CrossRef]

14. Venkatesan, K.; Ramanathan, K.; Vijayanandh, R.; Selvaraja, S.; Raj Kumarb, G.; SenthilKumarb, M. Comparative structural analysis of advanced multi-layer composite materials. *Mater. Today Proc.* **2020**, *27*, 2673–2687. [CrossRef]

15. Kukutschova, J.; Roubicek, V.; Malachova, K.; Pavlickova, Z.; Holusa, R.; Kubackova, J.; Micka, V.; MacCrimmon, D.; Filip, P. Wear mechanism in automotive brake materials, wear debris and its potential environmental impact. *Wear* **2009**, *267*, 807–817. [CrossRef]

16. Raj Kumar, G.; Vijayanandh, R.; Mohammad Bak, K.; ShyamChander, R.; Arawinth, R. Experimental Testing on Mechanical Properties Effect of Aluminum Foam. *Int. J. Mech. Prod. Eng. Res. Dev.* **2018**, *8*, 1047–1059.

17. Farag, M.M.; Drai, A.S. Mechanical and Tribological Behavior of Glass-Polyester Composite System under Graphite Filler Content. *Eng. Technol. J.* **2012**, *30*, 672–683.

18. Raj Kumar, G.; Vijayanandh, R.; Venkatesan, K.; Ramesh, M.; Senthil Kumar, M.; Balaji, S. Comparative Investigations on the Main Elements of Carbon Fiber Based Composites Using Computational Structural Simulations. *J. Phys. Conf. Ser.* **2020**, *1504*, 012003. [CrossRef]

19. Su, F.-H.; Zhang, Z.-Z.; Liu, W.-M. Mechanical and tribological property of Carbon Fabric composites filled with several nano particulates. *Wear* **2006**, *260*, 861–868. [CrossRef]

20. Venkatesan, K.; Geetha, S.; Vijayanandh, R.; Kumar, G.R.; Jagadeeshwaran, P.; Kumar, R.R. Advanced structural analysis of various composite materials with carbon nano-tubes for property enhancement. *AIP Conf. Proc.* **2020**, *2270*, 030005. [CrossRef]

21. Suresha, B.; Chandramohan, G.; Sampathkumaran, P.; Sethuramu, S. Investigation of the friction and wear behavior of glass-epoxy composite with and without graphite filler. *J. Reinf. Plast. Compos.* **2007**, *26*, 81–93. [CrossRef]

22. Mirrudula, P.; Kaviya Priya, P.; Malavika, M.; Kumar, G.R.; Vijayanandh, R.; Kumar, M.S. Comparative structural analysis of the sandwich composite using advanced numerical simulation. *AIP Conf. Proc.* **2020**, *2270*, 040005. [CrossRef]

23. Rohini Devi, G.; Rao Rama, K. Carbon–carbon composites—An overview. *Def. Sci. J.* **2013**, *43*, 369–383. [CrossRef]

24. Vijayanandh, R.; Venkatesan, K.; Ramesh, M.; Raj Kumar, G.; Senthil Kumar, M. Optimization of Orientation Of Carbon Fiber Reinforced Polymer Based On Structural Analysis. *Int. J. Sci. Technol. Res.* **2019**, *8*, 3020–3029.

25. Larsen, T.; Andersen, T.L.; Thorning, B.; Horsewell, A.; Vigild, M.E. Comparison of friction and wear for an epoxy reinforced by a glass or carbon/aramid hybrid weave. *Wear* **2007**, *262*, 1013–1020. [CrossRef]

26. Prasanth, S.I.; Kesavan, K.; Kiran, P.; Sivaguru, M.; Sudharsan, R.; Vijayanandh, R. Advanced structural analysis on E-glass fiber reinforced with polymer for enhancing the mechanical properties by optimizing the orientation of fiber. *AIP Conf. Proc.* **2020**, *2270*, 040006. [CrossRef]

27. Ruppe, J.P. Today and the future in aircraft wheel and brake development. *Can. Aeronaut. Space J.* **1981**, *26*, 209–215.

28. Bhagavathiyappan, S.; Balamurugan, M.; Rajamanickam, M.; Vijayanandh, R.; Kumar, G.R.; Kumar, M.S. Comparative computational impact analysis of multi-layer composite materials. *AIP Conf. Proc.* **2020**, *2270*, 040007. [CrossRef]

29. Tanaka, K. Friction and wear of semi crystalline polymers sliding against steel under water lubrication. *J. Lubr. Technol.* **1980**, *102*, 526–533. [CrossRef]

30. Mohamed Bak, K.; Raj Kumar, G.; Ramasamy, N.; Vijayanandh, R. Experimental and Numerical Studies on The Mechanical Characterization of Epdm/S-SbrNano Clay Composites. *IOP Conf. Ser. Mater. Sci. Eng.* **2020**, *912*, 052016. [CrossRef]

31. Ramesh, M.; Vijayanandh, R.; Raj Kumar, G.; Vijayakumar, M.; Jagadeeshwaran, P.; Senthil Kumar, M. Comparative Structural Analysis of Various Composite Materials based Unmanned Aerial Vehicle's Propeller by using Advanced Methodologies. *IOP Conf. Ser. Mater. Sci. Eng.* **2021**, *1017*, 012032. [CrossRef]

32. Vijayanandh, R.; Raj Kumar, G.; Jagadeeshwaran, P.; Vijayakumar, M.; Ramesh, M.; Won Jung, D. Carbon Nanotubes and Their Polymer Nanocomposites. In *Nanomaterials and Nanocomposites: Characterization, Processing, and Applications*; CRC Press: Boca Raton, FL, USA, 2021; pp. 139–165. ISBN 9780367483890.

33. Raj Kumar, G.; Balasubramaniyam, S.; Senthil Kumar, M.; Vijayanandh, R.; Raj Kumar, R.; Varun, S. Crash Analysis on the Automotive Vehicle Bumper. *Int. J. Eng. Adv. Technol.* **2019**, *8*, 1602–1607. [CrossRef]

34. Gates, D. Two-body and three-body abrasion: A critical discussion. *Wear* **1998**, *214*, 139–146. [CrossRef]

35. Arul Prakash, R.; Vijayanandh, R.; Ramesh, G.; Hariaran, S.; Janardhanan, Y.; Senthil, K.M.; Jagadeeshwaran, P. Investigation of Automotive Disc Brake's Material Based on Tribological Parameters by using Computational Structural Analysis. In *Tribology and Characterization of Surface Coatings*; Sarfraj, A., Vinayak, S.D., Eds.; Scrivener Publishing LLC: Beverly, MA, USA, 2022; Volume 10, pp. 211–238. [CrossRef]

36. Kumar, R.; Sesha, V.; Butt, M.M.; Ahmed, N.; Khan, S.A.; Afzal, A. Thermo-Mechanical Analysis and Estimation of Turbine Blade Tip Clearance of a Small Gas Turbine Engine under Transient Operating Conditions. *Appl. Therm. Eng.* **2020**, *179*, 115700. [CrossRef]

37. Sharath, B.N.; Venkatesh, C.V.; Afzal, A. Multi Ceramic Particles Inclusion in the Aluminium Matrix and Wear Characterization through Experimental and Response Surface-Artificial Neural Networks. *Materials* **2021**, *14*, 2895. [CrossRef]

38. Akhtar, M.N.; Khan, M.; Khan, S.A.; Afzal, A.; Subbiah, R.; Bakar, E.A. Determination of Non-Recrystallization Temperature for Niobium Microalloyed Steel. *Materials* **2021**, *14*, 2639. [CrossRef]

39. Jilte, R.; Afzal, A.; Panchal, S. A Novel Battery Thermal Management System Using Nano-Enhanced Phase Change Materials. *Energy* **2021**, *219*, 119564. [CrossRef]

40. Murugan, M.; Saravanan, A.; Elumalai, P.V.; Kumar, P.; AhamedSaleel, C.; Samuel, O.D.; Setiyo, M.; Enweremadu, C.C.; Afzal, A. An Overview on Energy and Exergy Analysis of Solar Thermal Collectors with Passive Performance Enhancers. *Alex. Eng. J.* **2022**, *61*, 8123–8147. [CrossRef]

41. Dhairiyasamy, R.; Saleh, B.; Govindasamy, M.; Aly, A.A.; Afzal, A.; Abdelrhman, Y. Effect of Particle Size on Thermophysical and Heat Transfer Properties of Ag Nanofluid in a Radiator–an Experimental Investigation. *Inorg. Nano Met. Chem.* **2021**. [CrossRef]

42. Afzal, A.; Nawfal, I.; Mahbubul, I.M.; Kumbar, S.S. An Overview on the Effect of Ultrasonication Duration on Different Properties of Nanofluids. *J. Therm. Anal. Calorim.* **2019**, *135*, 393–418. [CrossRef]

43. Islam, M.T.; Nguyen, A.V.; Afzal, A. Bubble's Rise Characteristics in Shear-Thinning Xanthan Gum Solution: A Numerical Analysis. *J. Taiwan Inst. Chem. Eng.* **2022**, *132*, 104219. [CrossRef]

44. Saleh, B.; Madhukesh, J.K.; Varun Kumar, R.S.; Afzal, A.; Abdelrhman, Y.; Aly, A.A.; Punith Gowda, R.J. Aspects of Magnetic Dipole and Heat Source/Sink on the Maxwell Hybrid Nanofluid Flow over a Stretching Sheet. *Proc. Inst. Mech. Eng. Part E J. Process. Mech. Eng.* **2022**. [CrossRef]

45. Afzal, A.; Abdul Mujeebu, M. Thermo-Mechanical and Structural Performances of Automobile Disc Brakes: A Review of Numerical and Experimental Studies. Arch. *Comput. Methods Eng.* **2019**, *26*, 1489–1513. [CrossRef]

46. Belhocine, A.; Afzal, A. A Predictive Tool to Evaluate Braking System Performance Using a Fully Coupled Thermo-Mechanical Finite Element Model. *Int. J. Interact. Des. Manuf.* **2020**, *14*, 225–253. [CrossRef]

47. Belhocine, A.; Afzal, A. Computational Finite Element Analysis of Brake Disc Rotors Employing Different Materials. *Aust. J. Mech. Eng.* **2020**, *20*, 637–650. [CrossRef]

48. Belhocine, A.; Afzal, A. Finite Element Modeling of Thermomechanical Problems under the Vehicle Braking Process. *Multiscale Multidiscip Model. Exp. Des.* **2020**, *3*, 53–76. [CrossRef]

49. Kesavan, K.; Kiran, P.; Sivaguru, M.; Indira Prasanth, S.; Sudharsan, R.; Raj Kumar, G.; Vijayanandh, R. Multi-objective Structural Analysis of Kevlar Fiber Reinforced Polymer Composite, Recent Advances in Smart Manufacturing and Materials. *Lect. Notes Mech. Eng.* **2021**, *11*, 137–151. [CrossRef]

50. Gnanasekaran, R.K.; Shanmugam, B.; Raja, V.; Kathiresan, S. Multi-disciplinary Optimizations on Flexural Behavioural Effects on Various Advanced Aerospace Materials: A Validated Investigation. *Mater. Plast.* **2022**, *59*, 214–233. [CrossRef]